

INVESTIGATING MOLECULAR MECHANISMS OF MAST CELL MIGRATION AND
DYNAMIC INTERACTIONS WITH INTESTINAL EPITHELIUM

A Dissertation

Presented to the Faculty of the Graduate School
of Cornell University

In Partial Fulfillment of the Requirements for the Degree of
Doctor of Philosophy

By

Jinmin Lee

January 2012

© 2012 Jinmin Lee

INVESTIGATING MOLECULAR MECHANISMS OF MAST CELL MIGRATION AND
DYNAMIC INTERACTIONS WITH INTESTINAL EPITHELIUM

Jinmin Lee, Ph.D.

Cornell University 2012

Migration is not only one of the very fundamental functions of cells, it is also crucial for immune cells to be at the right place at the right time to mount an effective immune response. Mast cells are the primary mediators of immunoglobulin E (IgE)-dependent allergic disorders, and they also function as effector and immunomodulatory cells in innate and adaptive immune responses. Crosslinking of IgE-FcεRI complexes at the mast cell surface by antigen activates a signaling cascade that causes mast cell activation, resulting in Ca²⁺ mobilization and granule exocytosis. Mast cells accumulate in the sites of inflammation in response to parasite and bacterial infections and in allergic reactions, but very little is known about the molecular mechanisms of this process. In this work, we use real-time video microscopy and a novel cell tracking analysis to probe this understudied area of mast cell biology. Using these methods, we demonstrate that rat basophilic leukemia (RBL) and bone marrow-derived rat mast cells exhibit spontaneous motility and directed migration up a gradient of antigen, and Ca²⁺ influx via the CRAC channel protein Orai1 plays an important role in regulating both of these processes. A mutant RBL cell line that lacks Syk tyrosine kinase shows reduced spontaneous motility and chemotaxis toward antigen, suggesting a role for Syk in these processes. To gain insights into the

physiological functions of mast cell migration, we investigated the dynamic interactions between mast cells and intestinal epithelial cells *in vitro* and *in situ*. Mucosal mast cells show transepithelial migration when these cells are introduced from either the apical and basolateral side of the polarized epithelial monolayers, suggesting dynamic interactions between mucosal mast cells and epithelial cells. Furthermore, using multiphoton imaging, we show endogenous and adoptively transferred mast cells localized in the intraepithelial regions of the intestinal villi in response to parasite infection *in situ*. Taken together, our results show that Orai1-dependent Ca^{2+} influx plays an essential role in the mechanism of directed mast cell migration, and they demonstrate distinct interactions between mast cells and intestinal epithelium, providing new insights into this process.

BIOGRAPHICAL SKETCH

Jinmin Lee was born on January 19, 1982 to Won Taek Lee and Kinam Han in Seoul, South Korea. In her childhood years, she spent most of her free time reading, making up stupid but harmless jokes with her friends, and occasionally wondered about *Life, the Universe, and Everything*. Her extensive family of scientists and physicians undoubtedly influenced her decision to study science. She received her Bachelor's degree in Biology at Sogang University in Seoul, South Korea, where she took Basic Immunology during her Senior year and quickly became fascinated with the fine complexity of immune systems. Wanting to learn more about this field, she decided to pursue a Master's degree in Biomedical Science with a concentration on Immunology at Yonsei University in Seoul, South Korea. In the summer of 2006, Jinmin moved across the Pacific Ocean to pursue a Ph.D in Immunology at Cornell University in Ithaca, New York. Here, she had the good fortune to join the laboratory of Drs. Barbara Baird and David Holowka, and studied molecular mechanisms of mast cell migration.

For my family

ACKNOWLEDGEMENTS

I am immensely grateful and indebted to the people who have helped and supported me throughout my scientific career and my life.

I would like to thank David Holowka for being an incredible advisor and mentor, for his constant guidance, encouragement, and infectious optimism. I am deeply thankful to Barbara Baird for always helping me to focus on my goal and providing great opportunities. It has been a wonderful experience to work under two very talented, dedicated mentors. Special thanks to my committee member Judy Appleton for her excellent suggestions, discussions, and enthusiasm.

I would especially like to thank past and present members of the Baird-Holowka lab for being wonderful colleagues and friends. Norah was a great friend with whom I had many enjoyable adventures inside and outside of the lab. Alice was a terrific and fun office mate. I greatly appreciate all the analysis work Sarah has done to help my research. I want to thank Ethan for giving me his TV and a plant (that met an untimely demise in my hands). Stephanie was always willing to answer my many questions. Kirsten for her enthusiasm and organizational skills. Kate, Sarah S., Josh, Chris for sharing numerous Friday evenings having fun conversations about science and otherwise. I appreciate all the help and advices Roy has given me about my project. I would like to thank: Kari, Amit, Deepti, Nat, Alexis, Lavanya, Marcela, Devin, Lily, Sil, and Prabs.

I would also like to thank my friends. My very best friends, Stella, Soh Min, Anna, Sooyeon, and Myung Hee are the sisters I never had. I thank them for being there throughout the years. I want to thank Lisa for being an excellent collaborator as well as a friend. I have learned many things and shared a lot of good times with Delbert, Sara, Jiyeon, Hyae-Soo, Mike, and Krystal. I am deeply grateful to Sungsoo for 42. Last, I must thank my parents for their love and support.

TABLE OF CONTENTS

Biographical Sketch	iii
Dedication	iv
Acknowledgements	v
Table of Contents	vii
List of Figures	ix
List of Abbreviations	xi
Chapter 1. Introduction	
Mast cell heterogeneity	2
Mast cells in immune response to pathogens	4
FcεRI-mediated signaling	8
Cell motility, migration and chemotaxis	11
Ca ²⁺ mobilization and store operated Ca ²⁺ entry in immune cells	14
Ca ²⁺ mobilization and cell motility	19
Current studies	21
References	24
Chapter 2. Molecular Mechanisms of Spontaneous and Directed Mast Cell Motility	
Abstract	40
Introduction	41
Materials and Methods	43
Results	48
Discussion	67
References	75
Chapter 3. Investigating the Dynamic Interactions of Mucosal Mast Cells and Intestinal Epithelial Cells	
Abstract	84
Introduction	85
Materials and Methods	87
Results	90
Discussion	100
References	106
Chapter 4. Summary and Future Directions	110
References	117

Appendices

A. Characterizing Motility of RBL Mast Cells on Different Substrates	119
B. Characterizing Roles for Fyn, Sphingosine Kinases 1 and 2, and Tec Family Kinases in Motility of Mouse Bone Marrow-Derived Mast Cells	126
C. Summary of Calcium Measurements of Rat Bone Marrow-Derived Mast Cells	132
D. Additional Results from Mast Cell Motility and Chemotaxis Study	140
E. MATLAB Code for Automated Tracking and Analysis	142

LIST OF FIGURES

1.1	FcεRI-mediated signaling pathways in mast cells.	9
1.2	Store operated Ca ²⁺ entry in mast cells.	15
2.1	Morphology and motility properties of RBL-2H3 mast cells and rat BMMCs.	49
2.2	Extracellular Ca ²⁺ is important for mast cell motility.	52
2.3	Involvement of Orai1/CRACM1 in RBL mast cell motility.	55
2.4	RBL-2H3 mast cells exhibit spontaneous Ca ²⁺ transients with influx dependence that correlates with motility.	57
2.5	Monitoring and analyzing mast cell chemotaxis in real time.	60
2.6	RBL-2H3 mast cells show chemotaxis toward antigen.	62
2.7	Directed migration of RBL-2H3 cells toward antigen is dependent on Syk kinase.	64
2.8	Orai1/CRACM1 contributes to RBL-2H3 mast cell chemotaxis toward antigen.	66
2.9	Average velocity and chemotactic index of chemotaxing mast cells under various conditions.	68
3.1	SLC-44 rat intestinal epithelial cell line makes tight junctions on a glass surface.	92
3.2	RBL-2H3 cells interacting with SLC-44 cell monolayers.	94
3.3	Schematic diagram of transwell transepithelial migration assay.	96
3.4	BMMCs interacting with SLC-44 cell monolayers.	97
3.5	<i>In situ</i> multiphoton imaging of endogenous mast cells in <i>Trichinella</i> -infected rat small intestine.	99
3.6	<i>In situ</i> multiphoton imaging of adoptively transferred RBL-2H3 mast cells in <i>Trichinella</i> -infected rat small intestine.	101

A.1	Morphology of RBL mast cells on different substrates.	121
A.2	Motility of RBL mast cells on different substrates.	123
B.1	Characterizing the role of Fyn and sphingosine kinases 1 and 2 in mouse BMMC motility.	129
B.2	Characterizing the role of Tec family kinases Itk and Btk in mouse BMMC motility.	130
C.1	Antigen-stimulated Ca^{2+} response of rat BMMCs.	134
C.2	Thapsigargin-stimulated Ca^{2+} response of rat BMMCs.	136
C.3	Stimulated Ca^{2+} response of rat BMMCs in the absence of extracellular Ca^{2+} .	138
D.1	Comparison of the motility coefficient and the chemotactic index of RBL-2H3 cells under various conditions.	141

LIST OF ABBREVIATIONS

2-APB	2-aminoethoxydiphenyl borate
APC	antigen presenting cell
BCR	B cell receptor
BiM	bisindolyl maleimide
BMMC	bone marrow-derived mast cell
BSS	buffered saline solution
Ca ²⁺	calcium
CAD	CRAC channel activating domain
CRAC	Ca ²⁺ release-activated Ca ²⁺
DAG	diacylglycerol
DC	dendritic cell
DMSO	dimethyl sulfoxide
DNP	2,4-dinitrophenyl
ECM	extracellular matrix
ER	endoplasmic reticulum
Gd ³⁺	gadolinium ion
IgE	immunoglobulin E
IL-3	interleukin-3
IP ₃	inositol-1,4,5-bisphosphate
ITAM	immune tyrosine activation motif
LAT	linker for the activation of T cells
MCP	mast cell protease
MHC	major histocompatibility complex
PI3K	phosphatidylinositol-3-OH kinase

PIP ₂	phosphatidylinositol-4,5-bisphosphate
PKC	protein kinase C
PLC γ	phospholipase C gamma
PLD	phospholipase D
PMN	polymorphonuclear leukocytes
PTEN	phosphatase and tensin homologue
RFP	red fluorescent protein
S1P	sphingosine-1-phosphate
SCF	stem cell factor
SH2	Src homology 2
SOC	store operated calcium
SOCE	store operated calcium entry
STIM	stromal interaction molecule
TCR	T cell receptor
TER	transepithelial electrical resistance
TLR	Toll-like receptor
TRPC	transient receptor potential channel
TNF	tumor necrosis factor
ZO-1	zona occludens-1

CHAPTER 1

INTRODUCTION

Allergic diseases have reached epidemic proportions worldwide, with their prevalence continuously increasing, especially in developed countries (1). Allergic diseases include asthma, food allergy, atopic dermatitis, anaphylaxis, and drug allergy. All of these allergic diseases can occur alone or in combination (2). Mast cells are a key cell type in the hematopoietic lineage that were first described by Paul Ehrlich in late 1800s (3), and they have long been recognized as a primary mediator of immunoglobulin E (IgE)-associated allergic reactions (4). Allergic reactions are described as symptomatic responses to a normally innocuous environmental antigen. More recently, mast cells are also acknowledged for their key role in recognizing pathogens and modulating appropriate immune responses (5), suggesting adaptable and multifunctional nature of these cells. Crosslinking of IgE bound to its high affinity receptor, Fc ϵ RI, activates a signaling cascade that results in the release of preformed granules in mast cells. Mast cells produce variety of biologically active products, including histamine, proteases, eicosanoids, cytokines, and chemokines. Histamine and proteases are stored in secretory granules, whereas eicosanoids and cytokines can be generated *de novo* after stimulation. This array of mediators as well as the expression of multiple types of receptors allows mast cells to participate in diverse functions (6).

Mast cell heterogeneity

Mast cells are derived from pluripotent hematopoietic stem cells in the bone marrow, and in particular, human mast cells are believed to arise from CD34⁺ stem cells. Mast cells circulate in the blood as progenitors, but acquire their differentiated mature phenotype within tissues, where they ultimately reside. These processes are regulated by stem cell factor (SCF), interleukin-3 (IL-3), IL-4, IL-9, nerve growth factor, and probably other factors (7). The mast cell growth factor SCF is produced mainly by stromal cells and either expressed on the cell surface or released in soluble form (8). The receptor for SCF is known as Kit (CD117) and is expressed on hematopoietic stem cells and is retained on mast cells throughout their development and differentiation but is down-regulated in other bone marrow-derived cells during differentiation. Unlike mast cells, basophils reach their mature phenotype in bone marrow before their release into blood (9). Mast cells are long-lived cells, and can proliferate in response to appropriate stimuli, despite their terminally differentiated phenotype (10).

Original observations of two histochemically distinct populations of mast cells (11), and the capacity of only one of these subsets to respond to compound 40/80 (12), led to the idea of mast cell heterogeneity. These distinct subsets express different proteoglycans and proteases (13, 14) and are commonly called mucosal mast cells and connective tissue (or serosal) mast cells. Mouse mucosal mast cells express chymases mMCP-1 (RMCPII in rat), and mMCP-2, and are mainly localized in the mucosal

epithelium and lamina propria. On the other hand, mouse connective tissue mast cells express chymases mMCP-4, -5, and tryptases and are thought to predominantly localize within submucosa composed of loose connective tissues (15). This heterogeneity probably contributes to the multifunctional roles that mast cells play. For example, mouse mMCP-4 expressing mast cells contribute to the regulation of homeostatic intestinal epithelial barrier function via this protease (16), whereas mice lacking mast cells and mice lacking mMCP-1 are defective in regulating intestinal permeability and parasite expulsion (17). Nonetheless, these two subsets of mast cells exhibit some 'plasticity'. When bone marrow derived mast cells from wild type mice were transferred to mast cell deficient mice, the cells show either mucosal or connective tissue phenotype depending on the tissue site to which they migrate, adopting the phenotype of mast cells that normally reside in that tissue site (18). IL-3 and SCF drive mast cell differentiation to mouse mucosal (19) or connective tissue (20) mast cells, respectively, and it is believed that under both normal and pathological situations, mast cells are conditioned by their cytokine environment (21). Human mast cells also show heterogeneity with two different protease types in their granule contents, but with less stringent tissue-type specificity (22).

Mast cells in immune response to pathogens

Mast cells are strategically located at the interface between host and environment such as skin and mucosa, which makes these cells ideally localized for immune surveillance (5). They are localized near blood vessels, lymphatic vessels, and nerve fibers. Especially at the earliest stages of infection, mast cells communicate the presence of a pathogen to many other cell types, including immune cells (23-26), epithelial cells (27), smooth muscle cells (28), and endothelial cells (29, 30) located nearby in the site of infection, and in the draining lymph nodes. Because their numerous granules contain preformed mediators, mast cells have great potential to be the first responders following pathogen recognition. These cellular communications by mast cells contribute to immune surveillance and host defense.

To initiate appropriate immune response against invading pathogens, mobilization of various cell types are required. Mast cells induce or increase cell trafficking of many different cell types under diverse pathological conditions that is mainly mediated by the release of their granule contents. At sites of bacterial infection, mast cell-derived tumor necrosis factor (TNF) promotes the influx of dendritic cells (DCs) and neutrophils (23, 29), and the production of the chemokine CCL20 by mast cells likely contributes to DC precursor recruitment from the blood into the tissues (31). In viral infection, mast cells induce the chemotaxis of CD8⁺ T cells by activation of Toll-

like receptor 3 (TLR3) on the mast cell surface and subsequent upregulation of CXCL10 (IP10) and CCL5 (RANTES) (25).

The first observation that mast cells could play a role in host defense came from the models of helminth infection in the gut (32, 33). In these early studies, mast cells were observed as clusters around sites of parasite infection, with many cells undergoing degranulation (32, 34-36). Different from bacteria, protozoa, fungi and viruses, most helminths do not replicate in the mammalian host. The infective stages must establish infection and then grow to sexual maturity, producing eggs or live offspring for transmission to the next host. The adult stages of these parasites can be long-lived, even for decades, and they adapt to the attack of host immune system. These distinct features, along with the multicellular nature of these pathogens, may explain why helminth induces a very different immune response profile from microbial pathogens. In mammals, this response belongs to the T helper cell type 2 (Th2) type, and it involves expanded populations of mast cells, eosinophils, basophils, and certain subtypes of macrophages, the antibodies IgG1, IgG4, and IgE, and the cytokines IL-3, IL-4, IL-5, IL-9, IL-10, and IL-13 (37-39).

The control or clearance of parasites by mast cells involves diverse mechanisms, including the recruitment of central immune cells, regulation of gut permeability and parasite expulsion, and containment of chronic infection (34-36, 40, 41). During protozoan parasite skin infection by *Leishmania*, mast cells are important for promoting

protective immunity which results in decrease skin lesion size (36). Mast cell proliferation, or mastocytosis, during gut infection by the parasite *Schistosoma* was shown to depend on SCF (42) or IgE (43). Mucosal mast cells proliferate in the infected gut in response to IL-9 (17) and IL-18 (44), and they release mast cell proteases that can degrade tight junctions (17), to increase fluid flow. Apparently, the requirement for mast cells during parasite infection varies greatly depending on the type of challenge. Expulsion of hookworm from the gut during secondary challenge depends on basophils rather than on mast cells, in contrast to expulsion during primary challenge (35). Rodents are natural hosts for a parasitic nematode, *Trichinella spiralis*, and primary infection induces a potent Th2 response leading to intestinal mastocytosis (45), and mast cell degranulation can be observed at the time of adult worm expulsion (32, 46). Mice deficient in IgE show a deficiency in parasite expulsion from the gut that might be explained by the decreased levels of mMCP-1, which were shown to influence the speed of expulsion from the gut (40). On the other hand, rapid expulsion of *T. spiralis* from the gut during secondary infection can occur in the absence of either mastocytosis or RMCPII release (47), suggesting that mast cells may play different roles depending on the type of challenge. In addition, differentiated mucosal mast cells are known to redistribute from the submucosa or crypt area to the lamina propria and intraepithelial regions of jejunal villi, and reversibly alter their protease phenotype during the course of an immune response to *T. spiralis* infections (48).

Immunoglobulin E (IgE) and FcεRI

Immunoglobulin E (IgE) is the fifth and final class of human antibody to be discovered (49), and it is produced by B cells following antigen presentation by antigen presenting cells (APC) to T helper type 2 (Th2) cells. Interleukin-4 (IL-4) and IL-13 secretion from Th2 cells induce B cells to switch production of IgM and other isotypes to antigen-specific IgE (6).

The receptor for IgE was initially identified by Metzger and colleagues using the rat basophilic leukemia (RBL) tumor mast cell line (50, 51). This receptor is abundantly expressed on both normal and RBL-2H3 mast cells (up to 3×10^5 receptors/cell), and it binds IgE with high affinity ($K_d \leq 10^{-10}$ M) (50), referred to as the high affinity receptor for IgE, or FcεRI. FcεRI is a heterotetrameric receptor expressed on the mast cell surface composed of three different subunits: an IgE-binding α -subunit, a membrane-tetraspanning β -subunit which amplifies the signal, and two identical γ -subunits linked by a disulfide bond contain immunoreceptor tyrosine-based activation motifs (ITAMs) that are essential for signal initiation (52).

FcεRI-mediated signaling

Mast cell signaling mediated by FcεRI has proven to be a useful model for understanding fundamental molecular mechanisms in immune cell activation. This is in part because of the relative simplicity of FcεRI-mediated signal initiation through its tyrosine phosphorylation cascade, and also the relatively immediate response of mast cell degranulation activated by this receptor.

Upon aggregation of IgE-FcεRI complexes by multivalent antigen, active Src family tyrosine kinase Lyn in ordered lipid microdomains (53), known as lipid rafts, becomes proximal to the cross-linked receptors and phosphorylates its ITAMs (54). This results in activation of tyrosine kinase Syk after ITAM binding. Activated Syk phosphorylates several downstream adaptor molecules and enzymes, including the linker for the activation of T cells (LAT). LAT is an adaptor protein with multiple tyrosines that serve as binding sites for SH2 domain-containing proteins when phosphorylated (55), including phospholipase C γ (PLC γ). PLC γ is phosphorylated by Syk after recruitment to the plasma membrane via interactions with LAT (56). Activated PLC γ hydrolyzes PIP $_2$ to produce inositol 1,4,5-trisphosphate (IP $_3$), and with protein kinase C (PKC) activation by diacylglycerol (DAG) production, initiates Ca $^{2+}$ mobilization. These stimulated events lead to degranulation and release of mediators of the allergic response including histamine. Additionally, cross-linking of FcεRI activates a second Src family kinase Fyn that phosphorylates the adaptor protein Gab2 to activate

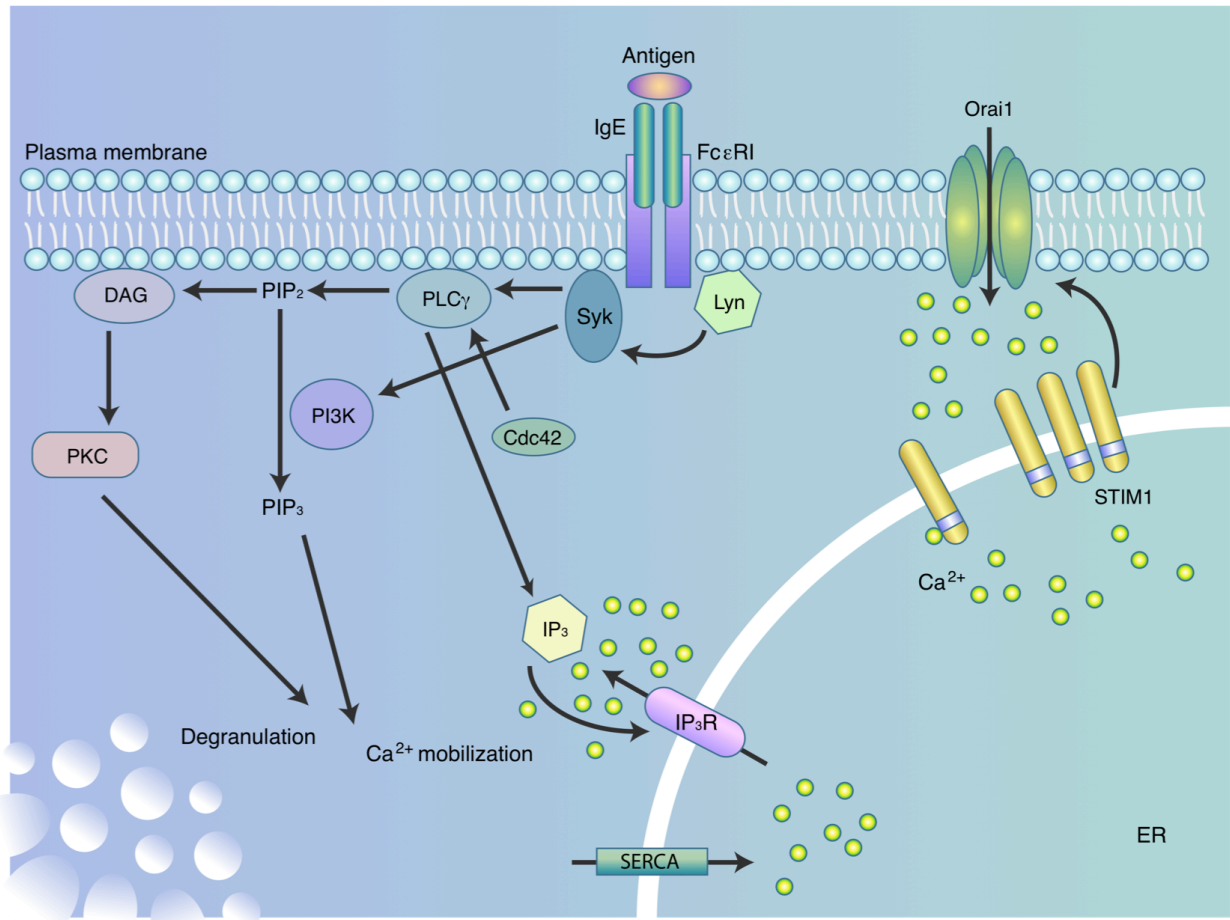


Figure 1.1. FcεRI-mediated signaling pathways in mast cells. A simplified schematic diagram of FcεRI signaling is shown. After antigen stimulation, IgE-FcεRI crosslinking at the cell surface leads to a tyrosine phosphorylation cascade, that results in downstream consequences of mast cell activation, such as Ca²⁺ mobilization and degranulation events.

the phosphatidylinositol-3-OH kinase (PI3K) pathway (57). Defects in FcεRI signaling in a mutant RBL cell line were reconstituted by activated Rho-family GTPases, Cdc42 and Rac, suggesting that activation of Cdc42 and/or Rac is also crucial for FcεRI-mediated signaling that leads to Ca²⁺ mobilization and degranulation (58, 59) (Figure 1.1).

Syk tyrosine kinase in immune cell adhesion

Syk is a 72 kDa non-receptor tyrosine kinase that contains two tandem Src homology 2 (SH2) domains and a kinase domain and is most highly expressed in hematopoietic cells. Syk also has a homolog protein, ZAP70, which is mostly restricted to the expression on T cells and natural killer (NK) cells. Syk has also been implicated in immune cell adhesion through integrin signal transduction (60). Integrins are a family of heterodimeric transmembrane receptors that play a key role in leukocyte adhesion and migration (60). Integrins and classical immunoreceptors were long believed to signal by conceptually different mechanisms, due to their structural and functional differences, but more recent data point otherwise. Syk-deficient neutrophils, monocytes, and macrophages (61-63) have defective integrin-mediated signaling; moreover, Syk is essential for firm leukocyte adhesion to the inflamed endothelium (64). Whether the mechanism underlying Syk activation in these processes is dependent on ITAMs (61, 65, 66) or not (65, 67) is still unresolved. However, it has been proposed that these two

mechanisms of integrin-Syk coupling may cooperatively regulate the activity of Syk (66).

Syk also plays a role for selectin mediated functions in immune cells. Selectins are transmembrane glycoproteins that participate in leukocyte rolling on the endothelium. Syk is involved in signal transduction by P-selectin glycoprotein ligand 1 (PSGL1), the major selectin receptor on leukocytes. Syk is activated by, and associated with PSGL1 in these cells (68, 69), and slow rolling is compromised in Syk-deficient neutrophils (69). These studies show that PSGL1-mediated Syk activation depends on an ITAM-mediated pathway (68, 70), however, one report suggested that Syk is activated via an ITAM-like motif in ezrin, radixin and moesin (ERM) family proteins (68), whereas the other suggested that phosphorylation of the ITAM-bearing adaptors such as DAP12 and FcR γ by the Src family kinase Fgr is involved (70).

Cell motility, migration, and chemotaxis

Cell migration is critical for various biological functions, such as embryogenesis, wound healing, and immune responses, and it can also contribute to the pathogenesis of diseases including cancer and transplant rejection. The basic mechanism of cell motility has been an interest of scientific investigations since the emergence of optical microscopy. Cell motility requires the actin cytoskeleton, asymmetric morphology of

the cell, and polarized intracellular signaling (71, 72). Polarization and development of leading and trailing edges of the cell mediates cell locomotion by dynamic extension and retraction of cellular protrusions, such as pseudopods, filopodia (73), or lamellopodia.

When cells are presented with a gradient of external factors or asymmetric environmental cues, a compass or steering mechanism coupled to basal motility machinery responds and cells undergo directed migration (74, 75). The types of the asymmetric environmental cues often define the kind of directed migration. Cells go through chemotaxis in response to soluble cues, electrotaxis in response to electric fields, durotaxis in response to mechanical signals in the environment, and haptotaxis in response to a gradient of cellular adhesion sites or substrate-bound chemoattractants. During embryogenesis, chemotaxis provides a key mechanism for individual and group cell migration, organ formation, and wiring of the nervous system. In the adult, chemotaxis is crucial for immune cell trafficking and in inflammation, regenerative processes such as wound healing, and maintenance of tissue architecture. Chemotaxis also seems to allow stem cells to target to and persist in their niches (76).

Even though an increasing number of cell types that carry out chemotaxis are being discovered, the signal transduction events mediating directed migration have been most comprehensively studied in *Dictyostelium* and neutrophils (77, 78). Chemotaxis requires the cell to sense the external soluble gradient and orient according

to the source of the signal. The known processes after initial activation by a chemotactic signal include signaling intermediate redistribution, GTPase-regulated actin polymerization (79), and activation of lipid kinases (80), which consequently generate asymmetric pools of phosphoinositides and F-actin that result in stable cell polarization and directionality (81, 82). Intracellular signaling mediated at the leading edge by the Rho family GTPases are involved in regulating directional migration by modulating leading edge formation. One member, GTPase Cdc42, is thought to be a regulator of cell polarity (81, 83). Polarized cells develop a small leading edge consisting of pseudopods, followed by the cell body that contains the nucleus, and a rear, near cylindrical tail termed the uropod. The leading edge is particularly sensitive to receptor engagement, including that by Fc receptors (FcRs), T cell antigen receptors (TCRs) and chemokine receptors (84). The interplay and non-overlapping distribution of PI3K and the lipid phosphatase PTEN (phosphatase and tensin homologue) generates phosphatidylinositol-3,4,5- trisphosphate (PtdIns(3,4,5)P₃, PIP₃) at the leading edge of chemotaxing cells (85). Rac1, a member of Rho family GTPases, may be a critical target of PI3K signaling at the leading edge (86). In neutrophils, phospholipase D (PLD) cooperates with PI3K-mediated signaling to activate Rac1 during chemotaxis (86).

The process that restricts lateral protrusions underlies directional migration. New protrusions are preferentially generated from the pre-existing leading edge, rather than in different locations around the cell (74, 87). Local signaling in a protrusion can direct the formation of new protrusions in response to an external guidance factors (74). Recently, some cells have been shown to migrate using plasma membrane blebbing

without lamellipodia, but the generality of this mechanism is yet unclear (88). Actin polymerization at the leukocyte lamellipodium is controlled in a way similar to what has been described in other cell types, and is locally triggered by signal amplification of the chemoattractant gradient that constitutes the polymerization stimulus. While lamellipodium extension is regulated by both actin polymerization and actomyosin-based contraction, posterior detachment seems to depend on contraction only (89).

Ca²⁺ mobilization and store operated Ca²⁺ entry in immune cells

Ca²⁺ is one of the most well studied second messengers, and is widely used by all eukaryotic cell types, including immune cells. Before stimulation through antigen, resting immune cells maintain a low concentration of Ca²⁺, but activation of immune cells via antigen engagement induces Ca²⁺ influx from the extracellular environment. In electrically non-excitabile cells like immune cells, store-operated Ca²⁺ entry (SOCE) is a major mechanism in Ca²⁺ entry.

The initial signaling events are quite similar in T and B lymphocytes and mast cells. Antigen recognition in these cells commonly triggers the tyrosine phosphorylation of immunoreceptor ITAM motifs and the recruitment and activation of protein tyrosine kinases. Crosslinking of antigen receptors causes phosphorylation and activation of

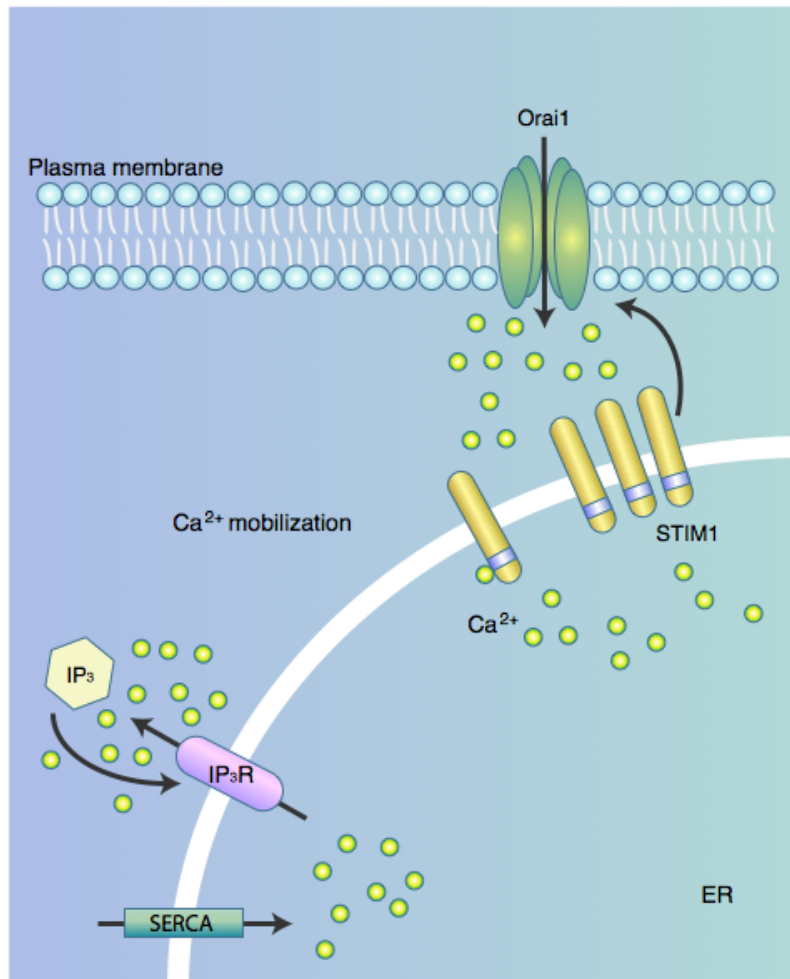


Figure 1.2. Store operated Ca^{2+} entry in mast cells. A simplified schematic diagram is shown. IP_3 produced by $\text{PLC}\gamma$ in response to $\text{Fc}\epsilon\text{RI}$ aggregation binds to IP_3 receptors in the ER membrane, causing the release of Ca^{2+} from these stores. Depletion of ER Ca^{2+} stores triggers the oligomerization of STIM1 and subsequent concentration at the ER-plasma membrane junctions causing Orai1 channels to open and mediate Ca^{2+} entry.

phospholipase C (PLC), and activated PLC generates inositol-1,4,5-trisphosphate (Ins(1,4,5)P₃) and diacylglycerol (DAG) by breaking down phosphatidylinositol-4,5-bisphosphate (PIP₂). IP₃ in turn binds to its receptor on the surface of internal Ca²⁺ stores, typically the endoplasmic reticulum (ER), and initiates the release of Ca²⁺ into the cytoplasm. This event is known as 'store depletion', and it triggers store-operated Ca²⁺ (SOC) channels in the plasma membrane to bring in more Ca²⁺ (Figure 1.2). Ca²⁺ release-activated Ca²⁺ (CRAC) channels are the most well characterized SOC channels in immune cells (90). CRAC channels are highly Ca²⁺ selective, have a very low conductance, and show inwardly rectifying current-voltage relationship.

The molecular compositions of CRAC signaling complex was identified less than a decade ago, when high-throughput, genome-wide screening of RNA-mediated interference (RNAi) began to be widely used as a method for unbiased discovery of proteins in biological pathways. Orai1 (also called Ca²⁺ release-activated Ca²⁺ modulator 1, CRACM1) has been identified as a pore-forming subunit of CRAC channels, and stromal interaction molecule 1 (STIM1) as the ER resident Ca²⁺ sensor (91-95). Orai1 has two homolog proteins, Orai2 and Orai3, while STIM1 has one homolog, STIM2, in mice and humans.

The canonical transient receptor potential (TRPC) family of protein channels have also been described to trigger elevation of intracellular Ca²⁺ either directly via coupled plasma membrane receptor stimulation, or possibly through store depletion

(96-98). TRPC channels have seven homologs in mammalian cells (TRPC1 – TRPC7). Direct involvement of TRPC proteins in SOCE is somewhat controversial, with no conclusive reports of TRPC store-operated Ca^{2+} currents in lymphocytes.

Orai (CRACM) The Orai1 monomer is a small protein of ~33 kDa with four transmembrane domains and amino and carboxyl ends that face the cytosol (93-95). Glycosylation increases its molecular weight on SDS gels (99, 100). Orai1 assembles as a tetrameric CRAC channel (101-103), and this channel opens in response to the signal communicated by STIM1. Orai1 can also form heteropolymers with Orai2 and Orai3, and possibly with some TRPC channel subunits (104, 105).

STIM STIM1 is a ~77 kDa single transmembrane protein that is mainly localized in the ER and in some reports at the plasma membrane. STIM1 was originally thought to be a secreted or plasma membrane protein of bone marrow stromal cells, giving rise to the name stromal interaction molecule (106). STIM1 predominantly resides in the ER (91, 92, 107, 108) and it is believed that ER-resident STIM1, not plasma membrane localized STIM1, regulates CRAC channel opening (91, 107, 109-111). STIM1 has an ER-luminal portion of ~22 kDa after cleavage of its signal sequence, with a single transmembrane sequence, and a ~51 kDa cytoplasmic region. ER-resident STIM1 carries out two basic functions in the CRAC signaling pathway: it senses ER store depletion and repletion, and it communicate the level of Ca^{2+} in the stores to the Ca^{2+} channels residing in the plasma membrane.

Orai1-STIM1 communications It has been proposed that STIM1 senses the depletion of Ca^{2+} stores via its amino-terminal Ca^{2+} -binding EF hand domain. Dissociation of Ca^{2+} from its binding site triggers a structural change in STIM1. STIM1 is localized throughout the ER membrane prior to store depletion, and store depletion induces the formation of oligomers of STIM1 in the ER through the EF-SAM region and ensuing translocation to discrete 'puncta' at ER-plasma membrane junctions (112, 113). The interactions that retain STIM1 at ER-plasma membrane junctions are not fully understood. One interaction maps to the short polybasic sequence at the carboxyl terminus of STIM1 (113-115), and involvement of this polybasic sequence has led to the hypothesis that STIM1 is recruited by negatively charged phospholipids such as PIP_2 and PIP_3 (113). A key upstream signaling mechanism for puncta formation is oligomerization of the STIM1 luminal domain, but how this oligomerization occurring in the ER lumen results in STIM1 relocation to the ER-plasma membrane junctions is less clear. STIM1 redistribution in cells shows prominent cooperativity with respect to ER-luminal Ca^{2+} concentration (116, 117). Since each STIM1 monomer has a single Ca^{2+} binding site, the cooperativity suggests that oligomeric STIM1 is involved in at least one step of redistribution. However, reported data do not discriminate between whether the oligomer is stable or transitory. Physiological stimuli can elicit significant Ca^{2+} entry without the presence of large puncta. For example, mast cells stimulated by crosslinking of IgE-Fc ϵ RI by antigen do not exhibit prominent puncta and only limited average proximity of STIM1 and Orai1 (118). Also in stimulated HEK293 cells, detectable STIM1

redistribution is modest or absent (119), even though these conditions are sufficient to elicit robust STIM1-Orai1 dependent elevation of Ca^{2+} or Ca^{2+} oscillations (118-120).

Orai1 is localized throughout the plasma membrane before store depletion. After store depletion, STIM1 relocation to puncta leads to the recruitment of Orai1 to the puncta, activating CRAC channels. Recruitment of Orai1 depends on its carboxyl terminus cytoplasmic tail (121, 122), and the basis for recruitment is thought to be a direct protein-protein interaction between Orai1 carboxyl terminus with STIM1 (114, 121, 123). Calloway et al. showed that a positively charged sequence of STIM1 in its CRAC channel activating domain (CAD) is necessary for SOCE activation, and this sequence directly interacts with an acidic coiled-coil of Orai1 in its C-terminal segment to gate Ca^{2+} influx, and gating Ca^{2+} depends on electrostatic interaction between Orai1 and STIM1 (118, 124).

Ca^{2+} mobilization and cell motility

Local changes in the intracellular Ca^{2+} concentration modulate directionally persistent cell migration in many cell types. Transient, spatially localized increases of intracellular Ca^{2+} guide neuronal growth cone migration during chemotaxis and haptotaxis (125, 126), and local Ca^{2+} influx can activate Cdc42 and Rac1 while inactivating RhoA to regulate growth cone motility (127). TRPM7 Ca^{2+} channels open

and induce local bursts of intracellular Ca^{2+} , termed 'Ca²⁺ flickers' at the leading edge in migrating fibroblasts undergoing chemokinesis. Symmetric addition of PDGF not only increases random migration of fibroblast but also increases number and amplitude of the Ca²⁺ flickers, and TRPM7 inhibition blocks chemotaxis of fibroblast toward PDGF (128). TRPC5 and TRPC6 channels play antagonistic roles in regulating fibroblast and kidney podocyte motility. Whereas TRPC5-mediated Ca²⁺ influx activates Rac1 to promote cell migration, TRPC6-mediated Ca²⁺ influx increases RhoA activity and inhibits cell migration (129). The downstream target of Ca²⁺ in fibroblast directional migration is yet unknown.

For immune cells, the role of Ca²⁺ in leukocyte migration is still not entirely clear. Polymorphonuclear leukocytes (PMNs) orient correctly across the chemoattractant gradient without extracellular Ca²⁺ (130, 131), and they migrate faster under these conditions (130). On the other hand, extracellular Ca²⁺ depletion causes leukocyte migration to slow and eventually stop (132-134), and buffering intracellular Ca²⁺ slows migration (135, 136). For mast cells, buffering of intracellular Ca²⁺ also causes a decrease in mast cell migration toward antigen (137, 138). To generate sustained signals necessary for cell activation efficiently, motile T cells must stop after they encounter APCs presenting specific antigen/MHC complexes. Intracellular Ca²⁺ rises after T cells interact with APCs *in vitro*, and consequently T cells round up and stop crawling. Ca²⁺ is sufficient to induce these processes, as ionomycin and thapsigargin show similar effects on T cell motility independent of the T cell receptor (TCR) (139, 140).

Furthermore, high K^+ and BAPTA/AM loading to inhibit elevation of intracellular Ca^{2+} reversibly blocks the immobilization of T cells (140). In contrast, Ca^{2+} is less effective at stopping naïve T cells interacting with APC, as naïve T cells still extend and retract lamellopodia after increases in intracellular Ca^{2+} (141). A Ca^{2+} -independent stop signal has been reported (142), suggesting that multiple signals may be involved in regulating naïve T cell motility.

More recently, a role for Orai1 and STIM1 in cell motility and migration has begun to emerge. Orai1 and STIM1 are essential in regulating breast tumor cell migration, and metastasis in mice (143). Orai1 regulates neutrophil arrest and polarization during recruitment (144), and Orai1 and STIM1 also play essential roles in PDGF-induced smooth muscle cell migration (145, 146). In intestinal epithelial cells, STIM1 redistribution to the plasma membrane enhances TRPC1 mediated Ca^{2+} signaling and cell migration after wounding (147).

Current studies

Trafficking of immune cells is pivotal for the immune system to carry out its functions. Evidence published more than a decade ago showed that mucosal mast cells must redistribute inside the tissue site, from the lamina propria to the jejunal villi of the gut, in response to parasite infection. This response requires mast cell motility and

likely driven by a chemotactic response, but very little has been characterized regarding the molecular mechanisms of mast cell motility or directed migration. RBL-2H3 mast cells and bone marrow- derived mast cells from the rat both have similar biochemical and functional characteristics of mucosal mast cells *in vivo* (148, 149). This dissertation examines the basal motility and chemotaxis of these mast cells, providing new insights into how immune cell migration is regulated.

In Chapter 2, we characterize the basal motility and chemotaxis of mast cells. Using real-time imaging, we demonstrate that RBL-2H3 cells and rat BMMCs show spontaneous motility on glass surfaces, and that these cells show chemotaxis toward antigen. This spontaneous motility of mast cells depends on actin polymerization, Rho family GTPases, and PI3K activity. We further show that Ca^{2+} influx and Syk tyrosine kinase play important roles in regulating both mast cell basal motility and chemotaxis toward antigen, and the Ca^{2+} influx channel protein Orail participates in these processes. Furthermore, we observe previously uncharacterized Ca^{2+} transients in non-stimulatory conditions in these cells. Ca^{2+} influx contributes to these Ca^{2+} transients with properties that correlate with its role in cell motility, suggesting a potential relationship between localized Ca^{2+} transients and mast cell motility.

Chapter 3 investigates the dynamic interactions between mast cells and intestinal epithelia *in vitro* and *in situ*. RBL mast cells show intimate interactions with the intestinal epithelial cell line SLC-44, and they exhibit transepithelial migration when

they are introduced from either apical or basolateral side of these polarized epithelial cells. In addition, transepithelial protrusions can be observed when rat BMMCs are introduced from the basolateral side and allowed to migrate overnight. Using multiphoton microscopy, transferred RBL-2H3 mast cells are detected in the interaepithelial region of the jejunal villi in the rat small intestine after *T. spiralis* infection *in situ*, further suggesting unique and dynamic interactions between mucosal mast cells and intestinal epithelia.

REFERENCES

1. Sicherer SH, Sampson HA. 2007. Peanut allergy: emerging concepts and approaches for an apparent epidemic. *J Allergy Clin Immunol* 120: 491-503
2. Holgate ST, Polosa R. 2008. Treatment strategies for allergy and asthma. *Nat Rev Immunol* 8: 218-30
3. Ehrlich P. 1877. Beitrage zur Kenntnis der Anilinfärbungen und ihrer Verwendung in der mikroskopischen Technik. *Arch. mikr. Anat.* 13: 263-77
4. Metcalfe DD, Baram D, Mekori YA. 1997. Mast cells. *Physiol Rev* 77: 1033-79
5. Abraham SN, St John AL. 2010. Mast cell-orchestrated immunity to pathogens. *Nat Rev Immunol* 10: 440-52
6. Beaven MA. 2009. Our perception of the mast cell from Paul Ehrlich to now. *Eur J Immunol* 39: 11-25
7. Brown JM, Wilson TM, Metcalfe DD. 2008. The mast cell and allergic diseases: role in pathogenesis and implications for therapy. *Clin Exp Allergy* 38: 4-18
8. Anderson DM, Lyman SD, Baird A, Wignall JM, Eisenman J, Rauch C, March CJ, Boswell HS, Gimpel SD, Cosman D, et al. 1990. Molecular cloning of mast cell growth factor, a hematopoietin that is active in both membrane bound and soluble forms. *Cell* 63: 235-43
9. Galli SJ. 2000. Mast cells and basophils. *Curr Opin Hematol* 7: 32-9
10. Abraham SN, Malaviya R. 1997. Mast cells in infection and immunity. *Infect Immun* 65: 3501-8
11. Enerback L. 1966. Mast cells in rat gastrointestinal mucosa. 2. Dye-binding and metachromatic properties. *Acta Pathol Microbiol Scand* 66: 303-12

12. Enerback L, Lundin PM. 1974. Ultrastructure of mucosal mast cells in normal and compound 48-80-treated rats. *Cell Tissue Res* 150: 95-105
13. Bienenstock J, Befus AD, Denburg J, Goodacre R, Pearce F, Shanahan F. 1983. Mast cell heterogeneity. *Monogr Allergy* 18: 124-8
14. Enerback L. 1997. The differentiation and maturation of inflammatory cells involved in the allergic response: mast cells and basophils. *Allergy* 52: 4-10
15. Miller HR, Pemberton AD. 2002. Tissue-specific expression of mast cell granule serine proteinases and their role in inflammation in the lung and gut. *Immunology* 105: 375-90
16. Groschwitz KR, Ahrens R, Osterfeld H, Gurish MF, Han X, Abrink M, Finkelman FD, Pejler G, Hogan SP. 2009. Mast cells regulate homeostatic intestinal epithelial migration and barrier function by a chymase/Mcpt4-dependent mechanism. *Proc Natl Acad Sci U S A* 106: 22381-6
17. McDermott JR, Bartram RE, Knight PA, Miller HR, Garrod DR, Grecnis RK. 2003. Mast cells disrupt epithelial barrier function during enteric nematode infection. *Proc Natl Acad Sci U S A* 100: 7761-6
18. Nakano T, Sonoda T, Hayashi C, Yamatodani A, Kanayama Y, Yamamura T, Asai H, Yonezawa T, Kitamura Y, Galli SJ. 1985. Fate of bone marrow-derived cultured mast cells after intracutaneous, intraperitoneal, and intravenous transfer into genetically mast cell-deficient W/W^v mice. Evidence that cultured mast cells can give rise to both connective tissue type and mucosal mast cells. *J Exp Med* 162: 1025-43
19. Razin E, Ihle JN, Seldin D, Mencia-Huerta JM, Katz HR, LeBlanc PA, Hein A, Caulfield JP, Austen KF, Stevens RL. 1984. Interleukin 3: A differentiation and growth factor for the mouse mast cell that contains chondroitin sulfate E proteoglycan. *J Immunol* 132: 1479-86
20. Tsai M, Takeishi T, Thompson H, Langley KE, Zsebo KM, Metcalfe DD, Geissler EN, Galli SJ. 1991. Induction of mast cell proliferation, maturation, and heparin synthesis by the rat c-kit ligand, stem cell factor. *Proc Natl Acad Sci U S A* 88: 6382-6

21. Okayama Y, Kawakami T. 2006. Development, migration, and survival of mast cells. *Immunol Res* 34: 97-115
22. Welle M. 1997. Development, significance, and heterogeneity of mast cells with particular regard to the mast cell-specific proteases chymase and tryptase. *J Leukoc Biol* 61: 233-45
23. Huang C, Friend DS, Qiu WT, Wong GW, Morales G, Hunt J, Stevens RL. 1998. Induction of a selective and persistent extravasation of neutrophils into the peritoneal cavity by tryptase mouse mast cell protease 6. *J Immunol* 160: 1910-9
24. Boyce JA. 2007. Mast cells and eicosanoid mediators: a system of reciprocal paracrine and autocrine regulation. *Immunol Rev* 217: 168-85
25. Orinska Z, Bulanova E, Budagian V, Metz M, Maurer M, Bulfone-Paus S. 2005. TLR3-induced activation of mast cells modulates CD8+ T-cell recruitment. *Blood* 106: 978-87
26. Ketavarapu JM, Rodriguez AR, Yu JJ, Cong Y, Murthy AK, Forsthuber TG, Guentzel MN, Klose KE, Berton MT, Arulanandam BP. 2008. Mast cells inhibit intramacrophage Francisella tularensis replication via contact and secreted products including IL-4. *Proc Natl Acad Sci U S A* 105: 9313-8
27. Bischoff SC. 2009. Physiological and pathophysiological functions of intestinal mast cells. *Semin Immunopathol* 31: 185-205
28. Funk CD. 2001. Prostaglandins and leukotrienes: advances in eicosanoid biology. *Science* 294: 1871-5
29. Shelburne CP, Nakano H, St John AL, Chan C, McLachlan JB, Gunn MD, Staats HF, Abraham SN. 2009. Mast cells augment adaptive immunity by orchestrating dendritic cell trafficking through infected tissues. *Cell Host Microbe* 6: 331-42
30. Boesiger J, Tsai M, Maurer M, Yamaguchi M, Brown LF, Claffey KP, Dvorak HF, Galli SJ. 1998. Mast cells can secrete vascular permeability factor/ vascular endothelial cell growth factor and exhibit enhanced release after immunoglobulin E-dependent upregulation of fc epsilon receptor I expression. *J Exp Med* 188: 1135-45

31. Galli SJ, Nakae S, Tsai M. 2005. Mast cells in the development of adaptive immune responses. *Nat Immunol* 6: 135-42
32. Woodbury RG, Miller HR, Huntley JF, Newlands GF, Palliser AC, Wakelin D. 1984. Mucosal mast cells are functionally active during spontaneous expulsion of intestinal nematode infections in rat. *Nature* 312: 450-2
33. Nawa Y, Kiyota M, Korenaga M, Kotani M. 1985. Defective protective capacity of W/W^v mice against *Strongyloides ratti* infection and its reconstitution with bone marrow cells. *Parasite Immunol* 7: 429-38
34. Wei OL, Hilliard A, Kalman D, Sherman M. 2005. Mast cells limit systemic bacterial dissemination but not colitis in response to *Citrobacter rodentium*. *Infect Immun* 73: 1978-85
35. Ohnmacht C, Voehringer D. 2010. Basophils protect against reinfection with hookworms independently of mast cells and memory Th2 cells. *J Immunol* 184: 344-50
36. Maurer M, Lopez Kostka S, Siebenhaar F, Moelle K, Metz M, Knop J, von Stebut E. 2006. Skin mast cells control T cell-dependent host defense in *Leishmania* major infections. *FASEB J* 20: 2460-7
37. Finkelman FD, Shea-Donohue T, Morris SC, Gildea L, Strait R, Madden KB, Schopf L, Urban JF, Jr. 2004. Interleukin-4- and interleukin-13-mediated host protection against intestinal nematode parasites. *Immunol Rev* 201: 139-55
38. Anthony RM, Rutitzky LI, Urban JF, Jr., Stadecker MJ, Gause WC. 2007. Protective immune mechanisms in helminth infection. *Nat Rev Immunol* 7: 975-87
39. Allen JE, Maizels RM. 2011. Diversity and dialogue in immunity to helminths. *Nat Rev Immunol* 11: 375-88
40. Gurish MF, Bryce PJ, Tao H, Kisselgof AB, Thornton EM, Miller HR, Friend DS, Oettgen HC. 2004. IgE enhances parasite clearance and regulates mast cell responses in mice infected with *Trichinella spiralis*. *J Immunol* 172: 1139-45

41. Knight PA, Wright SH, Lawrence CE, Paterson YY, Miller HR. 2000. Delayed expulsion of the nematode *Trichinella spiralis* in mice lacking the mucosal mast cell-specific granule chymase, mouse mast cell protease-1. *J Exp Med* 192: 1849-56
42. Newlands GF, Coulson PS, Wilson RA. 1995. Stem cell factor dependent hyperplasia of mucosal-type mast cells but not eosinophils in *Schistosoma mansoni*-infected rats. *Parasite Immunol* 17: 595-8
43. Asai K, Kitaura J, Kawakami Y, Yamagata N, Tsai M, Carbone DP, Liu FT, Galli SJ, Kawakami T. 2001. Regulation of mast cell survival by IgE. *Immunity* 14: 791-800
44. Sasaki Y, Yoshimoto T, Maruyama H, Tegoshi T, Ohta N, Arizono N, Nakanishi K. 2005. IL-18 with IL-2 protects against *Strongyloides venezuelensis* infection by activating mucosal mast cell-dependent type 2 innate immunity. *J Exp Med* 202: 607-16
45. Alizadeh H, Wakelin D. 1982. Comparison of rapid expulsion of *Trichinella spiralis* in mice and rats. *Int J Parasitol* 12: 65-73
46. Tuohy M, Lammas DA, Wakelin D, Huntley JF, Newlands GF, Miller HR. 1990. Functional correlations between mucosal mast cell activity and immunity to *Trichinella spiralis* in high and low responder mice. *Parasite Immunol* 12: 675-85
47. Blum LK, Thrasher SM, Gagliardo LF, Fabre V, Appleton JA. 2009. Expulsion of secondary *Trichinella spiralis* infection in rats occurs independently of mucosal mast cell release of mast cell protease II. *J Immunol* 183: 5816-22
48. Friend DS, Ghildyal N, Austen KF, Gurish MF, Matsumoto R, Stevens RL. 1996. Mast cells that reside at different locations in the jejunum of mice infected with *Trichinella spiralis* exhibit sequential changes in their granule ultrastructure and chymase phenotype. *J Cell Biol* 135: 279-90
49. Gould HJ, Sutton BJ. 2008. IgE in allergy and asthma today. *Nat Rev Immunol* 8: 205-17
50. Metzger H, Alcaraz G, Hohman R, Kinet JP, Pribluda V, Quarto R. 1986. The receptor with high affinity for immunoglobulin E. *Annu Rev Immunol* 4: 419-70

51. Siraganian RP, Metzger H. 1978. Evidence that the "mouse mastocytoma" cell line (MCT-1) is of rat origin. *J Immunol* 121: 2584-5
52. Kinet JP. 1999. The high-affinity IgE receptor (Fc epsilon RI): from physiology to pathology. *Annu Rev Immunol* 17: 931-72
53. Young RM, Holowka D, Baird B. 2003. A lipid raft environment enhances Lyn kinase activity by protecting the active site tyrosine from dephosphorylation. *J Biol Chem* 278: 20746-52
54. Field KA, Holowka D, Baird B. 1997. Compartmentalized activation of the high affinity immunoglobulin E receptor within membrane domains. *J Biol Chem* 272: 4276-80
55. Rivera J, Gilfillan AM. 2006. Molecular regulation of mast cell activation. *J Allergy Clin Immunol* 117: 1214-25; quiz 26
56. Turner H, Kinet JP. 1999. Signalling through the high-affinity IgE receptor Fc epsilon RI. *Nature* 402: B24-30
57. Parravicini V, Gadina M, Kovarova M, Odom S, Gonzalez-Espinosa C, Furumoto Y, Saitoh S, Samelson LE, O'Shea JJ, Rivera J. 2002. Fyn kinase initiates complementary signals required for IgE-dependent mast cell degranulation. *Nat Immunol* 3: 741-8
58. Field KA, Apgar JR, Hong-Geller E, Siraganian RP, Baird B, Holowka D. 2000. Mutant RBL mast cells defective in Fc epsilon RI signaling and lipid raft biosynthesis are reconstituted by activated Rho-family GTPases. *Mol Biol Cell* 11: 3661-73
59. Hong-Geller E, Holowka D, Siraganian RP, Baird B, Cerione RA. 2001. Activated Cdc42/Rac reconstitutes Fc epsilon RI-mediated Ca²⁺ mobilization and degranulation in mutant RBL mast cells. *Proc Natl Acad Sci U S A* 98: 1154-9
60. Mocsai A, Ruland J, Tybulewicz VL. 2010. The SYK tyrosine kinase: a crucial player in diverse biological functions. *Nat Rev Immunol* 10: 387-402

61. Mocsai A, Abram CL, Jakus Z, Hu Y, Lanier LL, Lowell CA. 2006. Integrin signaling in neutrophils and macrophages uses adaptors containing immunoreceptor tyrosine-based activation motifs. *Nat Immunol* 7: 1326-33
62. Mocsai A, Zhou M, Meng F, Tybulewicz VL, Lowell CA. 2002. Syk is required for integrin signaling in neutrophils. *Immunity* 16: 547-58
63. Vines CM, Potter JW, Xu Y, Geahlen RL, Costello PS, Tybulewicz VL, Lowell CA, Chang PW, Gresham HD, Willman CL. 2001. Inhibition of beta 2 integrin receptor and Syk kinase signaling in monocytes by the Src family kinase Fgr. *Immunity* 15: 507-19
64. Frommhold D, Mannigel I, Schymeinsky J, Mocsai A, Poeschl J, Walzog B, Sperandio M. 2007. Spleen tyrosine kinase Syk is critical for sustained leukocyte adhesion during inflammation in vivo. *BMC Immunol* 8: 31
65. Abtahian F, Bezman N, Clemens R, Sebzda E, Cheng L, Shattil SJ, Kahn ML, Koretzky GA. 2006. Evidence for the requirement of ITAM domains but not SLP-76/Gads interaction for integrin signaling in hematopoietic cells. *Mol Cell Biol* 26: 6936-49
66. Zou W, Kitaura H, Reeve J, Long F, Tybulewicz VL, Shattil SJ, Ginsberg MH, Ross FP, Teitelbaum SL. 2007. Syk, c-Src, the alphavbeta3 integrin, and ITAM immunoreceptors, in concert, regulate osteoclastic bone resorption. *J Cell Biol* 176: 877-88
67. Gao J, Zoller KE, Ginsberg MH, Brugge JS, Shattil SJ. 1997. Regulation of the pp72syk protein tyrosine kinase by platelet integrin alpha IIb beta 3. *EMBO J* 16: 6414-25
68. Urzainqui A, Serrador JM, Viedma F, Yanez-Mo M, Rodriguez A, Corbi AL, Alonso-Lebrero JL, Luque A, Deckert M, Vazquez J, Sanchez-Madrid F. 2002. ITAM-based interaction of ERM proteins with Syk mediates signaling by the leukocyte adhesion receptor PSGL-1. *Immunity* 17: 401-12
69. Zarbock A, Lowell CA, Ley K. 2007. Spleen tyrosine kinase Syk is necessary for E-selectin-induced alpha(L)beta(2) integrin-mediated rolling on intercellular adhesion molecule-1. *Immunity* 26: 773-83

70. Zarbock A, Abram CL, Hundt M, Altman A, Lowell CA, Ley K. 2008. PSGL-1 engagement by E-selectin signals through Src kinase Fgr and ITAM adapters DAP12 and FcR gamma to induce slow leukocyte rolling. *J Exp Med* 205: 2339-47
71. Petrie RJ, Doyle AD, Yamada KM. 2009. Random versus directionally persistent cell migration. *Nat Rev Mol Cell Biol* 10: 538-49
72. Mitchison TJ, Cramer LP. 1996. Actin-based cell motility and cell locomotion. *Cell* 84: 371-9
73. Gupton SL, Gertler FB. 2007. Filopodia: the fingers that do the walking. *Sci STKE* 2007: re5
74. Arrieumerlou C, Meyer T. 2005. A local coupling model and compass parameter for eukaryotic chemotaxis. *Dev Cell* 8: 215-27
75. Bourne HR, Weiner O. 2002. A chemical compass. *Nature* 419: 21
76. Swaney KF, Huang CH, Devreotes PN. 2010. Eukaryotic chemotaxis: a network of signaling pathways controls motility, directional sensing, and polarity. *Annu Rev Biophys* 39: 265-89
77. Schneider IC, Haugh JM. 2006. Mechanisms of gradient sensing and chemotaxis: conserved pathways, diverse regulation. *Cell Cycle* 5: 1130-4
78. Stephens L, Milne L, Hawkins P. 2008. Moving towards a better understanding of chemotaxis. *Curr Biol* 18: R485-94
79. Haddad E, Zugaza JL, Louache F, Debili N, Crouin C, Schwarz K, Fischer A, Vainchenker W, Bertoglio J. 2001. The interaction between Cdc42 and WASP is required for SDF-1-induced T-lymphocyte chemotaxis. *Blood* 97: 33-8
80. Vicente-Manzanares M, Rey M, Jones DR, Sancho D, Mellado M, Rodriguez-Frade JM, del Pozo MA, Yanez-Mo M, de Ana AM, Martinez AC, Merida I, Sanchez-Madrid F. 1999. Involvement of phosphatidylinositol 3-kinase in stromal cell-derived factor-1 alpha-induced lymphocyte polarization and chemotaxis. *J Immunol* 163: 4001-12

81. Allen WE, Zicha D, Ridley AJ, Jones GE. 1998. A role for Cdc42 in macrophage chemotaxis. *J Cell Biol* 141: 1147-57
82. Hannigan M, Zhan L, Li Z, Ai Y, Wu D, Huang CK. 2002. Neutrophils lacking phosphoinositide 3-kinase gamma show loss of directionality during N-formyl-Met-Leu-Phe-induced chemotaxis. *Proc Natl Acad Sci U S A* 99: 3603-8
83. Etienne-Manneville S. 2004. Cdc42--the centre of polarity. *J Cell Sci* 117: 1291-300
84. Friedl P, Weigelin B. 2008. Interstitial leukocyte migration and immune function. *Nat Immunol* 9: 960-9
85. Kolsch V, Charest PG, Firtel RA. 2008. The regulation of cell motility and chemotaxis by phospholipid signaling. *J Cell Sci* 121: 551-9
86. Nishikimi A, Fukuhara H, Su W, Hongu T, Takasuga S, Mihara H, Cao Q, Sanematsu F, Kanai M, Hasegawa H, Tanaka Y, Shibasaki M, Kanaho Y, Sasaki T, Frohman MA, Fukui Y. 2009. Sequential regulation of DOCK2 dynamics by two phospholipids during neutrophil chemotaxis. *Science* 324: 384-7
87. Andrew N, Insall RH. 2007. Chemotaxis in shallow gradients is mediated independently of PtdIns 3-kinase by biased choices between random protrusions. *Nat Cell Biol* 9: 193-200
88. Fackler OT, Grosse R. 2008. Cell motility through plasma membrane blebbing. *J Cell Biol* 181: 879-84
89. Meininger CJ, Yano H, Rottapel R, Bernstein A, Zsebo KM, Zetter BR. 1992. The c-kit receptor ligand functions as a mast cell chemoattractant. *Blood* 79: 958-63
90. Parekh AB, Putney JW, Jr. 2005. Store-operated calcium channels. *Physiol Rev* 85: 757-810
91. Liou J, Kim ML, Heo WD, Jones JT, Myers JW, Ferrell JE, Jr., Meyer T. 2005. STIM is a Ca²⁺ sensor essential for Ca²⁺-store-depletion-triggered Ca²⁺ influx. *Curr Biol* 15: 1235-41

92. Zhang SL, Yu Y, Roos J, Kozak JA, Deerinck TJ, Ellisman MH, Stauderman KA, Cahalan MD. 2005. STIM1 is a Ca²⁺ sensor that activates CRAC channels and migrates from the Ca²⁺ store to the plasma membrane. *Nature* 437: 902-5
93. Vig M, Peinelt C, Beck A, Koomoa DL, Rabah D, Koblan-Huberson M, Kraft S, Turner H, Fleig A, Penner R, Kinet JP. 2006. CRACM1 is a plasma membrane protein essential for store-operated Ca²⁺ entry. *Science* 312: 1220-3
94. Feske S, Gwack Y, Prakriya M, Srikanth S, Puppel SH, Tanasa B, Hogan PG, Lewis RS, Daly M, Rao A. 2006. A mutation in Orai1 causes immune deficiency by abrogating CRAC channel function. *Nature* 441: 179-85
95. Zhang SL, Yeromin AV, Zhang XH, Yu Y, Safrina O, Penna A, Roos J, Stauderman KA, Cahalan MD. 2006. Genome-wide RNAi screen of Ca(2+) influx identifies genes that regulate Ca(2+) release-activated Ca(2+) channel activity. *Proc Natl Acad Sci U S A* 103: 9357-62
96. Philipp S, Strauss B, Hirnet D, Wissenbach U, Mery L, Flockerzi V, Hoth M. 2003. TRPC3 mediates T-cell receptor-dependent calcium entry in human T-lymphocytes. *J Biol Chem* 278: 26629-38
97. Venkatachalam K, Ma HT, Ford DL, Gill DL. 2001. Expression of functional receptor-coupled TRPC3 channels in DT40 triple receptor InsP3 knockout cells. *J Biol Chem* 276: 33980-5
98. Putney JW, Jr. 2005. Capacitative calcium entry: sensing the calcium stores. *J Cell Biol* 169: 381-2
99. Prakriya M, Feske S, Gwack Y, Srikanth S, Rao A, Hogan PG. 2006. Orai1 is an essential pore subunit of the CRAC channel. *Nature* 443: 230-3
100. Gwack Y, Srikanth S, Feske S, Cruz-Guilloty F, Oh-hora M, Neems DS, Hogan PG, Rao A. 2007. Biochemical and functional characterization of Orai proteins. *J Biol Chem* 282: 16232-43
101. Mignen O, Thompson JL, Shuttleworth TJ. 2007. STIM1 regulates Ca²⁺ entry via arachidonate-regulated Ca²⁺-selective (ARC) channels without store depletion or translocation to the plasma membrane. *J Physiol* 579: 703-15

102. Lefkimmiatis K, Srikanthan M, Maiellaro I, Moyer MP, Curci S, Hofer AM. 2009. Store-operated cyclic AMP signalling mediated by STIM1. *Nat Cell Biol* 11: 433-42
103. Mignen O, Thompson JL, Shuttleworth TJ. 2008. Orai1 subunit stoichiometry of the mammalian CRAC channel pore. *J Physiol* 586: 419-25
104. Lis A, Peinelt C, Beck A, Parvez S, Monteilh-Zoller M, Fleig A, Penner R. 2007. CRACM1, CRACM2, and CRACM3 are store-operated Ca²⁺ channels with distinct functional properties. *Curr Biol* 17: 794-800
105. Ong HL, Cheng KT, Liu X, Bandyopadhyay BC, Paria BC, Soboloff J, Pani B, Gwack Y, Srikanth S, Singh BB, Gill DL, Ambudkar IS. 2007. Dynamic assembly of TRPC1-STIM1-Orai1 ternary complex is involved in store-operated calcium influx. Evidence for similarities in store-operated and calcium release-activated calcium channel components. *J Biol Chem* 282: 9105-16
106. Oritani K, Kincade PW. 1996. Identification of stromal cell products that interact with pre-B cells. *J Cell Biol* 134: 771-82
107. Wu MM, Buchanan J, Luik RM, Lewis RS. 2006. Ca²⁺ store depletion causes STIM1 to accumulate in ER regions closely associated with the plasma membrane. *J Cell Biol* 174: 803-13
108. Luik RM, Wu MM, Buchanan J, Lewis RS. 2006. The elementary unit of store-operated Ca²⁺ entry: local activation of CRAC channels by STIM1 at ER-plasma membrane junctions. *J Cell Biol* 174: 815-25
109. Mercer JC, Dehaven WI, Smyth JT, Wedel B, Boyles RR, Bird GS, Putney JW, Jr. 2006. Large store-operated calcium selective currents due to co-expression of Orai1 or Orai2 with the intracellular calcium sensor, Stim1. *J Biol Chem* 281: 24979-90
110. Xu P, Lu J, Li Z, Yu X, Chen L, Xu T. 2006. Aggregation of STIM1 underneath the plasma membrane induces clustering of Orai1. *Biochem Biophys Res Commun* 350: 969-76
111. Baba Y, Hayashi K, Fujii Y, Mizushima A, Watarai H, Wakamori M, Numaga T, Mori Y, Iino M, Hikida M, Kurosaki T. 2006. Coupling of STIM1 to store-

- operated Ca²⁺ entry through its constitutive and inducible movement in the endoplasmic reticulum. *Proc Natl Acad Sci U S A* 103: 16704-9
112. Stathopoulos PB, Li GY, Plevin MJ, Ames JB, Ikura M. 2006. Stored Ca²⁺ depletion-induced oligomerization of stromal interaction molecule 1 (STIM1) via the EF-SAM region: An initiation mechanism for capacitive Ca²⁺ entry. *J Biol Chem* 281: 35855-62
 113. Liou J, Fivaz M, Inoue T, Meyer T. 2007. Live-cell imaging reveals sequential oligomerization and local plasma membrane targeting of stromal interaction molecule 1 after Ca²⁺ store depletion. *Proc Natl Acad Sci U S A* 104: 9301-6
 114. Park CY, Hoover PJ, Mullins FM, Bachhawat P, Covington ED, Raunser S, Walz T, Garcia KC, Dolmetsch RE, Lewis RS. 2009. STIM1 clusters and activates CRAC channels via direct binding of a cytosolic domain to Orai1. *Cell* 136: 876-90
 115. Huang GN, Zeng W, Kim JY, Yuan JP, Han L, Muallem S, Worley PF. 2006. STIM1 carboxyl-terminus activates native SOC, I(crac) and TRPC1 channels. *Nat Cell Biol* 8: 1003-10
 116. Brandman O, Liou J, Park WS, Meyer T. 2007. STIM2 is a feedback regulator that stabilizes basal cytosolic and endoplasmic reticulum Ca²⁺ levels. *Cell* 131: 1327-39
 117. Luik RM, Wang B, Prakriya M, Wu MM, Lewis RS. 2008. Oligomerization of STIM1 couples ER calcium depletion to CRAC channel activation. *Nature* 454: 538-42
 118. Calloway N, Vig M, Kinet JP, Holowka D, Baird B. 2009. Molecular clustering of STIM1 with Orai1/CRACM1 at the plasma membrane depends dynamically on depletion of Ca²⁺ stores and on electrostatic interactions. *Mol Biol Cell* 20: 389-99
 119. Bird GS, Hwang SY, Smyth JT, Fukushima M, Boyles RR, Putney JW, Jr. 2009. STIM1 is a calcium sensor specialized for digital signaling. *Curr Biol* 19: 1724-9
 120. Wedel B, Boyles RR, Putney JW, Jr., Bird GS. 2007. Role of the store-operated calcium entry proteins Stim1 and Orai1 in muscarinic cholinergic receptor-

- stimulated calcium oscillations in human embryonic kidney cells. *J Physiol* 579: 679-89
121. Muik M, Frischauf I, Derler I, Fahrner M, Bergsmann J, Eder P, Schindl R, Hesch C, Polzinger B, Fritsch R, Kahr H, Madl J, Gruber H, Groschner K, Romanin C. 2008. Dynamic coupling of the putative coiled-coil domain of ORAI1 with STIM1 mediates ORAI1 channel activation. *J Biol Chem* 283: 8014-22
 122. Li Z, Lu J, Xu P, Xie X, Chen L, Xu T. 2007. Mapping the interacting domains of STIM1 and Orai1 in Ca²⁺ release-activated Ca²⁺ channel activation. *J Biol Chem* 282: 29448-56
 123. Zhou Y, Meraner P, Kwon HT, Machnes D, Oh-hora M, Zimmer J, Huang Y, Stura A, Rao A, Hogan PG. 2010. STIM1 gates the store-operated calcium channel ORAI1 in vitro. *Nat Struct Mol Biol* 17: 112-6
 124. Calloway N, Holowka D, Baird B. 2010. A basic sequence in STIM1 promotes Ca²⁺ influx by interacting with the C-terminal acidic coiled coil of Orai1. *Biochemistry* 49: 1067-71
 125. Gomez TM, Robles E, Poo M, Spitzer NC. 2001. Filopodial calcium transients promote substrate-dependent growth cone turning. *Science* 291: 1983-7
 126. Gomez TM, Zheng JQ. 2006. The molecular basis for calcium-dependent axon pathfinding. *Nat Rev Neurosci* 7: 115-25
 127. Jin M, Guan CB, Jiang YA, Chen G, Zhao CT, Cui K, Song YQ, Wu CP, Poo MM, Yuan XB. 2005. Ca²⁺-dependent regulation of rho GTPases triggers turning of nerve growth cones. *J Neurosci* 25: 2338-47
 128. Wei C, Wang X, Chen M, Ouyang K, Song LS, Cheng H. 2009. Calcium flickers steer cell migration. *Nature* 457: 901-5
 129. Tian D, Jacobo SM, Billing D, Rozkalne A, Gage SD, Anagnostou T, Pavenstadt H, Hsu HH, Schlondorff J, Ramos A, Greka A. 2010. Antagonistic regulation of actin dynamics and cell motility by TRPC5 and TRPC6 channels. *Sci Signal* 3: ra77

130. Marasco WA, Becker EL, Oliver JM. 1980. The ionic basis of chemotaxis. Separate cation requirements for neutrophil orientation and locomotion in a gradient of chemotactic peptide. *Am J Pathol* 98: 749-68
131. Zigmond SH. 1977. Ability of polymorphonuclear leukocytes to orient in gradients of chemotactic factors. *J Cell Biol* 75: 606-16
132. Gallin JI, Rosenthal AS. 1974. The regulatory role of divalent cations in human granulocyte chemotaxis. Evidence for an association between calcium exchanges and microtubule assembly. *J Cell Biol* 62: 594-609
133. Boucek MM, Snyderman R. 1976. Calcium influx requirement for human neutrophil chemotaxis: inhibition by lanthanum chloride. *Science* 193: 905-7
134. Mandeville JT, Ghosh RN, Maxfield FR. 1995. Intracellular calcium levels correlate with speed and persistent forward motion in migrating neutrophils. *Biophys J* 68: 1207-17
135. Sawyer DW, Sullivan JA, Mandell GL. 1985. Intracellular free calcium localization in neutrophils during phagocytosis. *Science* 230: 663-6
136. Marks PW, Maxfield FR. 1990. Transient increases in cytosolic free calcium appear to be required for the migration of adherent human neutrophils. *J Cell Biol* 110: 43-52
137. Jung ID, Lee HS, Lee HY, Choi OH. 2009. FcepsilonRI-mediated mast cell migration: signaling pathways and dependence on cytosolic free Ca²⁺ concentration. *Cell Signal* 21: 1698-705
138. Shimizu T, Owsianik G, Freichel M, Flockerzi V, Nilius B, Vennekens R. 2009. TRPM4 regulates migration of mast cells in mice. *Cell Calcium* 45: 226-32
139. Donnadieu E, Bismuth G, Trautmann A. 1994. Antigen recognition by helper T cells elicits a sequence of distinct changes of their shape and intracellular calcium. *Curr Biol* 4: 584-95

140. Negulescu PA, Krasieva TB, Khan A, Kerschbaum HH, Cahalan MD. 1996. Polarity of T cell shape, motility, and sensitivity to antigen. *Immunity* 4: 421-30
141. Delon J, Bercovici N, Liblau R, Trautmann A. 1998. Imaging antigen recognition by naive CD4+ T cells: compulsory cytoskeletal alterations for the triggering of an intracellular calcium response. *Eur J Immunol* 28: 716-29
142. Dustin ML, Bromley SK, Kan Z, Peterson DA, Unanue ER. 1997. Antigen receptor engagement delivers a stop signal to migrating T lymphocytes. *Proc Natl Acad Sci U S A* 94: 3909-13
143. Yang S, Zhang JJ, Huang XY. 2009. Orai1 and STIM1 are critical for breast tumor cell migration and metastasis. *Cancer Cell* 15: 124-34
144. Schaff UY, Dixit N, Procyk E, Yamayoshi I, Tse T, Simon SI. 2010. Orai1 regulates intracellular calcium, arrest, and shape polarization during neutrophil recruitment in shear flow. *Blood* 115: 657-66
145. Li J, Sukumar P, Milligan CJ, Kumar B, Ma ZY, Munsch CM, Jiang LH, Porter KE, Beech DJ. 2008. Interactions, functions, and independence of plasma membrane STIM1 and TRPC1 in vascular smooth muscle cells. *Circ Res* 103: e97-104
146. Bisailon JM, Motiani RK, Gonzalez-Cobos JC, Potier M, Halligan KE, Alzawahra WF, Barroso M, Singer HA, Jour'd'heuil D, Trebak M. 2010. Essential role for STIM1/Orai1-mediated calcium influx in PDGF-induced smooth muscle migration. *Am J Physiol Cell Physiol* 298: C993-1005
147. Rao JN, Rathor N, Zou T, Liu L, Xiao L, Yu TX, Cui YH, Wang JY. 2010. STIM1 translocation to the plasma membrane enhances intestinal epithelial restitution by inducing TRPC1-mediated Ca²⁺ signaling after wounding. *Am J Physiol Cell Physiol* 299: C579-88
148. MacDonald AJ, Pick J, Bissonnette EY, Befus AD. 1998. Rat mucosal mast cells: the cultured bone marrow-derived mast cell is biochemically and functionally analogous to its counterpart in vivo. *Immunology* 93: 533-9

149. Seldin DC, Adelman S, Austen KF, Stevens RL, Hein A, Caulfield JP, Woodbury RG. 1985. Homology of the rat basophilic leukemia cell and the rat mucosal mast cell. *Proc Natl Acad Sci U S A* 82: 3871-5

CHAPTER 2

MOLECULAR MECHANISMS OF SPONTANEOUS AND DIRECTED MAST CELL MOTILITY

Abstract

Migration is a fundamental function of immune cells, and a role for Ca^{2+} in immune cell migration has been an interest of scientific investigations for many decades. Mast cells are the major effector cells in IgE-mediated immune responses, and crosslinking of IgE-Fc ϵ RI complexes at the mast cell surface by antigen activates a signaling cascade that causes mast cell activation, resulting in Ca^{2+} mobilization and granule exocytosis. These cells accumulate in the sites of inflammation in response to parasite and bacterial infections. Here, we show that Ca^{2+} influx via Orai1 plays an important role in regulating both spontaneous motility and directional migration of mast cells. Using real-time imaging, we observed that rat basophilic leukemia (RBL-2H3) and bone marrow-derived rat mast cells exhibit both spontaneous motility and chemotaxis toward antigen. Inhibition of Ca^{2+} influx, or knockdown of the Ca^{2+} entry channel protein, Orai1, by shRNA causes inhibition of both of these processes. In addition, a mutant RBL cell line that lacks tyrosine kinase Syk shows impaired spontaneous motility and chemotaxis toward antigen, whereas expression of Syk rescues the capability of these Syk- cells to chemotaxis to antigen. Our data identify a novel Ca^{2+} influx-mediated, Orai1 dependent mechanism in mast cell migration.

Introduction

Mast cells are key effector cells in IgE-associated immune responses, including allergic disorders and protective immune responses against certain bacteria and parasites (1). Mast cells carry out adaptive immune functions through antigen- and IgE-dependent clustering of the high affinity IgE receptor, FcεRI (2). Crosslinking of IgE-FcεRI complexes at the mast cell surface activates a signaling cascade that causes mast cell activation, resulting in Ca²⁺ mobilization and consequent release of preformed mediators of the allergic response and inflammation (3). The RBL-2H3 mast cell line has structural and functional characteristics of differentiated mucosal mast cells (4), and has been utilized for comprehensive biochemical and cell biological investigations of mast cell function. Mast cell recruitment into the site of inflammation is associated with helminth and bacterial infections (5, 6), and chronic allergic disorders (7). In particular, differentiated mucosal mast cells are known to redistribute from the submucosa or crypt area to the lamina propria and intraepithelial regions of jejunal villi during the course of an immune response to certain parasitic infections (8). This process depends on mast cell motility and is likely to be driven by chemotactic responses, but the mechanisms underlying this process are poorly understood.

The directed migration of leukocytes in response to soluble cues, known as chemotaxis, is induced by various extracellular signals, including chemokines and cytokines, lipid mediators, bacterial factors and ECM degradation products (9-11). Chemotactic ligands have been identified for mast cells, including sphingosine 1-

phosphate (S1P) (12), stem cell factor (SCF) (13), arachidonic acid metabolites leukotriene B4 (14), and PGE₂ (15) as well as several chemokines (16). In addition, mast cell chemotaxis toward IgE-specific antigen was first described with MC/9 mouse mast cells (17), followed by others (17-19).

A role for Ca²⁺ in directed hematopoietic cell migration has been implicated (20-22) but is controversial (23, 24). Leukocyte migration slows and stops when the extracellular Ca²⁺ is depleted (20, 21, 25), and similarly, migration slows when the intracellular Ca²⁺ is buffered (26, 27). In contrast, polymorphonuclear leukocytes (PMNs) orient correctly across the chemoattractant gradient without extracellular Ca²⁺ (23, 24), and migrate faster (24). In T cells, a rise in intracellular [Ca²⁺] after APC interaction causes T cells to stop crawling (28, 29). All of these observations suggest that the role of Ca²⁺ in hematopoietic cell polarization and migration maybe different for different cell types. One of the key mechanisms in mammalian cells to regulate Ca²⁺ influx is through the Ca²⁺ release-activated Ca²⁺ (CRAC) channel, in which the depletion of intracellular Ca²⁺ stores triggers sustained Ca²⁺ influx through the coupling of ER store Ca²⁺ sensor STIM1 to the plasma membrane channel protein Orai1 (CRACM1). Recently, evidence linking Orai1 and STIM1 to cancer cell migration and metastasis (30), neutrophil recruitment and polarization (31), and vascular smooth muscle cell migration (32, 33) have been described.

In the course of investigating mast cell motility and directional migration, we found that Ca²⁺ influx plays a key role in regulating mast cell random motility via the store operated Ca²⁺ entry channel protein Orai1. Furthermore, we show that antigen

directly elicits a chemotactic response from mast cells, and this directed migration is dependent on tyrosine kinase Syk, extracellular $[Ca^{2+}]$, and Orai1 as assessed using real-time imaging. These results demonstrate the importance of Ca^{2+} homeostasis in both mast cell motility and directed migration toward antigen, while revealing a novel role for Syk and Orai1 in these processes.

Materials and Methods

Chemicals, reagents, and constructs

Cytochalasin D, wortmannin, U-73122, 2-aminoethoxydiphenyl borate (2-APB), and $GdCl_3$ were purchased from Sigma-Aldrich Chemical Co. (Saint Louis, MO). Recombinant rat SCF and IL-3 were from Peprotech Inc. (Rocky Hill, NJ). Sphingosine-1-phosphate (S1P) is from Enzo Life Sciences, Inc. (Farmingdale, NY). Mouse monoclonal anti-dinitrophenyl (DNP) IgE was purified as previously described (34). Multivalent antigen (DNP-BSA) contained an average 15 DNP groups per protein and was prepared as previously described (35). GFP-(PLC- γ 1)-(SH2)₂ (36) and Syk-CFP (ATCC id: 10373748) cDNA constructs were gifts from Dr. Tobias Meyer (Stanford University). Small hairpin RNA (shRNA) plasmids targeting Orai1, STIM1, and TRPC1 (OriGene, Rockville, MD) were previously described and characterized in RBL cells (37). GCaMP3 construct (38) was obtained from Addgene (Cambridge, MA).

Cell Culture

The RBL-2H3 and other cell lines were maintained as monolayers in minimal essential medium supplemented with 20% (vol/vol) fetal bovine serum and 10 µg/ml gentamicin. All tissue culture reagents were obtained from Invitrogen Corp. unless otherwise noted. For transient transfection, cells were plated in 35 mm culture dish at 70 - 80 % confluence and transfected with fluorescent tagged Syk or tandem SH2 domain of PLC γ using FuGENE HD (Roche Diagnostics, Indianapolis, IN) per manufacturer's instructions with modifications to enhance transfection efficiency in the RBL cells as previously described (39). For knock-down studies, cells were transiently transfected with either using FuGENE HD or by electroporation using Gene Pulser X (Bio-Rad) with 20 µg each of inhibitory shRNA plasmids against Orai1 or STIM1 which also contains genetically encoded fluorescent protein expression sequence, or with 20 µg of inhibitory plasmids targeting TRPC1 along with 8 µg of the expression vector that encodes monomeric red fluorescent protein (mRFP) as previously described (40). Cells were used 48 hours after transfection. Rat BMMCs were differentiated from bone marrow-derived stem cells of Lewis strain rats by culturing for 14 - 28 days in the presence of rat stem cell factor (SCF, 50 ng/ml) and rat IL-3 (100 ng/ml) as previously described (41).

Motility assay

RBL-2H3 cells or rat BMMCs were plated at low density ($\sim 1.5 \times 10^5$ cells/dish) overnight in 35-mm dishes with cover slip inserts (MatTek Corp., Ashland, MA). Time-lapse video

microscopy of live cells was collected for 2-3 hours with images taken in every 1-2 minutes. Images were collected using 40x/0.65NA or 10x/0.22NA dry objectives with a Leica DMIR microscope with a Photometrics Quantix CCD camera (Roper Scientific, Tucson, AZ), and a thermally regulated air gun (ASI 400 Air Stream Incubator, Nevtek, Williamsville, VA) was used to maintain the temperature at 37°C throughout the experiment. To quantify cell migration, we developed an automated tracking and analysis algorithm using MATLAB¹, in which the cell bodies were tracked automatically, then mean squared displacement (MSD) was calculated based on migration tracks. MSD measures average displacement of the cell body between two time points in the cell migration tracks. MSD was calculated for each time interval τ as follows where j represents a frame number and each frame corresponds to 2 min:

$$\text{MSD} = 4D(\tau)\tau = \left\langle \sum_{j=0}^{\text{final frame} - \tau} (r(j) - r(j + \tau))^2 \right\rangle$$

D is a diffusion coefficient and r is a position of the cell body. MSD was plotted versus τ to determine the motility coefficient as a measure of how much area the cells cover in a unit of time. The slope of the linear segment of the curve (between $\tau = 10$ min to $\tau = 20$ min under these conditions) were used to represent the motility coefficient, and calculated as follows:

$$\text{Motility coefficient} = 4D = \Delta\text{MSD}/\tau$$

¹ S. Veatch developed the MATLAB code. S. Shelby modified the code.

Live Cell Calcium Imaging

In preparation for Ca²⁺ imaging, RBL cells were transiently transfected with Ca²⁺ sensor GCaMP3 by electroporation, then plated onto 35 mm MatTek dishes. After 24 hours, cells were washed with buffered salt solution (BSS; 135 mM NaCl, 5 mM KCl, 1.8 mM CaCl₂, 1 mM MgCl₂, 1 mg/ml glucose, 20 mM HEPES (pH 7.2-7.4)), and imaged using a heated (37°C) stage with 25x oil immersion objective on a Zeiss 710 confocal microscope. GCaMP3-transfected cells were excited at 488 nm, and fluorescence was monitored at 473 - 590 nm. Time-lapse images were taken every 2 seconds for 10 – 20 min. For measurement without extracellular Ca²⁺, cells were washed in BSS without Ca²⁺ (135 mM NaCl, 5 mM KCl, 3 mM MgCl₂, 1 mM EGTA, 1 mg/ml glucose, 20 mM HEPES (pH 7.2-7.4)) and imaged in the same buffer. Pharmacological reagents 2-APB (final concentration of 10 μM) or GdCl₃ (final concentration of 2 μM) were added just prior to initiating data collection.

Chemotaxis assay

RBL-2H3 cells or rat BMMCs were plated into the narrow observation channel separating the two reservoirs in an Ibidi chemotaxis μ-slide (Ibidi LLC, Madison, WI) in complete medium. RBL mast cells were plated into uncoated Ibidi μ-slide, and rat BMMCs into collagen IV coated Ibidi μ-slide. In the cases indicated, cells were sensitized overnight with anti-DNP IgE (final concentration of 2 μg/ml). After 24 hours of incubation, one of the reservoirs was filled with complete medium with 25 mM HEPES, pH 7.2-7.4. The lower reservoir was filled with potential chemoattractant-

containing media as indicated. Chemoattractant concentrations indicated represent the final concentration used to fill the reservoir. For cells without extracellular Ca^{2+} , cells cultured overnight were washed in media containing 4 mM EGTA and 3 mM MgCl_2 , then equilibrated with the same media for the duration of the experiment. Images were collected using 10x/0.22NA dry objective with a custom built Leica microscope as described above and maintained at 37°C throughout the experiment. After 16 hours of collecting time-lapse images every 10 min, cells were tracked using the Manual Tracking Plugin for ImageJ. Manual Tracking Plugin provides a way to retrieve XY coordinates and velocity by manually clicking on the structure of interest. Then chemotactic index (y Forward Migration Index, yFMI) was determined by using the Chemotaxis Tool Plugin for ImageJ for the tracked cells. Using XY coordinates retrieved by Manual Tracking Plugin, Chemotaxis Tool Plugin provides a way to visualize and quantify chemotaxis process. yFMI is calculated to quantify chemotactic response of cells, by dividing the net y value of a given track by accumulated distance. The value for yFMI was calculated as follows:

$$\text{yFMI} = \text{Forward progress} / \text{Total path length} = \Sigma\Delta y / \Sigma((\Delta x^2 + \Delta y^2)^{-1/2})$$

with Δx and Δy assessed for each 10 min interval throughout the observation period of 16 h (42). For all the experiments with transiently transfected cells, only the fluorescent protein-tagged cells were analyzed.

Statistical analysis

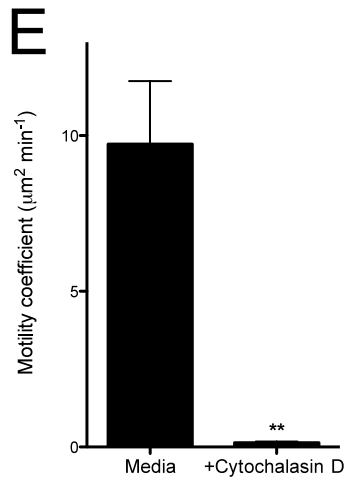
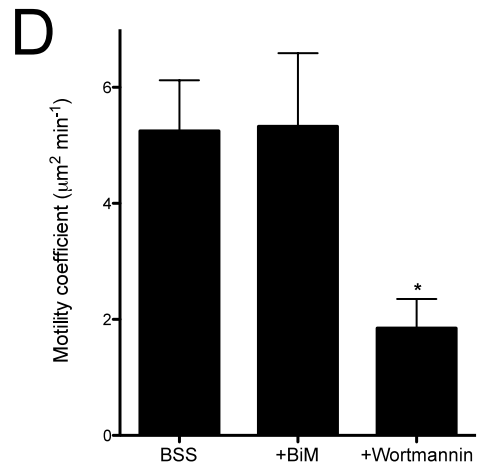
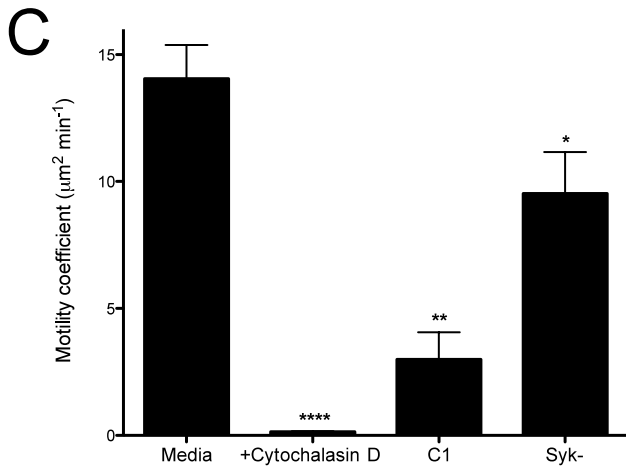
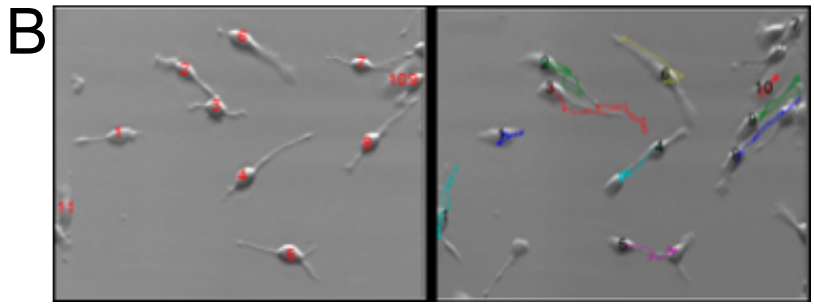
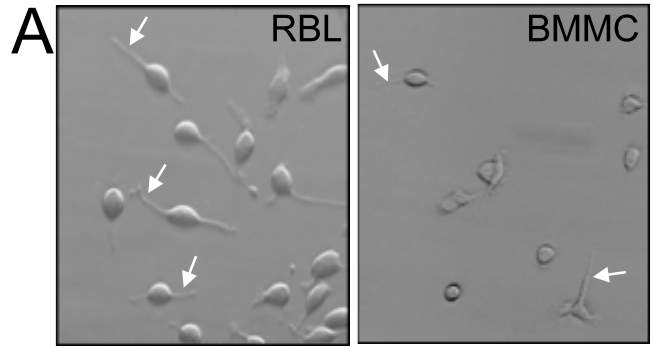
Statistical analysis was performed using unpaired two-tailed Student t test. Summary data were represented as means \pm SEM. A value of $P < 0.05$ was considered significant.

Results

Mast cells exhibit spontaneous motility.

Using RBL-2H3 mast cells as a model, we initially characterized the motility of mast cells using real time video microscopy. RBL-2H3 mast cells often exhibit distinctive extended protrusions after several hours in culture on glass surfaces (Fig. 2.1A left panel), and they show spontaneous random migration in which the cell body moves, often along tracks that are defined by the elongated protrusions (Fig. 2.1A left panel, Fig. 2.1B and Supplementary Movie 2.1). To evaluate motility characteristics of mast cells, we developed an automated tracking method, which yields a motility coefficient for cells tracked as described in Materials and Methods. The motility coefficient is a measure of the area an average cell surveys per unit time, and it is analogous to a two-dimensional diffusion coefficient (43). In agreement with previous findings with other hematopoietic cells, inhibition of actin polymerization by 1 μ M cytochalasin D completely blocked cell motility, and inhibition of phosphoinositide 3-kinase (PI3K) by 200 nM wortmannin substantially reduced cell motility as shown by

Figure 2.1. Morphology and motility properties of RBL-2H3 mast cells and rat BMMCs. (A) Phase contrast images of RBL-2H3 cells (left) and rat BMMCs (right) in media. Note polarized morphologies with extended protrusions that are common for these cells after several hours on glass surfaces (arrows). (B) Representative images of a first (left) and last (right) snapshots of time-lapse images of RBL-2H3 cells that automatically tracked using MATLAB as described in Materials and Methods. Numbers identify identical cells in both images, and colored lines on right panel represent the cell migration tracks. (C, D) Average motility coefficients of RBL-2H3 cells analyzed using MATLAB as described in Materials and Methods. Error bars show standard error of mean (SEM) for $n = 15 - 97$ cells for each sample. Cell motility was monitored for 1.5 - 3h in media (C) or in BSS with 1 mg/ml BSA (D). Inhibitors (1 μ M cytochalasin D, 1 μ M bisindolymaleimide I hydrochloride (BiM), or 200 nM wortmannin) were added just prior to motility measurements. For wortmannin, cell motility was monitored in the absence of BSA. C1, the mutant RBL cell line RBL-C1. Syk-, the mutant RBL cell line lacking tyrosine kinase Syk. (E) Average motility coefficients of rat BMMCs \pm SEM for $n = 30 - 67$ per each sample. Cytochalasin D (1 μ M) was added just prior to motility measurements. * $P < 0.05$, ** $P < 0.01$, **** $P < 0.0001$ compared to untreated control.



average motility coefficient (Fig. 2.1C, D). To further investigate the molecular bases of mast cell motility, we utilized the mutant RBL cell line RBL-C1, which is deficient in FcεRI-mediated activation of Cdc42 and Rac1, as well as in Cdc42-dependent biosynthetic trafficking (44). These cells exhibit substantially reduced motility, suggesting significant roles for these Rho family GTPases in this process (Fig. 2.1C). In addition, we used an RBL cell variant that lacks the tyrosine kinase Syk (45) to show that this protein contributes to spontaneous RBL cell motility. In contrast, inhibition of protein kinase C (PKC) with bisindolylmaleimide I (BiM) does not alter cell motility (Fig. 1C, D), suggesting selectivity in the intracellular signaling pathway that regulates mast cell motility.

Similar to RBL mast cells, primary rat bone marrow derived mast cells (BMMC) have IgE receptors and the mast cell-specific ganglioside detected with monoclonal antibody against AA4, and they exhibit a mucosal mast cell phenotype (46). Even though they have more heterogeneous morphology than RBL cells, we observed extended protrusions in a subset of these cells, very reminiscent of those seen with RBL-2H3 mast cells (Fig. 2.1A, right panel). Rat BMMC also show spontaneous migration on glass, and have similar motility characteristics as RBL-2H3 mast cells, with a slightly lower average motility coefficient value in media (Fig. 2.1E). As for RBL cells, cytochalasin D completely inhibit this motility. These results provide clear evidence that mast cells migrate spontaneously, and actin polymerization, Rho GTPases, protein tyrosine kinase Syk, and PI3K are involved in regulating this motility.

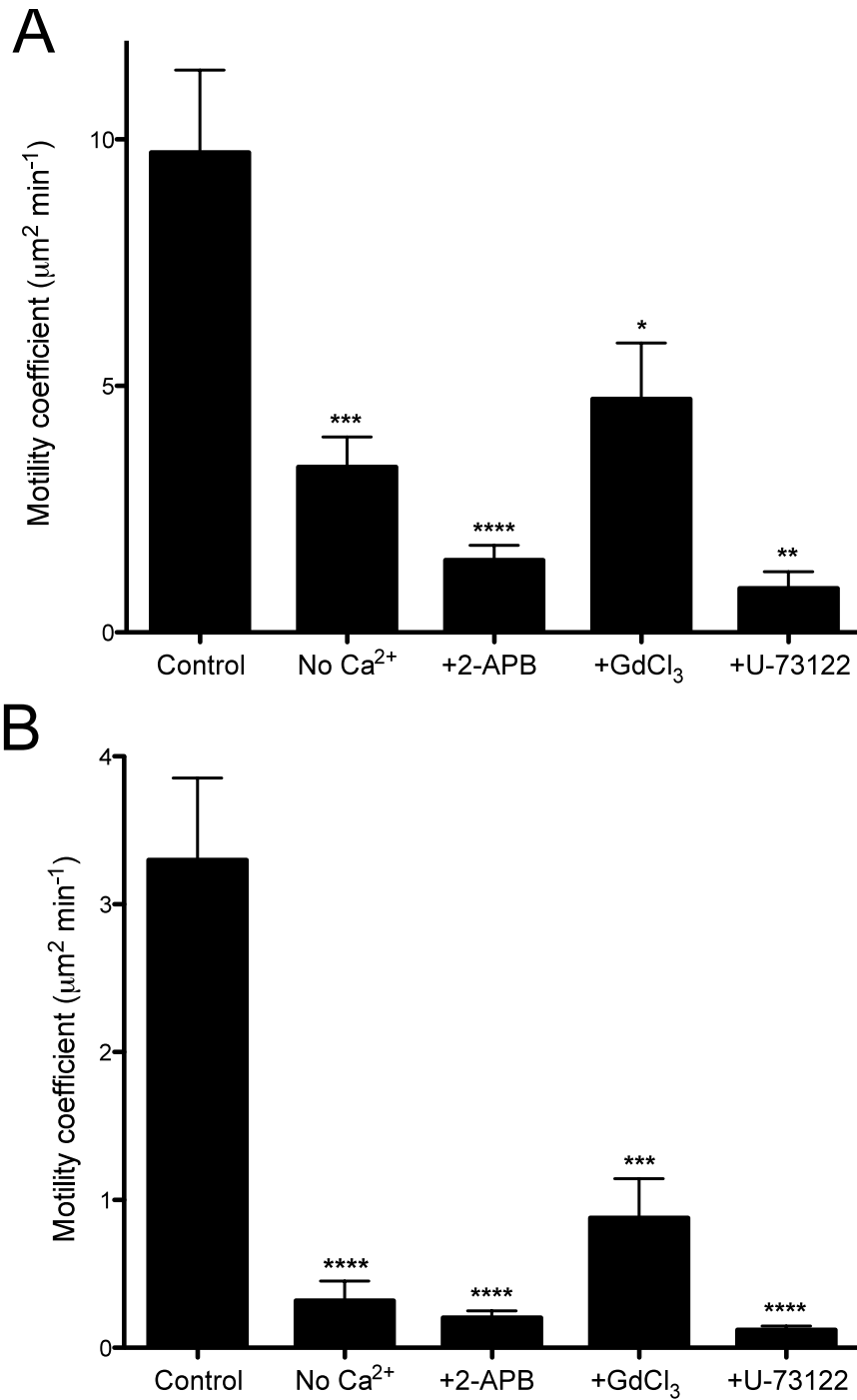


Figure 2.2. Extracellular Ca^{2+} is important for mast cell motility. Motility of RBL-2H3 cells (A) and rat BMMCs (B) was monitored for 1.5 h in BSS, and average motility coefficients \pm SEM ($n = 14 - 88$ per each sample) are shown. No Ca^{2+} ; BSS without CaCl_2 + 1 mM EGTA and 2 mM MgCl_2 . SOCE inhibitor 2-APB (10 μM), Orai1 channel inhibitor GdCl_3 (2 μM), and the phospholipase C inhibitor U-73122 (2 μM) were added prior to motility measurements. * $P < 0.05$, ** $P < 0.01$, *** $P < 0.001$, **** $P < 0.0001$ compared to control.

Ca²⁺ influx regulates basal mast cell motility.

As Ca²⁺ mobilization contributes to a diverse range of cell functions, including cell motility and adhesion, and is vital to several mast cell functions (3, 47), we next investigated whether Ca²⁺ plays a role in mast cell spontaneous migration using pharmacological inhibitors. All the experiments shown in Figure 2.2 were carried out in BSS, as serum components in media can bind pharmacologic agents to interfere with their activity. Without the growth factors that are present in media, mast cells in BSS exhibited reduced motility, as evidenced for RBL cells in Figure 2.1C vs. D. RBL mast cells in the absence of extracellular Ca²⁺ exhibit substantially reduced cell motility in comparison to control cells in BSS (Fig. 2.2A). Chelating intracellular Ca²⁺ by BAPTA-AM did not further reduce their migration (data not shown), so we hypothesized that impaired Ca²⁺ influx might be responsible for the reduction in motility. 2-APB was first described as an inhibitor of IP₃ receptor (IP₃R)-mediated Ca²⁺ release (48), but subsequently shown to inhibit store operated calcium entry (SOCE) in T cells at the concentrations between 10-50 μM (49). In RBL-2H3 cells, 2-APB has an inhibitory effect on Ca²⁺ influx, but fails to inhibit IP₃R-mediated Ca²⁺ release from ER stores at concentrations up to 40 μM (40). As shown in Figure 2.2A, 10 μM 2-APB causes a large reduction in RBL cell motility. Because RBL cells do not express voltage gated Ca²⁺ channels (50), Gd³⁺ can be used to specifically block Ca²⁺ release-activated Ca²⁺ (CRAC) channels in these cells (51). When 2 μM Gd³⁺ was added to assess the role of CRAC channels in RBL cell motility, we observed a significant reduction in motility, although

not as severe as when 2-APB was used. In addition, the phospholipase C (PLC) inhibitor, U-73122, also caused a decrease in cell motility at a final concentration of 2 μM (Fig. 2.2A).

These same trends of reduced motility are observed in primary rat BMMCs as well (Fig. 2.2B). For these cells, spontaneous motility in BSS is only about one third the rate it is in full media (Compare Fig. 2.2E to Fig. 2.1E), suggesting the factors in the serum contribute even more substantially to this process. Collectively, these data demonstrate that absence of extracellular Ca^{2+} and pharmacological inhibition of Ca^{2+} influx causes reduction in spontaneous motility of RBL mast cells and rat BMMCs.

To further evaluate the molecular bases of Ca^{2+} influx in mast cell motility in RBL cells, we knocked down Orai1 and STIM1, the major components of CRAC channel activation. A previous study showed that these shRNA vectors resulted in substantial reduction in antigen-stimulated SOCE (36). We found that expression of the shRNA for Orai1 significantly reduced RBL cell motility to about 50 % decrease in average motility coefficient compared to control vector transfected cells (Fig. 2.3). By comparison, STIM1 shRNA caused a smaller, statistically insignificant reduction in motility to about 25%, and TRPC1 shRNA did not reduce this compared to controls. These results support a role for Ca^{2+} influx via Orai1 in mast cell motility.

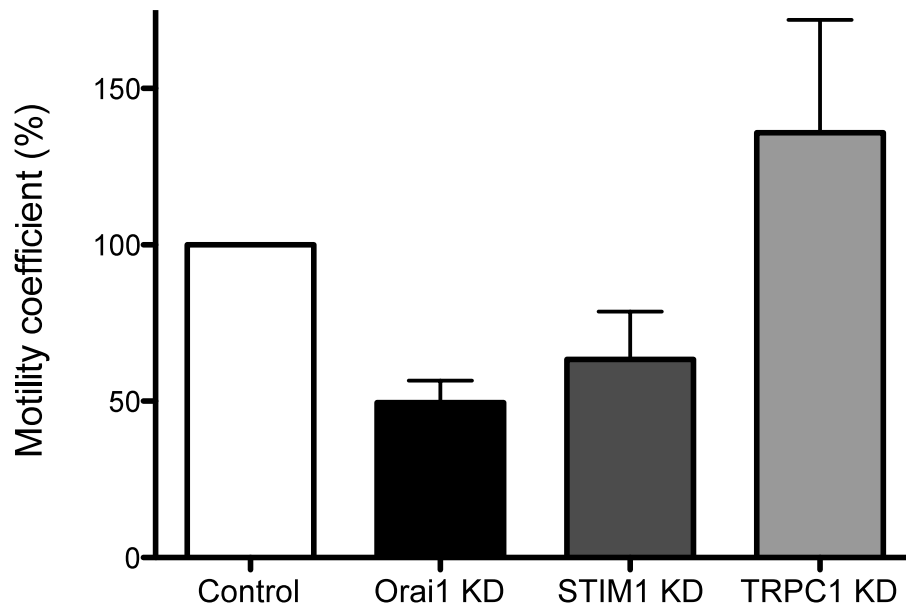
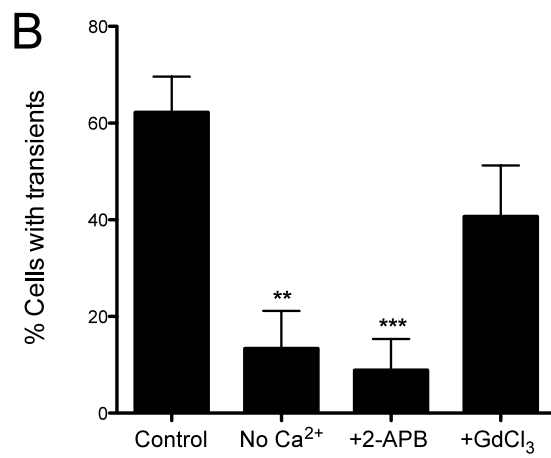
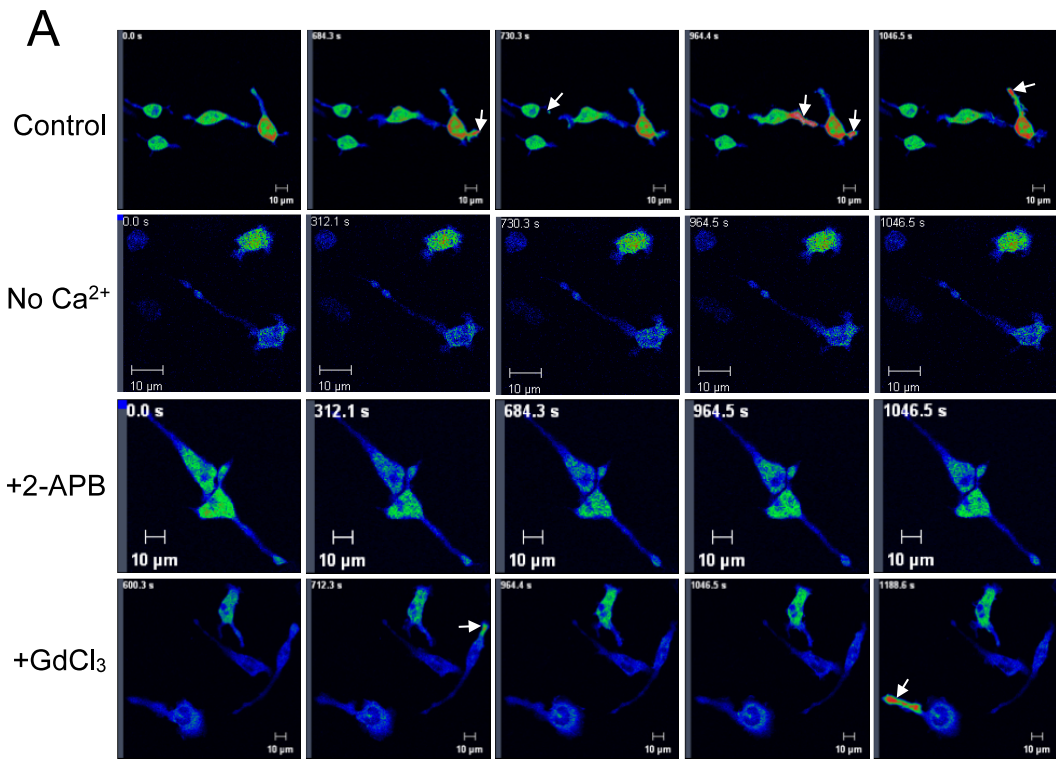


Figure 2.3. Involvement of Orai1/CRACM1 in RBL mast cell motility. RBL-2H3 cells were transiently transfected with shRNA specific for Orai1, STIM1, or parallel control empty vectors, respectively. TRPC1 shRNA was co-transfected with mRFP, and in control experiments RBL cells were transiently transfected with mRFP only. Cell motility was monitored for 1.5h in media, and the percent decreases in motility coefficients are shown \pm SEM (n = 45 - 75 cells per each sample).

RBL-2H3 mast cells exhibit spontaneous Ca²⁺ transients.

Changes in intracellular Ca²⁺ through stimulated events including Ca²⁺ puffs, waves, and oscillations follow FcεRI-mediated activation in mast cells as previously described (40), but spontaneous Ca²⁺ events have not been previously characterized. As spontaneous motility in mast cells is regulated by Ca²⁺ influx, we investigated Ca²⁺ mobilization events in non-stimulatory conditions using the genetically encoded Ca²⁺ indicator, GCaMP3, and real-time confocal microscopy. GCaMP3 has been reported to have increased fluorescence quantum yield, higher affinity for Ca²⁺, and significantly better signal-to-noise ratio than GCaMP2 (38), making it potentially better suited for monitoring transient Ca²⁺ mobilization events. As represented in Figure 2.4A, we found short-lived, localized intracellular Ca²⁺ transients, that are frequently seen in extended protrusions (Fig. 2.4A and Supplementary Movie 2.2). During the 20 min of real-time confocal microscopy, an average of 62.3% ± 7.4% of GCaMP3 transfected cells exhibited Ca²⁺ transients (Figure 2.4B). Strikingly, when the cells were monitored in the absence of extracellular Ca²⁺, the number of cells that show spontaneous Ca²⁺ transients was markedly decreased to 14.3% ± 6.4% SEM. Adding 2-APB also caused substantial reduction in number of cells with Ca²⁺ transients (8.9% ± 6.5% SEM), and Gd³⁺ caused a smaller reduction to 40.7% ± 10.6% SEM (Fig. 2.4B), reminiscent of trends observed in RBL cell motility under these conditions (Fig. 2.3A).

Figure 2.4. RBL-2H3 mast cells exhibit spontaneous Ca²⁺ transients with influx dependence that correlates with motility. (A) Confocal images of representative RBL-2H3 mast cells expressing GCaMP3. Time-lapse images were taken every 2 seconds for 20 min. Note localized, transient Ca²⁺ transients frequently occurring in protrusions (arrows). No Ca²⁺; BSS without CaCl₂ + 1 mM EGTA and 2 mM MgCl₂. Inhibitors 2-APB (10 μM), or GdCl₃ (2 μM), were added just prior to collecting time-lapse images. (B) Summary of average percentages of cells with Ca²⁺ transients out of total GCaMP3 expressing cells ± SEM (n = 27 - 42 per each condition) monitored in 3 experiments. Cells with at least one Ca²⁺ transient during 20 min were scored for all cases shown. ** *P* < 0.01, *** *P* < 0.001 compared to control.

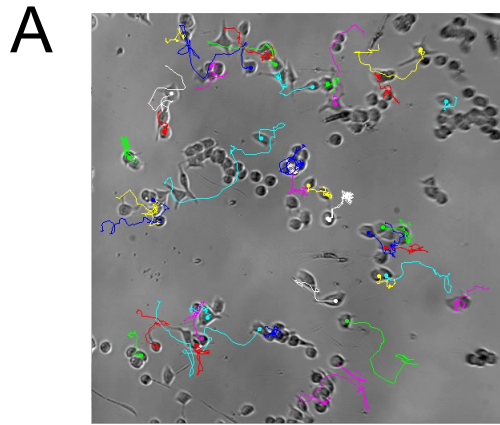


Mast cells show directed migration toward antigen.

To directly visualize mast cell chemotaxis in real time, we established a chemotaxis assay using the chemotaxis μ -slide chamber (Ibidi Corp.). RBL-2H3 cells were plated into the narrow observation channel separating the two 40 μ L reservoirs, and the putative chemoattractant was added to one of the reservoirs to establish a spatially well defined chemotactic gradient. After imaging cells for 16 hours, the cells were manually tracked using the Image J Manual Tracking Plugin (Fig. 2.5A and Supplementary Movie 2.3), and then the tracked information was processed using the Chemotaxis Tool Plugin for ImageJ. As shown in the representative experiments in Figure 2.5B and the corresponding Supplementary Movie 2.4, anti-DNP IgE sensitized RBL-2H3 cells exhibit net chemotaxis toward antigen (10 ng/mL DNP-BSA), when the cell migration tracks are plotted after normalizing the start point to $x = 0$ and $y = 0$. In this representation, the y axis is the direction between reservoirs, and the red tracks represent the cells with net migration toward the lower, chemoattractant containing reservoir.

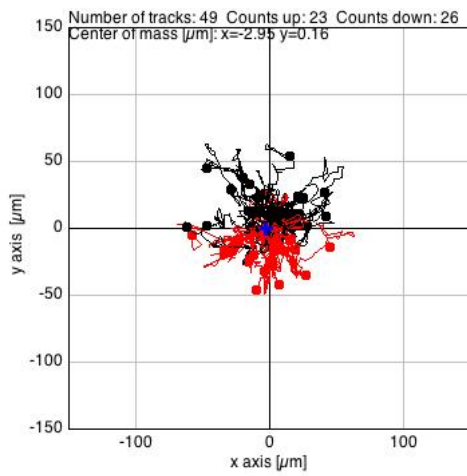
To measure directed migration in a more quantifiable manner, we calculated y Forward Migration Index (y FMI), where y FMI was determined by dividing the net y value of a given cell track by accumulated distance. As summarized in Figure 2.6, RBL cells migrated toward antigen in a dose dependent manner, with a maximal response at 10 ng/ml DNP-BSA, but they did not migrate significantly toward a higher dose of antigen. As expected, RBL cells did not chemotax toward antigen when the cells were

Figure 2.5. Monitoring and analyzing mast cell chemotaxis in real time. (A) Representative image of RBL-2H3 cells in Ibidi chemotaxis μ -slide after 16 h. Colored lines show migration tracks derived from ImageJ Manual Tracking plugin program. (B) Representative plots from single experiment showing migration tracks of RBL-2H3 cells with and without 10 ng/mL DNP-BSA. (C) Representative plots for rat BMMCs with and without 100 nM SCF. The migration tracks were plotted after normalizing the starting point to $x = 0$ and $y = 0$ using ImageJ plugin Chemotaxis Tool. Red tracks indicate cells with net migration toward the lower (chemoattractant)-containing chamber.

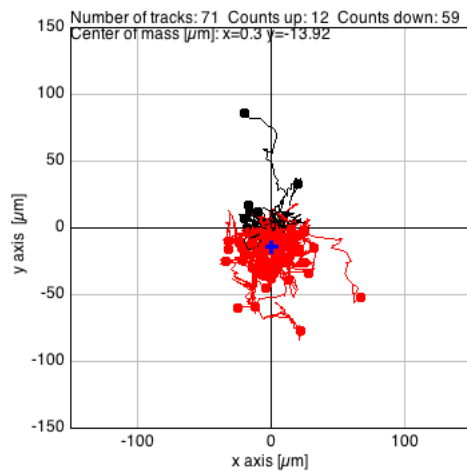


B

Control

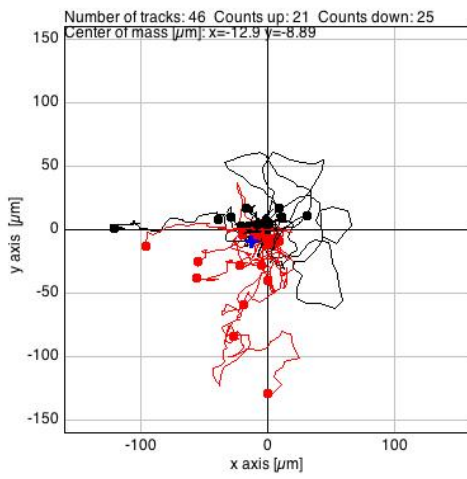


+ Antigen

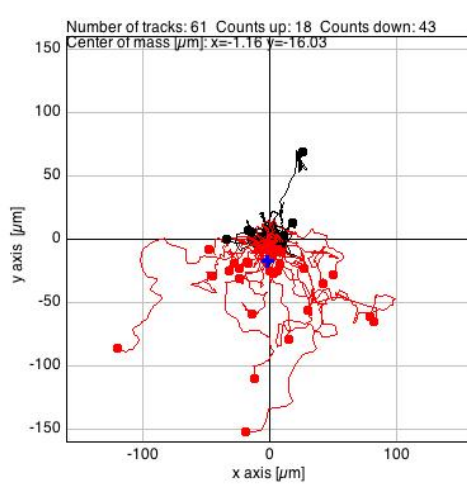


C

Control



+ SCF



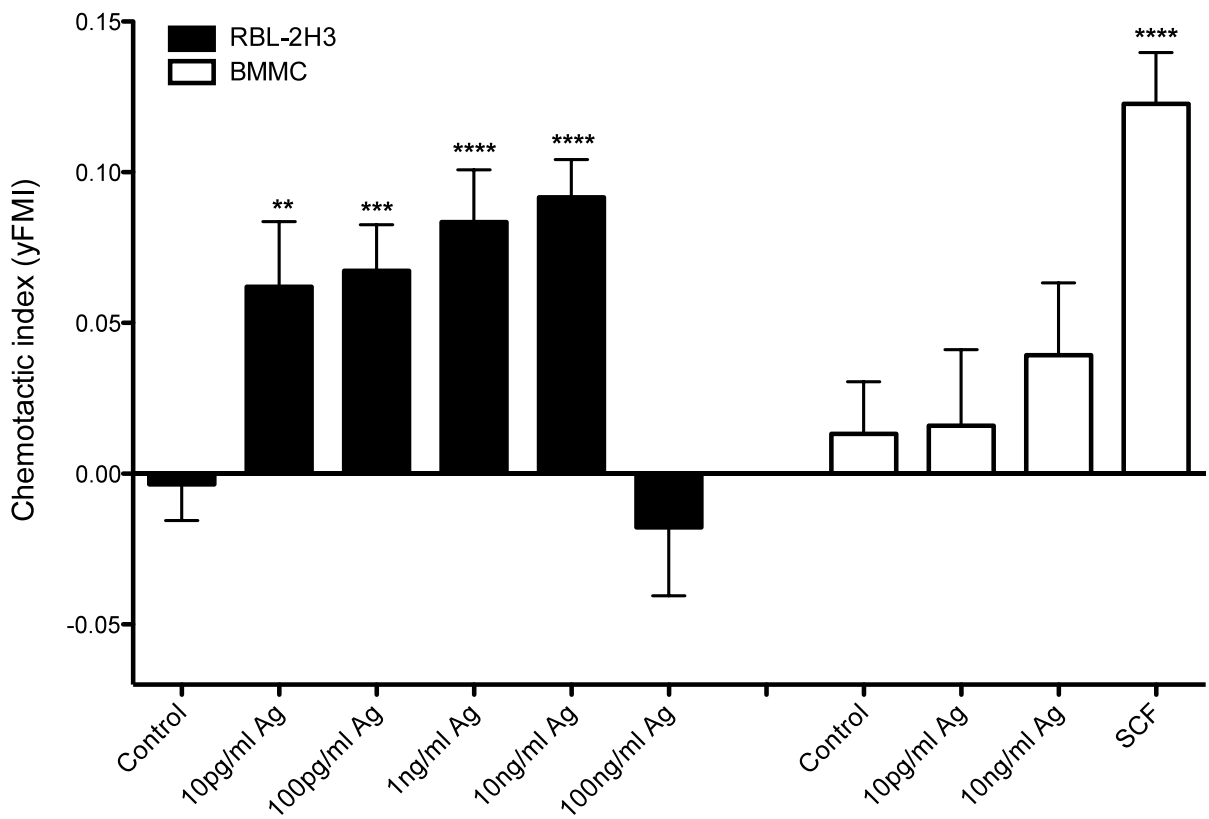


Figure 2.6. RBL-2H3 mast cells show chemotaxis toward antigen. Mast cell chemotaxis is represented as the average y Forward Migration Index (yFMI) \pm SEM (n = 36 - 137 cells per each condition). yFMI is determined by dividing the net y value of a given track by accumulated distance. RBL-2H3 cells (black bars) or rat BMMCs (open bars) were sensitized with anti-DNP IgE, plated onto Ibidi chemotaxis μ -slide chambers overnight, then monitored for 16 hours in the absence (control) or presence of varying doses of DNP-BSA or SCF as indicated. SCF; BMMCs with 100 nM SCF. ** $P < 0.01$, *** $P < 0.001$, **** $P < 0.0001$ compared to respective control.

not sensitized with anti-DNP IgE (data not shown). Rat BMMCs showed only a small chemotactic response toward antigen over a similar dose range, but they exhibited substantial directed migration toward stem cell factor (SCF), which is a known chemoattractant for BMMCs (Fig. 2.5C and Fig. 2.6, ref. 13). RBL mast cells express constitutively active c-kit (1), a ligand for SCF, making directed migration of RBL cells toward SCF unlikely. These results provide compelling evidence that mast cells can sense and directly migrate in response to an antigen gradient.

Syk plays an important role in mast cell chemotaxis toward antigen.

To investigate whether directed migration is affected by the absence of tyrosine kinase Syk, we assessed the chemotactic ability of Syk⁻ cells. As shown in Figure 2.7, Syk⁻ cells sensitized with IgE failed to show chemotaxis toward antigen at 10 ng/ml. A chemotactic response could be obtained by transiently expressing Syk-CFP (Fig. 2.7), indicating a key role for Syk in the chemotactic response toward antigen. In contrast, when the tandem SH2 domain of phospholipase C γ (GFP-(PLC γ 1)-(SH2)₂) was transiently expressed, cells failed to chemotax toward antigen, supporting a role for the kinase domain of Syk in this process. Chemotaxing cells turn forward and backward repeatedly during observation period. Both Syk⁻ cells in the absence or presence of antigen as a chemoattractant, as well as Syk⁻ cells transiently expressing GFP-(PLC γ 1)-(SH2)₂ in the presence of antigen show final γ FMI values that are negative, indicating

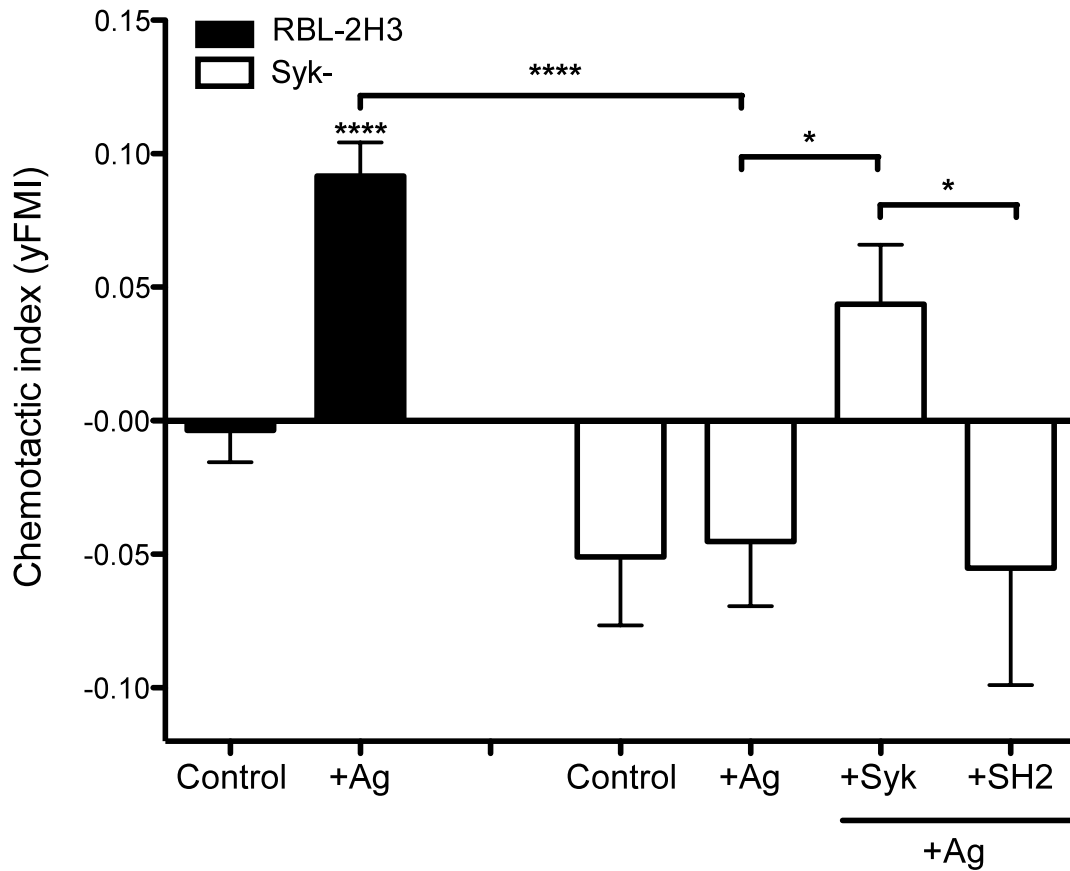


Figure 2.7. Directed migration of RBL-2H3 cells toward antigen is dependent on Syk kinase. Syk⁻ cells were sensitized with anti-DNP IgE, plated onto Ibidi chemotaxis μ -slide chambers overnight, then monitored for 16 hours in the absence (control) or presence of 10 ng/mL DNP-BSA (+Ag). +Syk: Syk⁻ cells transiently expressing Syk-CFP cells. +SH2: Syk⁻ cells transiently expressing PLC γ -(SH2)₂-GFP. Average yFMI \pm SEM (n = 27 - 108 cells per each condition) are shown. * $P < 0.05$, **** $P < 0.0001$ compared to respective control as indicated.

that their net direction is backward when compared to their initial starting point (Fig. 2.7). The reason for this is unclear at the present time.

Ca²⁺ channel protein Orai1 is important for RBL-2H3 cell migration toward antigen.

Because we observed decreased random motility of RBL-2H3 mast cells in the absence of extracellular Ca²⁺ and when the Ca²⁺ channel protein Orai1 was knocked down, we next asked whether the absence of extracellular Ca²⁺ or a reduction in Orai1 also impairs mast cell chemotaxis toward antigen. As shown in Figure 2.8, when RBL-2H3 cells were monitored in excess EGTA, they show significantly reduced chemotaxis toward 10 ng/ml antigen when compared to cells in normal media. Cells transiently transfected with shRNA specific for Orai1 also show markedly reduced chemotaxis toward 10 ng/ml antigen when compared to untransfected cells and to control empty vector shRNA transfected cells. These data strongly support that Ca²⁺ influx via Orai1 plays an important role not only in spontaneous mast cell motility (Fig. 2.3) but also in directed migration to antigen. Previous reports have shown that mast cells generate and secrete sphingosine-1-phosphate (S1P) upon crosslinking of FcεRI (12, 19, 51), and S1P can act as a chemoattractant for mast cells (12). It has been speculated that mast cell chemotaxis toward antigen might be due to S1P secreted by FcεRI activation of cells. When S1P was used as a chemoattractant, RBL-2H3 mast cells show directed migration toward S1P as previously demonstrated (12). However, this chemotaxis fails to show a dependence on extracellular Ca²⁺, suggesting an alternative molecular basis for this

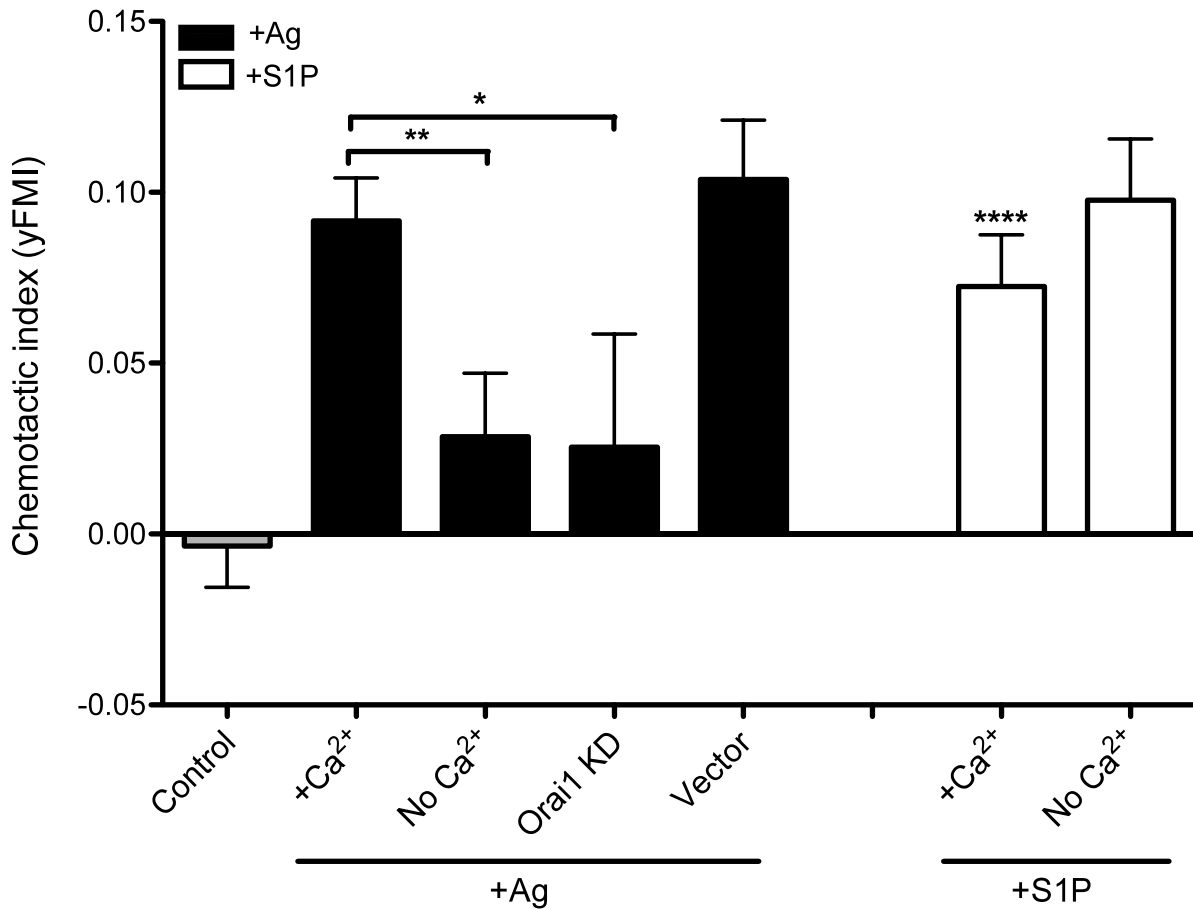


Figure 2.8. Orai1/CRACM1 contributes to RBL-2H3 mast cell chemotaxis toward antigen. RBL-2H3 cells were sensitized with anti-DNP IgE, plated onto Ibidi chemotaxis μ -slide chambers overnight, then monitored for 16 hours in the absence (control) or presence of 10 ng/mL DNP-BSA (+Ag). +S1P: chemotaxis of RBL cells in the presence of 1 μ M S1P. No Ca²⁺: RBL-2H3 cells in media with 4 mM EGTA and 3 mM MgCl₂. RBL-2H3 cells were transiently transfected with shRNA against Orai1 (Orai1 KD) or with corresponding empty vector (Vector), sensitized with anti-DNP IgE, plated onto Ibidi chemotaxis μ -slide chambers overnight, then monitored for 16 hours. Average yFMI \pm SEM (n = 11 - 108 cells per each condition) are shown. * $P < 0.05$, ** $P < 0.01$, **** $P < 0.0001$ compared to respective control as indicated.

process. Moreover, the velocities of RBL cells chemotaxing toward S1P are decreased in excess EGTA, indicating that extracellular Ca^{2+} -does influence this aspect of migration in the presence of S1P (Fig. 2.9).

Discussion

Involvement of Ca^{2+} in regulating leukocyte migration has been an interest in the field for many decades (20, 24). Our results using real-time video microscopy provide direct evidence that Ca^{2+} influx is important for mast cell spontaneous motility and directed migration toward antigen. Using pharmacological inhibitors as well as genetic manipulations, we present compelling evidence that SOCE, in particular Orai1, is important for regulating these processes (Fig. 2.2, 2.3 and Fig. 2.8).

In agreement with the view that phosphatidylinositol 3-kinases (PI3K) is a key regulator in chemotaxis and cell polarity in T cells and neutrophils (52-56), mast cell spontaneous motility was blocked by PI3K inhibition with 200 nM wortmannin treatment (Fig. 2.1). More recently, this view has been challenged with equally compelling reports demonstrating that PI3K is dispensable and only important under certain conditions (57-59). Currently, there are emerging theories attempting to bridge these seemingly inconsistent results, including the possibility that the PI3K requirement in chemotaxis depends on the differentiation state or primed status of cells (60). Since

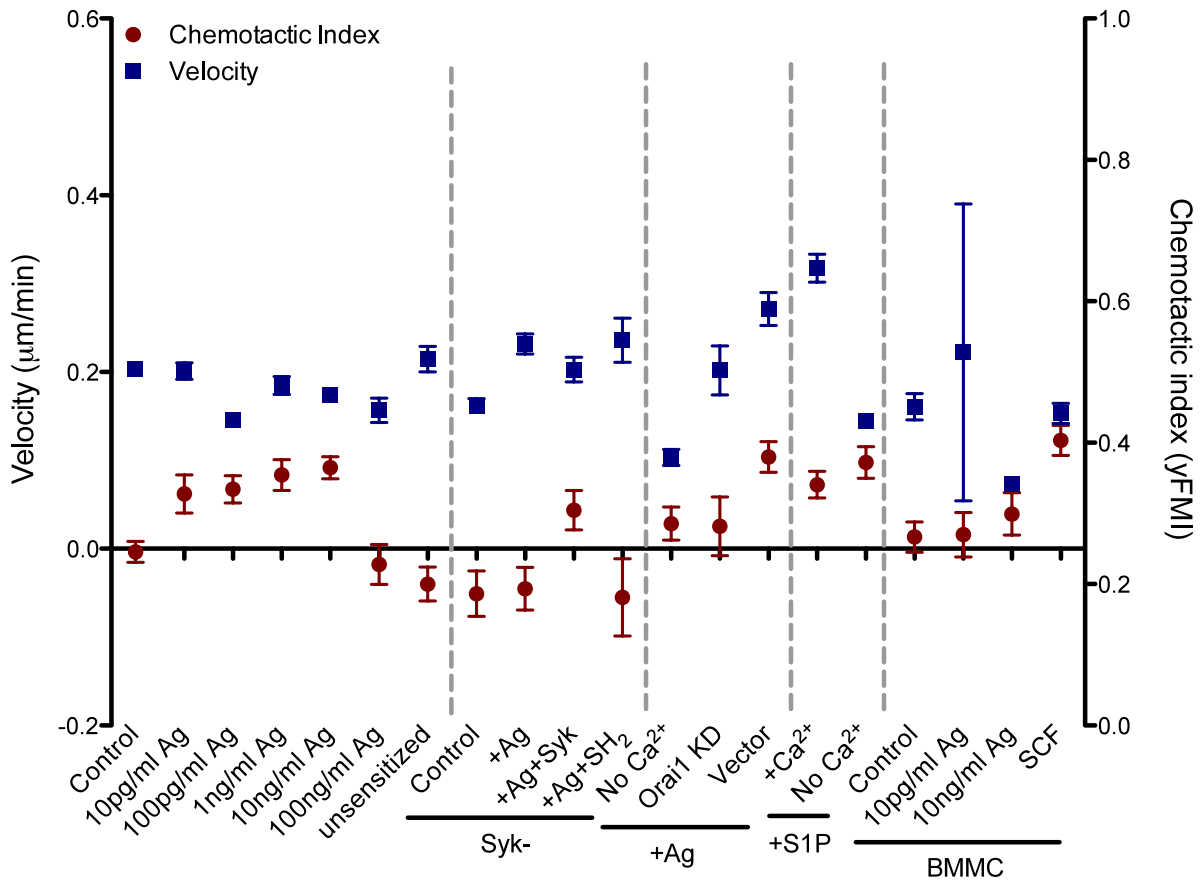


Figure 2.9. Average velocity and chemotactic index of chemotaxing mast cells under various conditions. Average velocity (blue rectangle) and y Forward Migration Index (yFMI, chemotactic index, red circle) of mast cells in Ibidi chemotaxis μ -slide are shown \pm SEM (n= 11 – 137). Same experiments were used to acquire both velocity and yFMI. yFMI of these cells are also separately shown in Fig. 2.6 – Fig. 2.8.

we saw inhibition of basal motility with PI3K inhibition, it will be interesting to determine if more “primed” condition, i.e., cells undergoing chemotaxis, would make the PI3K requirement differ from that of spontaneously migrating cells. Additionally, by studying the motility properties of RBL-C1 mutant cell line, which is deficient in Cdc42-dependent biosynthetic trafficking and FcεRI-mediated activation of Cdc42 and Rac1, we demonstrated that Rho family GTPases also play a significant role in mast cell motility (Fig. 2.1).

It was previously shown that Ca^{2+} influx is necessary for maintaining phosphatidylinositol-3,4,5-triphosphate (PIP_3) at the leading edge in spontaneously polarizing macrophages through positive feedback-loop consists of PI3K, F-actin, and extracellular Ca^{2+} influx (22). Furthermore, adding exogenous PIP_3 stimulates Ca^{2+} influx, and inhibiting PI3K blocks Ca^{2+} influx in RBL-2H3 mast cell (61), T cells (62), and neutrophils (63). Since we observed inhibitory effects on mast cell motility by inhibiting either PI3K or Ca^{2+} influx, it will be interesting to determine whether spatial regulation of PI3K and its subsequent preferential localization of PIP_3 to the leading edge is a downstream target of Ca^{2+} influx through Orai1 in regulating mast cell basal motility.

We characterized spontaneous Ca^{2+} transients that have not been previously described in mast cells using genetically encoded Ca^{2+} indicator GCaMP3 with real-time confocal microscopy. Interestingly, we observed local Ca^{2+} transients in unstimulated cells, often more frequently in extended cell protrusions, and these can be inhibited by

chelating extracellular Ca^{2+} or by blocking SOCE or Orai1 (Fig. 2.4). These trends are similar to those observed in cell motility (Fig. 2.2). A recent study by Wei et al. reported that high Ca^{2+} microdomains, 'Ca²⁺ flickers', are asymmetrically localized to the leading edge of migrating fibroblasts and promote the turning behavior of these cells (64). Similarly, we observed some tendency of more frequent stimulated Ca^{2+} mobilization events in the protrusions of RBL cells to which the cell body is moving (R. Cohen and J. Lee, unpublished results), suggesting a possibility of correlation between localized Ca^{2+} transients and RBL cell motility.

We investigated chemotaxis of mast cells by establishing real-time imaging of this process utilizing Ibidi μ -slide chemotaxis chambers. This method allows us to directly visualize and analyze directed cell migration, and is especially well suited for long-term studies of slow migrating cells (65). We demonstrated that mast cells exhibit chemotaxis toward antigen (Fig. 2.5 and Fig. 2.6), and this process depends on tyrosine kinase Syk and Ca^{2+} influx via Orai1 (Fig. 2.7 and Fig. 2.8). We observed RBL mast cells chemotax toward antigen in a dose dependent manner, with a maximal response toward 10 ng/ml antigen, but did not observe chemotaxis toward a 10-fold higher dose of antigen. Mast cells show similar average velocity in the presence or absence of various doses of antigen as a chemoattractant, implying that antigen directly elicits a chemotactic response by altering the directionality and sensing of mast cells, rather than causing enhancement of chemokinesis in these cells (Fig. 2.9). However, relations between velocity and directionality and sensing of mast cells under other conditions

seem to be more complicated (Fig. 2.9). With 100 ng/ml antigen, mast cells begin to halt their migration and undergo degranulation. When higher dose of 1 μ g/ml antigen was added globally to RBL mast cells, cells flatten out, ruffle, and stop crawling (data not shown). Similarly, RBL mast cells initially flatten out and stop crawling when 100 ng/ml antigen was used as a chemoattractant (data not shown). At this concentration of antigen, mast cells show near maximal degranulation response (data not shown). These data suggest that there might be an antigen dose-sensitive mechanism that regulates the chemotactic response of mast cells and intersects with mast cell degranulation response.

Syk negative mutant RBL cells (Syk⁻ cells) are deficient in their directed migration toward antigen, and this defect can be restored by transient overexpression of Syk-CFP (Fig. 2.7). Involvement of Syk in mouse BMMC chemotaxis toward antigen has been described previously (18), but little has been explored about their detailed mechanism. Syk contains two tandem SRC homology 2 (SH2) domains and a carboxy-terminal tyrosine kinase domain. When we transiently overexpress two tandem SH2 domains of PLC γ (GFP-(PLC γ 1)-(SH2)₂) to Syk⁻ mutant cells, it fails to reconstitute the deficiency in Syk⁻ cell chemotaxis toward antigen (Fig. 2.7), indicating that binding of tandem SH2 domain to Fc ϵ RI ITAMs (35) is not sufficient for this reconstitution, implicating the kinase activity of Syk.

Syk has been implicated in macrophage chemotaxis (66), lamellipodium formation and chemotaxis of human leukocytes (67), and integrin-mediated signal

transduction leading to leukocyte adhesion and migration (68-70). Syk is also important in Fc γ RI mediated signaling in macrophages and neutrophils (71, 72), and essential for Fc ϵ RI mediated signaling in mast cells (73). Together with our finding that Syk plays a key role in mast cell basal motility and chemotaxis toward antigen, it seems to imply a universal role for Syk in immune cell migration.

Mast cell chemotaxis toward antigen has been demonstrated previously, including RBL-2H3 cells and mouse BMMCs (12, 17-19, 74), and involvement of Ca²⁺ in this process was suggested recently (75, 76). Our principle new finding is that this process is mediated by Ca²⁺ influx via Orai1 (Fig. 2.8). Evidence for a role for Orai1 and/or STIM1 in cell migration has just began to emerge in various cell types. Yang et al. have reported that breast cancer cell migration and tumor metastasis depend on Orai1 and STIM1 (30), and Orai1 has been shown to regulate integrin dependent arrest and migration of neutrophils (31). A role for Orai1, STIM1, and TRPC1 in vascular smooth muscle cell migration has been described as well (32, 33). We observed smaller inhibition of basal motility of mast cells by knocking down Orai1 when compared to the inhibition of chemotaxis toward antigen, suggesting that Orai1 might be playing a more significant role in regulating mast cell chemotaxis toward antigen. Knockdown of TRPC1 by shRNA failed to cause inhibition in mast cell basal motility, and with STIM1 knockdown, we only saw relatively small inhibition. It is possible that Orai1 may couple to STIM2 under these conditions, but we cannot rule out the possibility of insufficient knockdown of STIM1 as an explanation for the results we obtained.

Rat BMMCs show smaller, statistically insignificant chemotaxis toward similar antigen dosages that are optimal for RBL-2H3 cells (Fig. 2.6). It is possible that the heterogenous expression of FcεRI on the surface of BMMCs, in which a substantial subpopulation of BMMCs does not express detectable surface expression of FcεRI (D. Holowka, unpublished results) could contribute to these results, thus limiting the average chemotaxis response.

S1P is a known chemoattractant for mast cells (12). Indeed, we were able to confirm directed migration of RBL-2H3 cells toward S1P (Fig. 2.8). S1P generation and secretion succeeds FcεRI aggregation in mast cells following activation of sphingosine phosphate kinase (SphKs). In dendritic cells, secreted S1P can act in autocrine and paracrine fashion, binding to its G-protein coupled receptor S1PR1, then activating one of its downstream target Rac to enhance migration (77). It was previously reported that in RBL-2H3 cells, knocking down either S1PR1 or SphK1 caused reduction in their chemotaxis toward antigen (12), which led to the idea that secreted S1P after FcεRI aggregation might be mediating mast cell chemotaxis toward antigen. Whether autocrine-paracrine action of chemotactic factors that are released from the activated mast cells after FcεRI crosslinking is required (12, 18) or not (17, 74) is unclear. Although we cannot rule out the possibility that secreted S1P is mediating chemotaxis toward antigen, our data clearly demonstrates that, in contrast to chemotaxis toward antigen, RBL-2H3 chemotaxis toward S1P is independent of extracellular Ca^{2+} , suggesting different pathway(s) are involved in these processes. This discrepancy could be at least

in part attributed to the different time scale of these experiments: Jolly et al. looked at migration after 3 hours, but we observed migration for 16 hours. The suggested mechanisms involved are not necessarily mutually exclusive. Perhaps, secreted S1P mediated chemotaxis toward antigen is more important for initial, shorter time period, but that Ca^{2+} influx becomes more important over longer time periods.

The present study shows that Ca^{2+} influx plays an essential role in mast cell basal motility and directed migration toward antigen and that Orai1 contributes to these processes. Basal motility also depends on Rho GTPases, protein tyrosine kinase Syk, and PI3K. Furthermore, we observed spontaneous Ca^{2+} transients that are inhibited by SOCE and Orai1 inhibitors, with a trend resembling that of cell motility. Antigen can directly induce a chemotactic response from IgE-sensitized mast cells. To understand the molecular mechanisms underlying this process, we compared chemotaxis toward antigen in the presence or absence of extracellular Ca^{2+} , or with knock down of Orai1 with specific shRNA, using real-time imaging. Our results reveal that without extracellular Ca^{2+} or with Orai1 knocked-down, mast cells exhibit markedly reduced chemotaxis toward antigen, suggesting a role for Ca^{2+} influx via Orai1 in regulating mast cell motility, providing new insight into the mechanism of immune cell migration.

REFERENCES

1. Beaven MA. 2009. Our perception of the mast cell from Paul Ehrlich to now. *Eur J Immunol* 39: 11-25
2. Kinet JP. 1999. The high-affinity IgE receptor (Fc epsilon RI): from physiology to pathology. *Annu Rev Immunol* 17: 931-72
3. Rivera J, Gilfillan AM. 2006. Molecular regulation of mast cell activation. *J Allergy Clin Immunol* 117: 1214-25; quiz 26
4. Seldin DC, Adelman S, Austen KF, Stevens RL, Hein A, Caulfield JP, Woodbury RG. 1985. Homology of the rat basophilic leukemia cell and the rat mucosal mast cell. *Proc Natl Acad Sci U S A* 82: 3871-5
5. Echtenacher B, Mannel DN, Hultner L. 1996. Critical protective role of mast cells in a model of acute septic peritonitis. *Nature* 381: 75-7
6. Madden KB, Urban JF, Jr., Ziltener HJ, Schrader JW, Finkelman FD, Katona IM. 1991. Antibodies to IL-3 and IL-4 suppress helminth-induced intestinal mastocytosis. *J Immunol* 147: 1387-91
7. Brightling CE, Bradding P, Symon FA, Holgate ST, Wardlaw AJ, Pavord ID. 2002. Mast-cell infiltration of airway smooth muscle in asthma. *N Engl J Med* 346: 1699-705
8. Friend DS, Ghildyal N, Austen KF, Gurish MF, Matsumoto R, Stevens RL. 1996. Mast cells that reside at different locations in the jejunum of mice infected with *Trichinella spiralis* exhibit sequential changes in their granule ultrastructure and chymase phenotype. *J Cell Biol* 135: 279-90
9. Laskin DL, Kimura T, Sakakibara S, Riley DJ, Berg RA. 1986. Chemotactic activity of collagen-like polypeptides for human peripheral blood neutrophils. *J Leukoc Biol* 39: 255-66

10. Senior RM, Gresham HD, Griffin GL, Brown EJ, Chung AE. 1992. Entactin stimulates neutrophil adhesion and chemotaxis through interactions between its Arg-Gly-Asp (RGD) domain and the leukocyte response integrin. *J Clin Invest* 90: 2251-7
11. Adair-Kirk TL, Atkinson JJ, Broekelmann TJ, Doi M, Tryggvason K, Miner JH, Mechem RP, Senior RM. 2003. A site on laminin alpha 5, AQARSAASKVKVSMKF, induces inflammatory cell production of matrix metalloproteinase-9 and chemotaxis. *J Immunol* 171: 398-406
12. Jolly PS, Bektas M, Olivera A, Gonzalez-Espinosa C, Proia RL, Rivera J, Milstien S, Spiegel S. 2004. Transactivation of sphingosine-1-phosphate receptors by FcepsilonRI triggering is required for normal mast cell degranulation and chemotaxis. *J Exp Med* 199: 959-70
13. Meininger CJ, Yano H, Rottapel R, Bernstein A, Zsebo KM, Zetter BR. 1992. The c-kit receptor ligand functions as a mast cell chemoattractant. *Blood* 79: 958-63
14. Weller CL, Collington SJ, Brown JK, Miller HR, Al-Kashi A, Clark P, Jose PJ, Hartnell A, Williams TJ. 2005. Leukotriene B₄, an activation product of mast cells, is a chemoattractant for their progenitors. *J Exp Med* 201: 1961-71
15. Weller CL, Collington SJ, Hartnell A, Conroy DM, Kaise T, Barker JE, Wilson MS, Taylor GW, Jose PJ, Williams TJ. 2007. Chemotactic action of prostaglandin E₂ on mouse mast cells acting via the PGE₂ receptor 3. *Proc Natl Acad Sci U S A* 104: 11712-7
16. Taub D, Dastyk J, Inamura N, Upton J, Kelvin D, Metcalfe D, Oppenheim J. 1995. Bone marrow-derived murine mast cells migrate, but do not degranulate, in response to chemokines. *J Immunol* 154: 2393-402
17. Ishizuka T, Okajima F, Ishiwara M, Iizuka K, Ichimonji I, Kawata T, Tsukagoshi H, Dobashi K, Nakazawa T, Mori M. 2001. Sensitized mast cells migrate toward the antigen: a response regulated by p38 mitogen-activated protein kinase and Rho-associated coiled-coil-forming protein kinase. *J Immunol* 167: 2298-304
18. Kitaura J, Kinoshita T, Matsumoto M, Chung S, Kawakami Y, Leitges M, Wu D, Lowell CA, Kawakami T. 2005. IgE- and IgE+Ag-mediated mast cell migration in an autocrine/paracrine fashion. *Blood* 105: 3222-9

19. Olivera A, Urtz N, Mizugishi K, Yamashita Y, Gilfillan AM, Furumoto Y, Gu H, Proia RL, Baumruker T, Rivera J. 2006. IgE-dependent activation of sphingosine kinases 1 and 2 and secretion of sphingosine 1-phosphate requires Fyn kinase and contributes to mast cell responses. *J Biol Chem* 281: 2515-25
20. Gallin JI, Rosenthal AS. 1974. The regulatory role of divalent cations in human granulocyte chemotaxis. Evidence for an association between calcium exchanges and microtubule assembly. *J Cell Biol* 62: 594-609
21. Boucek MM, Snyderman R. 1976. Calcium influx requirement for human neutrophil chemotaxis: inhibition by lanthanum chloride. *Science* 193: 905-7
22. Evans JH, Falke JJ. 2007. Ca²⁺ influx is an essential component of the positive-feedback loop that maintains leading-edge structure and activity in macrophages. *Proc Natl Acad Sci U S A* 104: 16176-81
23. Zigmond SH. 1977. Ability of polymorphonuclear leukocytes to orient in gradients of chemotactic factors. *J Cell Biol* 75: 606-16
24. Marasco WA, Becker EL, Oliver JM. 1980. The ionic basis of chemotaxis. Separate cation requirements for neutrophil orientation and locomotion in a gradient of chemotactic peptide. *Am J Pathol* 98: 749-68
25. Mandeville JT, Ghosh RN, Maxfield FR. 1995. Intracellular calcium levels correlate with speed and persistent forward motion in migrating neutrophils. *Biophys J* 68: 1207-17
26. Sawyer DW, Sullivan JA, Mandell GL. 1985. Intracellular free calcium localization in neutrophils during phagocytosis. *Science* 230: 663-6
27. Marks PW, Maxfield FR. 1990. Transient increases in cytosolic free calcium appear to be required for the migration of adherent human neutrophils. *J Cell Biol* 110: 43-52
28. Donnadieu E, Bismuth G, Trautmann A. 1994. Antigen recognition by helper T cells elicits a sequence of distinct changes of their shape and intracellular calcium. *Curr Biol* 4: 584-95

29. Negulescu PA, Krasieva TB, Khan A, Kerschbaum HH, Cahalan MD. 1996. Polarity of T cell shape, motility, and sensitivity to antigen. *Immunity* 4: 421-30
30. Yang S, Zhang JJ, Huang XY. 2009. Orai1 and STIM1 are critical for breast tumor cell migration and metastasis. *Cancer Cell* 15: 124-34
31. Schaff UY, Dixit N, Procyk E, Yamayoshi I, Tse T, Simon SI. 2010. Orai1 regulates intracellular calcium, arrest, and shape polarization during neutrophil recruitment in shear flow. *Blood* 115: 657-66
32. Li J, Sukumar P, Milligan CJ, Kumar B, Ma ZY, Munsch CM, Jiang LH, Porter KE, Beech DJ. 2008. Interactions, functions, and independence of plasma membrane STIM1 and TRPC1 in vascular smooth muscle cells. *Circ Res* 103: e97-104
33. Bisailon JM, Motiani RK, Gonzalez-Cobos JC, Potier M, Halligan KE, Alzawahra WF, Barroso M, Singer HA, Jour'dheuil D, Trebak M. 2010. Essential role for STIM1/Orai1-mediated calcium influx in PDGF-induced smooth muscle migration. *Am J Physiol Cell Physiol* 298: C993-1005
34. Posner RG, Lee B, Conrad DH, Holowka D, Baird B, Goldstein B. 1992. Aggregation of IgE-receptor complexes on rat basophilic leukemia cells does not change the intrinsic affinity but can alter the kinetics of the ligand-IgE interaction. *Biochemistry* 31: 5350-6
35. Naal RM, Holowka EP, Baird B, Holowka D. 2003. Antigen-stimulated trafficking from the recycling compartment to the plasma membrane in RBL mast cells. *Traffic* 4: 190-200
36. Stauffer TP, Meyer T. 1997. Compartmentalized IgE receptor-mediated signal transduction in living cells. *J Cell Biol* 139: 1447-54
37. Ma HT, Peng Z, Hiragun T, Iwaki S, Gilfillan AM, Beaven MA. 2008. Canonical transient receptor potential 5 channel in conjunction with Orai1 and STIM1 allows Sr²⁺ entry, optimal influx of Ca²⁺, and degranulation in a rat mast cell line. *J Immunol* 180: 2233-9
38. Tian L, Hires SA, Mao T, Huber D, Chiappe ME, Chalasani SH, Petreanu L, Akerboom J, McKinney SA, Schreiter ER, Bargmann CI, Jayaraman V, Svoboda

- K, Looger LL. 2009. Imaging neural activity in worms, flies and mice with improved GCaMP calcium indicators. *Nat Methods* 6: 875-81
39. Gosse JA, Wagenknecht-Wiesner A, Holowka D, Baird B. 2005. Transmembrane sequences are determinants of immunoreceptor signaling. *J Immunol* 175: 2123-31
 40. Cohen R, Torres A, Ma HT, Holowka D, Baird B. 2009. Ca²⁺ waves initiate antigen-stimulated Ca²⁺ responses in mast cells. *J Immunol* 183: 6478-88
 41. Haig DM, Huntley JF, MacKellar A, Newlands GF, Inglis L, Sangha R, Cohen D, Hapel A, Galli SJ, Miller HR. 1994. Effects of stem cell factor (kit-ligand) and interleukin-3 on the growth and serine proteinase expression of rat bone-marrow-derived or serosal mast cells. *Blood* 83: 72-83
 42. Foxman EF, Kunkel EJ, Butcher EC. 1999. Integrating conflicting chemotactic signals. The role of memory in leukocyte navigation. *J Cell Biol* 147: 577-88
 43. Sumen C, Mempel TR, Mazo IB, von Andrian UH. 2004. Intravital microscopy: visualizing immunity in context. *Immunity* 21: 315-29
 44. Field KA, Apgar JR, Hong-Geller E, Siraganian RP, Baird B, Holowka D. 2000. Mutant RBL mast cells defective in Fc epsilon RI signaling and lipid raft biosynthesis are reconstituted by activated Rho-family GTPases. *Mol Biol Cell* 11: 3661-73
 45. Zhang J, Berenstein EH, Evans RL, Siraganian RP. 1996. Transfection of Syk protein tyrosine kinase reconstitutes high affinity IgE receptor-mediated degranulation in a Syk-negative variant of rat basophilic leukemia RBL-2H3 cells. *J Exp Med* 184: 71-9
 46. MacDonald AJ, Pick J, Bissonnette EY, Befus AD. 1998. Rat mucosal mast cells: the cultured bone marrow-derived mast cell is biochemically and functionally analogous to its counterpart in vivo. *Immunology* 93: 533-9
 47. Kim TD, Eddlestone GT, Mahmoud SF, Kuchtey J, Fewtrell C. 1997. Correlating Ca²⁺ responses and secretion in individual RBL-2H3 mucosal mast cells. *J Biol Chem* 272: 31225-9

48. Maruyama T, Kanaji T, Nakade S, Kanno T, Mikoshiba K. 1997. 2APB, 2-aminoethoxydiphenyl borate, a membrane-penetrable modulator of Ins(1,4,5)P₃-induced Ca²⁺ release. *J Biochem* 122: 498-505
49. Prakriya M, Lewis RS. 2001. Potentiation and inhibition of Ca(2+) release-activated Ca(2+) channels by 2-aminoethyldiphenyl borate (2-APB) occurs independently of IP(3) receptors. *J Physiol* 536: 3-19
50. Hoth M, Penner R. 1992. Depletion of intracellular calcium stores activates a calcium current in mast cells. *Nature* 355: 353-6
51. Broad LM, Cannon TR, Taylor CW. 1999. A non-capacitative pathway activated by arachidonic acid is the major Ca²⁺ entry mechanism in rat A7r5 smooth muscle cells stimulated with low concentrations of vasopressin. *J Physiol* 517 (Pt 1): 121-34
52. Hirsch E, Katanaev VL, Garlanda C, Azzolino O, Pirola L, Silengo L, Sozzani S, Mantovani A, Altruda F, Wymann MP. 2000. Central role for G protein-coupled phosphoinositide 3-kinase gamma in inflammation. *Science* 287: 1049-53
53. Sasaki T, Irie-Sasaki J, Jones RG, Oliveira-dos-Santos AJ, Stanford WL, Bolon B, Wakeham A, Itie A, Bouchard D, Koziaradzki I, Joza N, Mak TW, Ohashi PS, Suzuki A, Penninger JM. 2000. Function of PI3Kgamma in thymocyte development, T cell activation, and neutrophil migration. *Science* 287: 1040-6
54. Niggli V, Keller H. 1997. The phosphatidylinositol 3-kinase inhibitor wortmannin markedly reduces chemotactic peptide-induced locomotion and increases in cytoskeletal actin in human neutrophils. *Eur J Pharmacol* 335: 43-52
55. Servant G, Weiner OD, Herzmark P, Balla T, Sedat JW, Bourne HR. 2000. Polarization of chemoattractant receptor signaling during neutrophil chemotaxis. *Science* 287: 1037-40
56. Yoo SK, Deng Q, Cavnar PJ, Wu YI, Hahn KM, Huttenlocher A. 2010. Differential regulation of protrusion and polarity by PI3K during neutrophil motility in live zebrafish. *Dev Cell* 18: 226-36

57. Andrew N, Insall RH. 2007. Chemotaxis in shallow gradients is mediated independently of PtdIns 3-kinase by biased choices between random protrusions. *Nat Cell Biol* 9: 193-200
58. Ferguson GJ, Milne L, Kulkarni S, Sasaki T, Walker S, Andrews S, Crabbe T, Finan P, Jones G, Jackson S, Camps M, Rommel C, Wymann M, Hirsch E, Hawkins P, Stephens L. 2007. PI(3)Kgamma has an important context-dependent role in neutrophil chemokinesis. *Nat Cell Biol* 9: 86-91
59. Hoeller O, Kay RR. 2007. Chemotaxis in the absence of PIP3 gradients. *Curr Biol* 17: 813-7
60. Afonso PV, Parent CA. 2011. PI3K and chemotaxis: a priming issue? *Sci Signal* 4: pe22
61. Ching TT, Hsu AL, Johnson AJ, Chen CS. 2001. Phosphoinositide 3-kinase facilitates antigen-stimulated Ca(2+) influx in RBL-2H3 mast cells via a phosphatidylinositol 3,4,5-trisphosphate-sensitive Ca(2+) entry mechanism. *J Biol Chem* 276: 14814-20
62. Hsu AL, Ching TT, Sen G, Wang DS, Bondada S, Authi KS, Chen CS. 2000. Novel function of phosphoinositide 3-kinase in T cell Ca2+ signaling. A phosphatidylinositol 3,4,5-trisphosphate-mediated Ca2+ entry mechanism. *J Biol Chem* 275: 16242-50
63. Tian W, Laffafian I, Dewitt S, Hallett MB. 2003. Exclusion of exogenous phosphatidylinositol-3,4,5-trisphosphate from neutrophil-polarizing pseudopodia: stabilization of the uropod and cell polarity. *EMBO Rep* 4: 982-8
64. Wei C, Wang X, Chen M, Ouyang K, Song LS, Cheng H. 2009. Calcium flickers steer cell migration. *Nature* 457: 901-5
65. Zantl R, Horn E. 2011. Chemotaxis of slow migrating Mammalian cells analysed by video microscopy. *Methods Mol Biol* 769: 191-203
66. Park H, Cox D. 2011. Syk regulates multiple signaling pathways leading to CX3CL1 chemotaxis in macrophages. *J Biol Chem* 286: 14762-9

67. Schymeinsky J, Then C, Sindrilaru A, Gerstl R, Jakus Z, Tybulewicz VL, Scharffetter-Kochanek K, Walzog B. 2007. Syk-mediated translocation of PI3Kdelta to the leading edge controls lamellipodium formation and migration of leukocytes. *PLoS One* 2: e1132
68. Mocsai A, Abram CL, Jakus Z, Hu Y, Lanier LL, Lowell CA. 2006. Integrin signaling in neutrophils and macrophages uses adaptors containing immunoreceptor tyrosine-based activation motifs. *Nat Immunol* 7: 1326-33
69. Vines CM, Potter JW, Xu Y, Geahlen RL, Costello PS, Tybulewicz VL, Lowell CA, Chang PW, Gresham HD, Willman CL. 2001. Inhibition of beta 2 integrin receptor and Syk kinase signaling in monocytes by the Src family kinase Fgr. *Immunity* 15: 507-19
70. Mocsai A, Zhou M, Meng F, Tybulewicz VL, Lowell CA. 2002. Syk is required for integrin signaling in neutrophils. *Immunity* 16: 547-58
71. Crowley MT, Costello PS, Fitzer-Attas CJ, Turner M, Meng F, Lowell C, Tybulewicz VL, DeFranco AL. 1997. A critical role for Syk in signal transduction and phagocytosis mediated by Fcgamma receptors on macrophages. *J Exp Med* 186: 1027-39
72. Kiefer F, Brumell J, Al-Alawi N, Latour S, Cheng A, Veillette A, Grinstein S, Pawson T. 1998. The Syk protein tyrosine kinase is essential for Fcgamma receptor signaling in macrophages and neutrophils. *Mol Cell Biol* 18: 4209-20
73. Costello PS, Turner M, Walters AE, Cunningham CN, Bauer PH, Downward J, Tybulewicz VL. 1996. Critical role for the tyrosine kinase Syk in signalling through the high affinity IgE receptor of mast cells. *Oncogene* 13: 2595-605
74. Kuehn HS, Radinger M, Brown JM, Ali K, Vanhaesebroeck B, Beaven MA, Metcalfe DD, Gilfillan AM. 2010. Btk-dependent Rac activation and actin rearrangement following FcepsilonRI aggregation promotes enhanced chemotactic responses of mast cells. *J Cell Sci* 123: 2576-85
75. Jung ID, Lee HS, Lee HY, Choi OH. 2009. FcepsilonRI-mediated mast cell migration: signaling pathways and dependence on cytosolic free Ca²⁺ concentration. *Cell Signal* 21: 1698-705

76. Shimizu T, Owsianik G, Freichel M, Flockerzi V, Nilius B, Vennekens R. 2009. TRPM4 regulates migration of mast cells in mice. *Cell Calcium* 45: 226-32
77. Konig K, Diehl L, Rommerscheidt-Fuss U, Golletz C, Quast T, Kahl P, Kolanus W, Knolle P, Buettner R, Heukamp LC. 2010. Four-and-a-half LIM domain protein 2 is a novel regulator of sphingosine 1-phosphate receptor 1 in CCL19-induced dendritic cell migration. *J Immunol* 185: 1466-75

CHAPTER 3

INVESTIGATING THE DYNAMIC INTERACTIONS OF MUCOSAL MAST CELLS AND INTESTINAL EPITHELIAL CELLS

Abstract

Mucosal mast cells play an important role in host defense against helminth infection. These cells are suggested to redistribute from the lamina propria of the small intestine to jejunal villi in response to *Trichinella spiralis* infection, implying a role for mast cell migration in pathological conditions. In this study, we investigated the dynamic interactions between mucosal mast cells and intestinal epithelial cells *in vitro* and *in situ*. We show that RBL-2H3 mast cells exhibit adhesion and transepithelial migration on cultured intestinal epithelial monolayers when introduced from the apical surface. Furthermore, rat BMMCs show transepithelial migration with extended protrusions when introduced from the basolateral side of the polarized epithelial monolayers using a Transwell co-culture system. We further explored these interactions in live tissue by observing labeled mast cells in intestinal segments from *T. spiralis* infected rats using multiphoton microscopy. We find endogenous cells expressing mast cell-specific ganglioside on their surface, as well as cells labeled with monoclonal anti-IgE in these segments. In addition, we detect labeled, adoptively transferred RBL-2H3 mucosal mast cells in the intraepithelial region of the intestinal villi. Together, these results provide evidence for dynamic interactions between mucosal mast cells and intestinal epithelial cells.

Introduction

Mast cells are the primary mediators of immunoglobulin E (IgE)-dependent allergic disorders, but they also play key roles as effectors and immunomodulatory cells in innate and adaptive immune responses against pathogens (1). Mast cells are strategically located at the interface between host and environment such as skin and mucosal surfaces, which makes these cells ideally localized for immune surveillance (1). Rodent mast cells can be broadly categorized into two types: mucosal and connective tissue mast cell types. Mucosal mast cells in the mouse express chymases mMCP-1, which is equivalent to rat RMCPII, and mMCP-2, and these cells are predominantly localized in the mucosal epithelium and lamina propria. In contrast, connective tissue mast cells in the mouse express chymases mMCP-4, -5, and tryptases, and primarily localize within submucosa which is composed of loose connective tissues (2). It has been documented that while mouse mMCP-4-expressing mast cells contribute to the regulation of homeostatic intestinal epithelial barrier function (3), mice lacking mMCP-1 or mast cells are defective in modulating intestinal permeability and parasite expulsion (4), suggesting that the two different subpopulations of mast cells might be playing a distinct role in non-disease and disease states in mice.

Whereas homing of mast cell progenitors is relatively well studied (5), little is known about the motility and migration of fully mature mast cells at specific tissue sites. Previous studies provided evidence that mucosal mast cell precursors migrate to mucosal tissues in response to appropriate stimuli (5), but interaction with mucosal tissue is required for these precursors to fully differentiate (5). Intestinal infection of

animals by parasitic nematodes, including *Trichinella spiralis*, induces intestinal mastocytosis during the effector phase of the inflammatory response. Furthermore, differentiated mucosal mast cells are known to redistribute from the submucosa or crypt area to the lamina propria and intraepithelial regions of jejunal villi during the course of an immune response to certain parasitic infections (6), and mast cell infiltration in to the submucosa of asthmatic airways has been reported (7). Although migration of fully differentiated mucosal mast cells inside mucosal tissue was suggested several decades ago (6), surprisingly little is known about this process.

The intestinal epithelial barrier is maintained by tight junctions (TJs) that are composed of the transmembrane proteins occludin, claudin, and junctional adhesion molecules (8). Zona Occludens-1 (ZO-1), ZO-2, and ZO-3 consist of membrane associated guanylate kinase homolog proteins that are associated with the carboxyl termini of occludin and claudin, and link these transmembrane proteins to the actin cytoskeleton to serve as platforms for various signaling molecules (9). In recent years, it has been shown that the transwell epithelial culture system is useful for dissecting the molecular events in leukocyte transepithelial migration (10). Furthermore, dynamic imaging of intestinal tissue preparations and intravital imaging using two-photon microscopy have revealed a novel role for dendritic cell extensions in the gut (11).

Previous experimental data indicated that RBL-2H3 mast cells represent an immortalized, differentiated mucosal mast cell line (12). Similarly, rat bone marrow-derived mast cells (BMMCs) have biochemical and functional characteristics of their *in vivo* mucosal counterparts, even though their maturation state is uncertain (13). Here we

show that RBL-2H3 mast cells undergo adhesion and motility on cultured monolayers of rat intestinal epithelial cells and exhibit transepithelial migration under these conditions. Furthermore, rat BMMCs show transepithelial extensions when they are introduced from the basolateral side of polarized epithelial monolayers, further suggesting dynamic interactions between mucosal mast cells and epithelial cells. In addition, using multiphoton confocal microscopy of *ex vivo* intestinal tissue from infected rats, we visualized fluorescently labeled endogenous and adoptively transferred mast cells in the epithelial layer of jejunal villi, demonstrating intimate association between the mucosal mast cells and the epithelial layer that lines the intestinal microvilli.

Materials and Methods

Reagents

Mouse monoclonal IgE specific for 2,4-dinitrophenyl (DNP) was purified as described previously (14) and was fluorescently modified with Alexa488 as previously described (15). The fluorescently modified IgE had ~7-10 dye molecules per protein. Monoclonal anti- α -galactosyl GD1b ganglioside, AA4 (16) was provided by Dr. R. Siraganian (NIH). Monoclonal anti-IgE B5 antibody was described previously (17). Anti-ZO-1 rabbit polyclonal antibody, Alexa555-CTxB, Alexa568 goat anti-rabbit antibody, and Cell Trace™ far red DDAO-SE were from Invitrogen (Carlsbad, CA).

Cell culture

SLC-44 rat intestinal epithelial cells (18) were maintained as monolayers in minimal essential medium supplemented with 10 µg/ml gentamicin and 10% (vol/vol) fetal bovine serum. In preparation for confocal microscopy, cells were harvested with EDTA for 5 min at room temperature, then plated at 50% confluence on 35 mm MatTek dishes. Next day, cells were fixed in 4% paraformaldehyde with 0.1% glutaldehyde for 15 min at room temperature, then permeabilized with 0.01% saponin, and labeled for 1 hour with rabbit anti-ZO-1 antibody (1:50; Invitrogen, Carlesbad, CA) as the primary antibody, followed by secondary antibody labeling with Alexa568 goat anti-rabbit antibody (1:200; Invitrogen) for 1 hour. Confocal images were obtained using a Leica TCS SP2 laser scanning confocal system (Leica Microsystems, Exton, PA) with a 63x/0.9NA water-immersion objective.

Real-time imaging

To monitor interactions between mast cells and epithelial cell monolayer in real time, SLC-44 cells were plated overnight on 35-mm MatTek dishes. Next day, RBL-2H3 cells were labeled with Alexa488-IgE for at least an hour at 37°C, then added to the apical side of the polarized SLC-44 cell monolayer. After 2 hours of incubation at 37°C to allow cells to adhere and start migrate, RBL mast cell migration was monitored by acquiring time-lapse images every 2 minutes for 3 hours at 37°C using a 40x/0.65NA dry objective with a Leica microscope described in Chapter 2.

Transwell transepithelial migration assay

SLC-44 cells were plated at a low density on upside down transwell inserts with a porous membrane (pore size = 5 μm , Millipore, Billerica, MA). After overnight incubation to allow cells to firmly attach to the porous membrane filter, upside down transwell inserts were oriented correctly and hung onto appropriate-sized cell culture plates. SLC-44 cells were then cultured for 14 days while changing media (minimal essential medium supplemented with 10 $\mu\text{g}/\text{ml}$ gentamicin and 5% (vol/vol) fetal bovine serum) every day to allow cells to form tight junctions. After 14 days, Alexa488-IgE labeled RBL-2H3 cells or Alexa488-anti-AA4 labeled 14-28 days cultured rat BMMCs were added to the upper chamber of the transwell inserts to introduce mast cells from the basolateral side of the polarized epithelial monolayers, and cultured for overnight. Cells were then fixed in 4% paraformaldehyde with 0.1% glutaldehyde for 15 min at room temperature. Fixed cells were permeabilized with 0.01% saponin, and labeled for 1 hour with rabbit anti-ZO-1 antibody (1:50; Invitrogen, Carlebad, CA) as the primary antibody, followed by Alexa568 goat anti-rabbit antibody (1:200; Invitrogen). Z-series images were collected using a Leica TCS SP2 laser scanning confocal system (Leica Microsystems, Exton, PA) with a 63x/0.9NA water-immersion objective.

Multiphoton microscopy

Albino Oxford (AO) or Lewis strain rats were infected with *T. spiralis* as previously described (19). Briefly, adult rats were infected by 250-400 first stage larvae (L_1), then

rats were euthanized 14-18 days post-infection and small intestines were collected¹. Small intestine segments (~ 1 cm) were bathed in Alexa488-AA4 mAb or Alexa488-B5 anti-IgE mAb solution for at least an hour at 4°C before imaging. For mast cell adoptive transfer experiments, RBL-2H3 cells were resuspended in BSS at $\sim 5 \times 10^7$ cells/ml and pre-warmed to 37°C. 50 µg Cell Trace™ far-red DDAO-SE (Invitrogen) was dissolved in DMSO to a final concentration of 10 mM, then added to the pre-warmed cells at 1:500, and incubated for 10 min at 37°C. Cells were then washed and injected in lateral tail vein of the rat post 13-17 days of infection. Next day, rats were euthanized and small intestines were collected. Small intestines were kept at 4°C in PBS, then segmented just before imaging. Small intestine segments were laid on an imaging apparatus covered with PBS. Z-series images were collected using custom built multiphoton confocal microscope (20) with a 780 nm illumination and 20x/0.95NA objective².

Results

RBL-2H3 mast cells cross the intestinal epithelial cell monolayer.

As a starting point to characterize the dynamics of mucosal mast cells and their intestinal mucosal tissue interactions, we explored interactions between RBL-2H3 mast

¹ Lisa Blum infected the rats and collected the small intestines in Dr. Judy Appleton's lab at Cornell University.

² Dr. Rebecca Williams collected the Z-series images using multiphoton microscopy.

cells and a rat intestinal epithelial cell line, SLC-44 (18). These epithelial cells polarize and form tight junctions when cultured on glass surfaces, orienting with the basolateral side attached to the glass surface and the apical surface facing media. We confirmed this by staining SLC-44 cells with antibody against tight junction specific protein Zona Occludens-1 (ZO-1) (Fig. 3.1), where ZO-1 clearly localized in between cell to cell junctions.

As shown in Figure 3.2, RBL mast cells were added from the top onto the apical side of polarized epithelial monolayers, and RBL-2H3 cells were distinguished from the SLC-44 cells by labeling Fc ϵ RI with Alexa488-IgE (Fig. 3.2A; Figure 3.2C shows a corresponding bright-field image of Figure 3.2A). Figure 3.2A and 3.2C show the first images of the time-lapse series (see Movie 3.1) with nine distinguishable fluorescently labeled RBL mast cells adhere on epithelial cell monolayer. Some of these cells show smaller cell bodies and large lamellopodia-like morphologies, suggesting cells in the process of transmigration. Figure 3.2B and 3.2D show the last images of the time-lapse series after 3 hours, and Alexa488-IgE labeled mast cells were still distinctly visible by fluorescence with more flattened morphology (Fig. 3.2B, arrows), but could not be observed in a corresponding bright-field image of the apical plane (Fig. 3.2D), suggesting that RBL mast cells migrated from the apical side to the basolateral side of the polarized epithelial monolayer (Fig. 3.2, arrows and Supplementary Movie 3.1). Movie 3.1 depicts transmigration of RBL-2H3 mast cells, where some of the cell bodies of mast cells get smaller as time proceeds and eventually “vanish” from the apical plane of the epithelial monolayers at the end of the movie. We observed average of 44.7 %

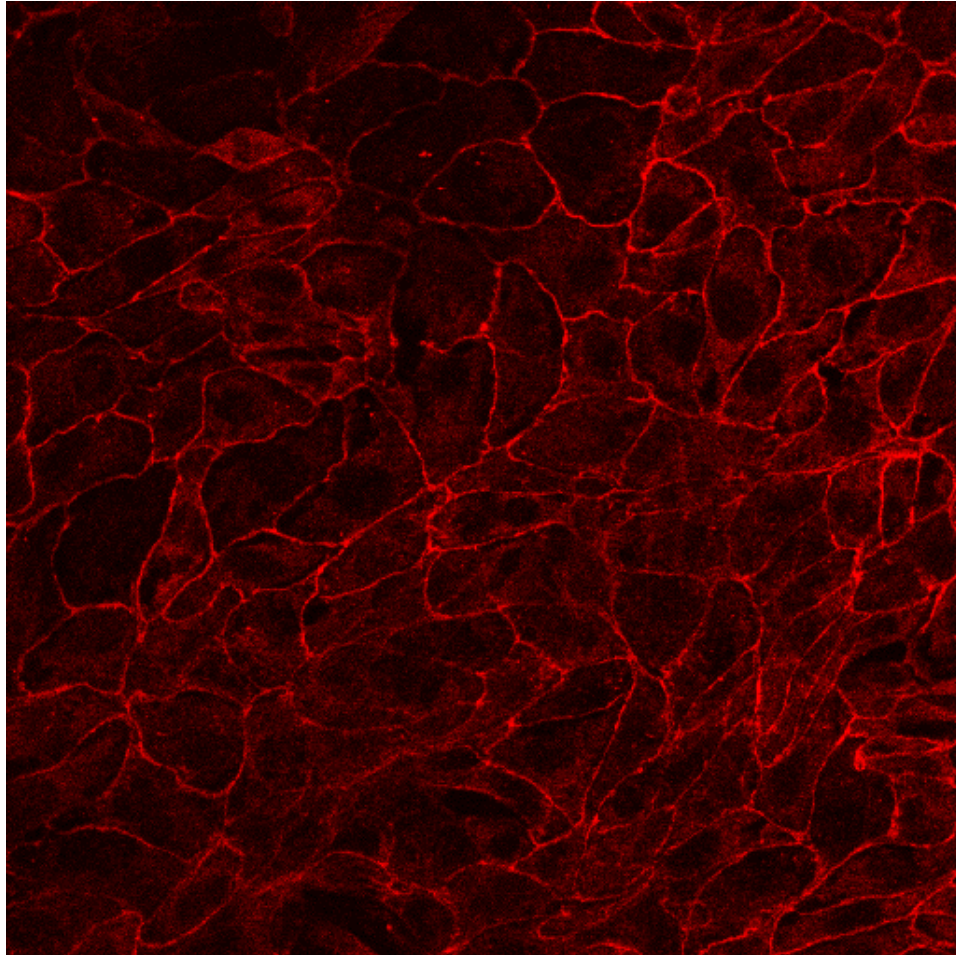


Figure 3.1. SLC-44 rat intestinal epithelial cell line makes tight junctions on a glass surface. Representative confocal image of SLC-44 cells. Cells were plated overnight, until they form monolayers, then fixed, permeablized, and labeled with anti-ZO1 and Alexa555-secondary antibody (red).

RBL mast cells out of total fluorescently labeled cells in the field undergoing transepithelial migration in 2 separate experiments (n = 29). In contrast, when fluorescently labeled RBL cells were introduced onto the top of the CHO cell monolayers, we did not observe this type of migration (data not shown), suggesting that this migratory behavior is a result of particular interactions between the RBL mast cells and SLC-44 intestinal epithelial monolayers. Although mast cells normally encounter epithelial cells from the basolateral side from the lamina propria of intestinal tissue, these results demonstrate that RBL cells have the capability to actively interact with intestinal epithelial cells.

Mast cells show transepithelial protrusions.

To assess whether mast cells can interact with polarized epithelial monolayer when they are introduced from the basolateral side of the SLC-44 cell monolayers, we utilized a transwell co-culture system (21). As shown in the schematic diagram in Figure 3.3, SLC-44 cells were first plated on top of inverted transwell insert at low density, then cultured for overnight to allow the cells to adhere firmly. This transwell insert was then inserted into a culture well in conventional orientation, such that the epithelial cells were attached to the bottom surface of the porous membrane. These cells were grown for 2 weeks in media with reduced FBS (5%) to form a monolayer with tight junctions. During this time, transepithelial electrical resistance (TER) was

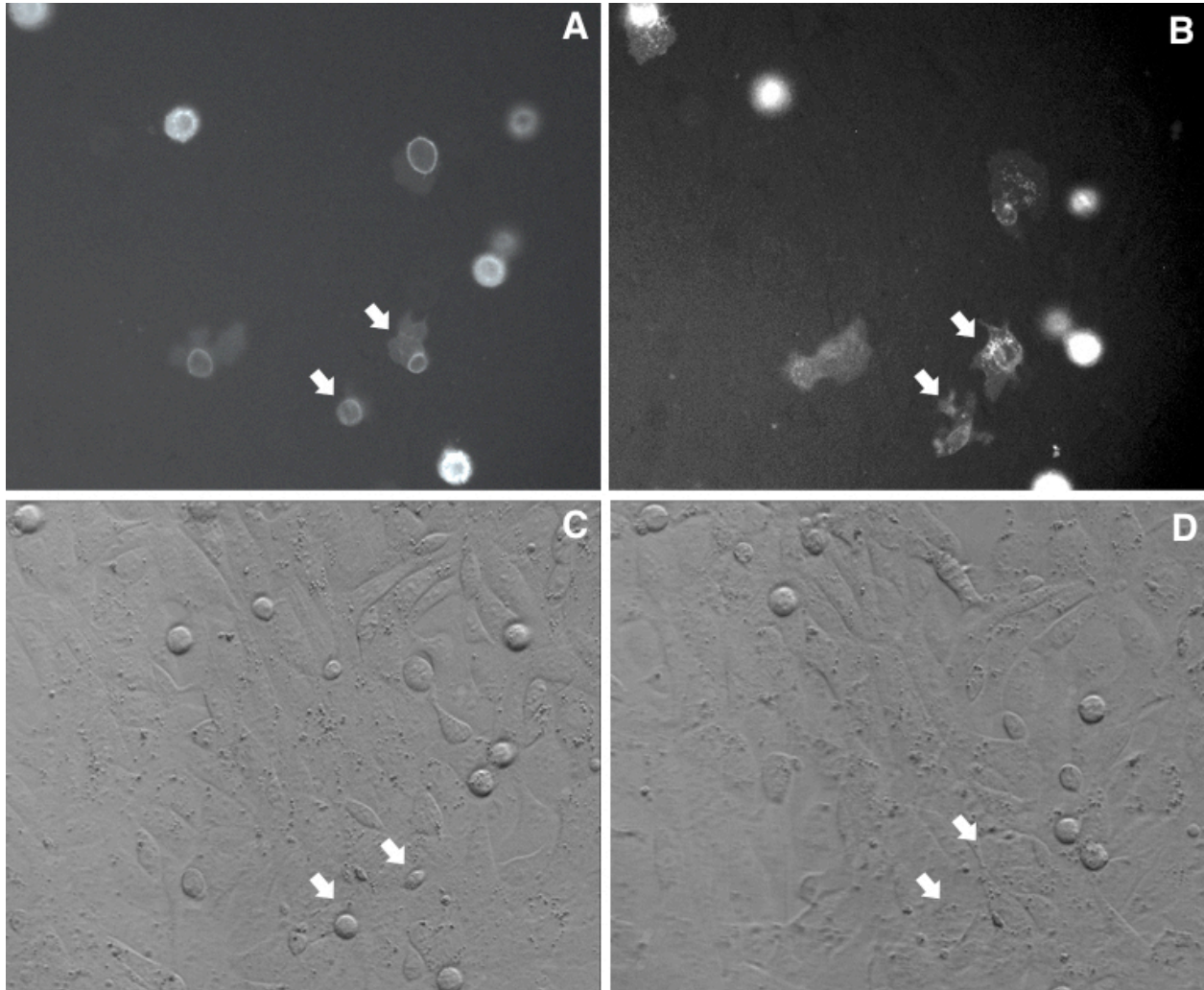


Figure 3.2. RBL-2H3 cells interacting with SLC-44 cell monolayers. Representative images of the RBL mast cells labeled with Alexa488-IgE (A, B) on SLC-44 cell monolayers (C, D), before (A, C) and after 3h at 37°C (B, D). Images correspond to the very first and the last images of Supplementary Movie 3.1. Arrows point to two RBL cells in (A) and (C) that clearly migrate to the basolateral side in (B) and (D).

measured to check the integrity of the epithelial monolayer (data not shown). After 2 weeks, fluorescently labeled mast cells were added to the upper chamber of the transwell insert at the upper surface of the porous membrane to introduce mast cells from the basolateral side of the polarized epithelial cell monolayer. The cells are then cultured for varying times, permitting mast cell migration through the porous membrane and interaction with the epithelial cell monolayer.

Figure 3.4 shows reconstructed Z-series images taken as optical cross-sections across the mast cells, transwell insert, and epithelial cells. A rat BMMC (yellow) found among the epithelial cells (red) with protrusions extending toward the porous membrane (Fig. 3.4, arrows) after ~20 hours of initial addition of labeled rat BMMCs. The porous membrane has autofluorescence that is seen as an orange/brown color with black pores in Figure 3.4. This data suggest that rat BMMC can cross the porous membrane towards the epithelial cells and interact with the epithelial cells. RBL-2H3 mast cells also interacted with SLC-44 cells in a similar way when they were added from the basolateral side and allowed to migrate (data now shown). Collectively, these data illustrate the occurrence of mast cell transepithelial migration with protrusions, further supporting the idea of dynamic interactions between mucosal mast cells and intestinal epithelial monolayers.

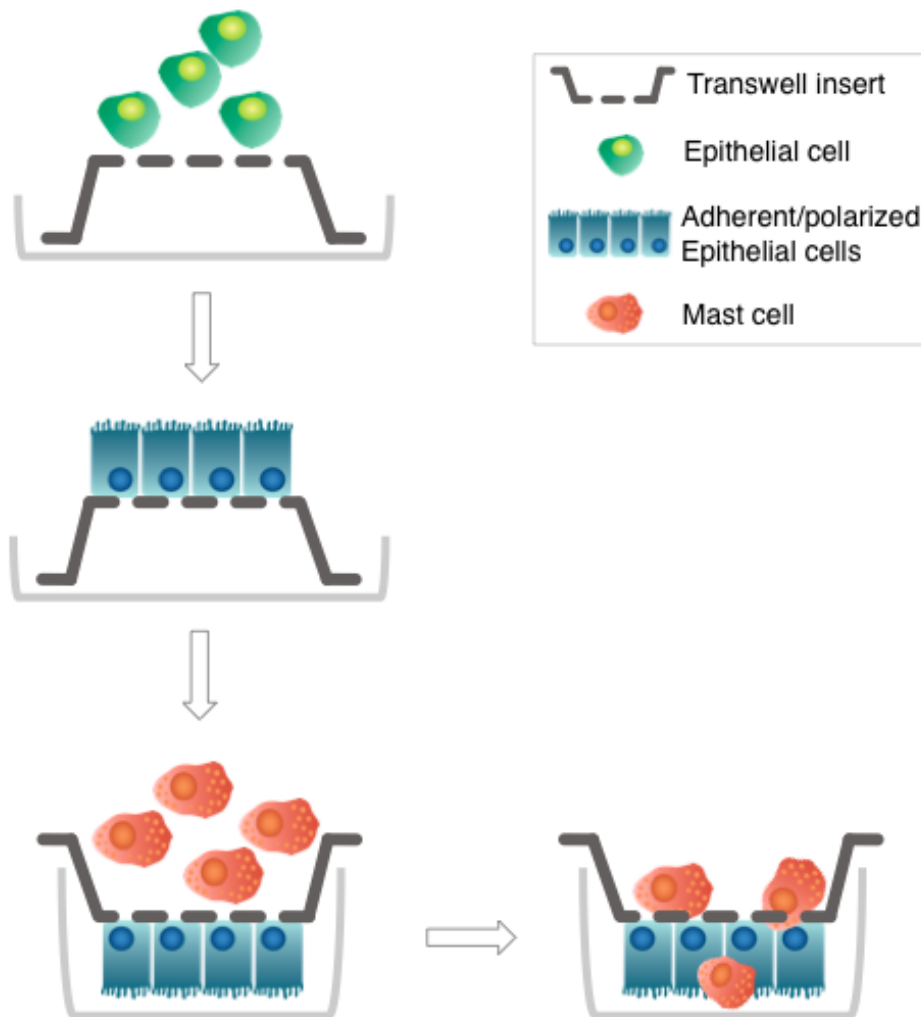


Figure 3.3. Schematic diagram of transwell transepithelial migration assay. SLC-44 cells were plated onto upside down transwell inserts with a porous membrane (5 μm pores). Next day, transwell inserts were hung in the normal orientation in 6 well culture plate with the basolateral side of the epithelial cells attached to the porous membrane, then the cells were cultured for additional 13 days. Fluorescently labeled mast cells were then introduced from the basolateral side and allowed to migrate overnight, fixed and labeled with anti-ZO-1, then Z-series images were collected with a confocal microscope.

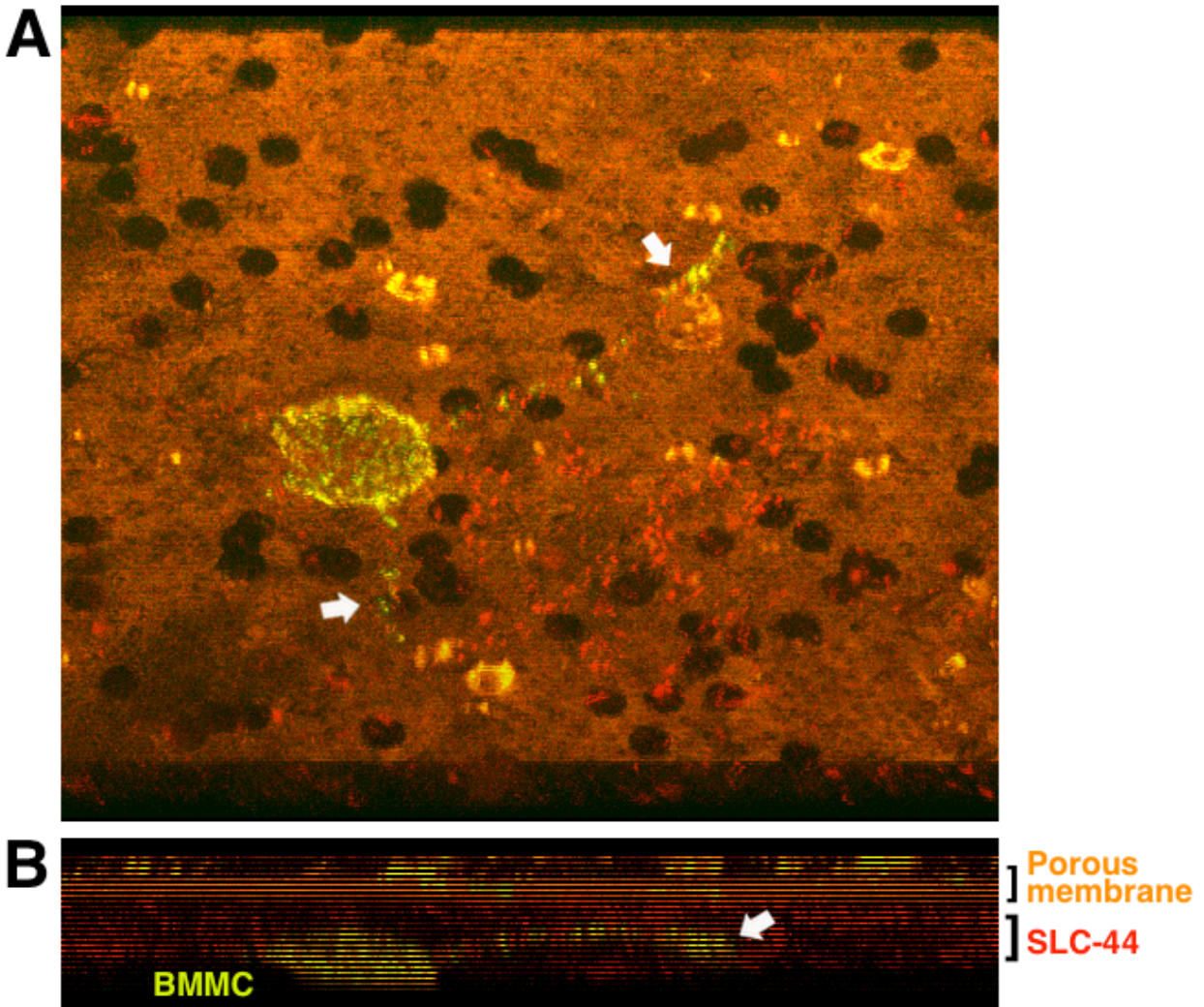


Figure 3.4. BMMCs interacting with SLC-44 cell monolayers. (A) A representative 3D projection image showing a rat BMMC with protrusions (arrows) that was labeled with Alexa488-anti-mast cell ganglioside mAb (yellow). This cell migrated across the porous membrane (orange), then from the basolateral to the apical side of an SLC-44 cell monolayer. (A) View from the tilted lower surface (apical side). (B) View from the side. Both images show the same field. Epithelial cells were labeled with anti-ZO-1 (red). Pore size = 5 μm.

***In situ* imaging of rat small intestine after *T. spiralis* infection.**

As shown above, we could detect transepithelial migration of mast cells *in vitro*, and we next determined whether we could observe mast cell interacting with epithelial cells in live tissue. Thus, we investigated mucosal mast cell migration *in situ* by carrying out multiphoton imaging of labeled mast cells in intestinal segments. For robust imaging, we took advantage of the *Trichinella spiralis* infection model of the rat, in which this infection causes intestinal mucosal mastocytosis, a local abnormal expansion of mucosal mast cells in the gut (6). Figure 3.5A shows a small intestine section pinned on a microscope stage and ready to be imaged. In initial experiments, we labeled intestinal segments separately with Alexa488-conjugated AA4 monoclonal antibody (mAb) and Alexa488-conjugated B5 anti-IgE mAb by incubating each tissue sections with antibody solution for at least 1 hour at 4°C. AA4 mAb binds specifically to a ganglioside only found on the surface of rat mast cells (16, 22), and B5 mAb is specific for rat IgE (17). AA4 mAb is exclusive for mast cells, whereas anti-IgE B5 mAb could label other IgE-bound cells in the gut, such as basophils. As shown in Figure 3.5B, a single cell is clearly surface-labeled by A488-AA4 (Fig. 3.5B, middle panel, arrow), and several cells appear to exhibit some green labeling after incubation with A488-B5 (Fig. 3.5B, right panel). Although we did observe occasional labeled cells consistent with endogenous mucosal mast cells in the epithelial villi, the labeling method employed was technically limiting in sufficient penetration of the antibody solution to label all the endogenous mast cells.

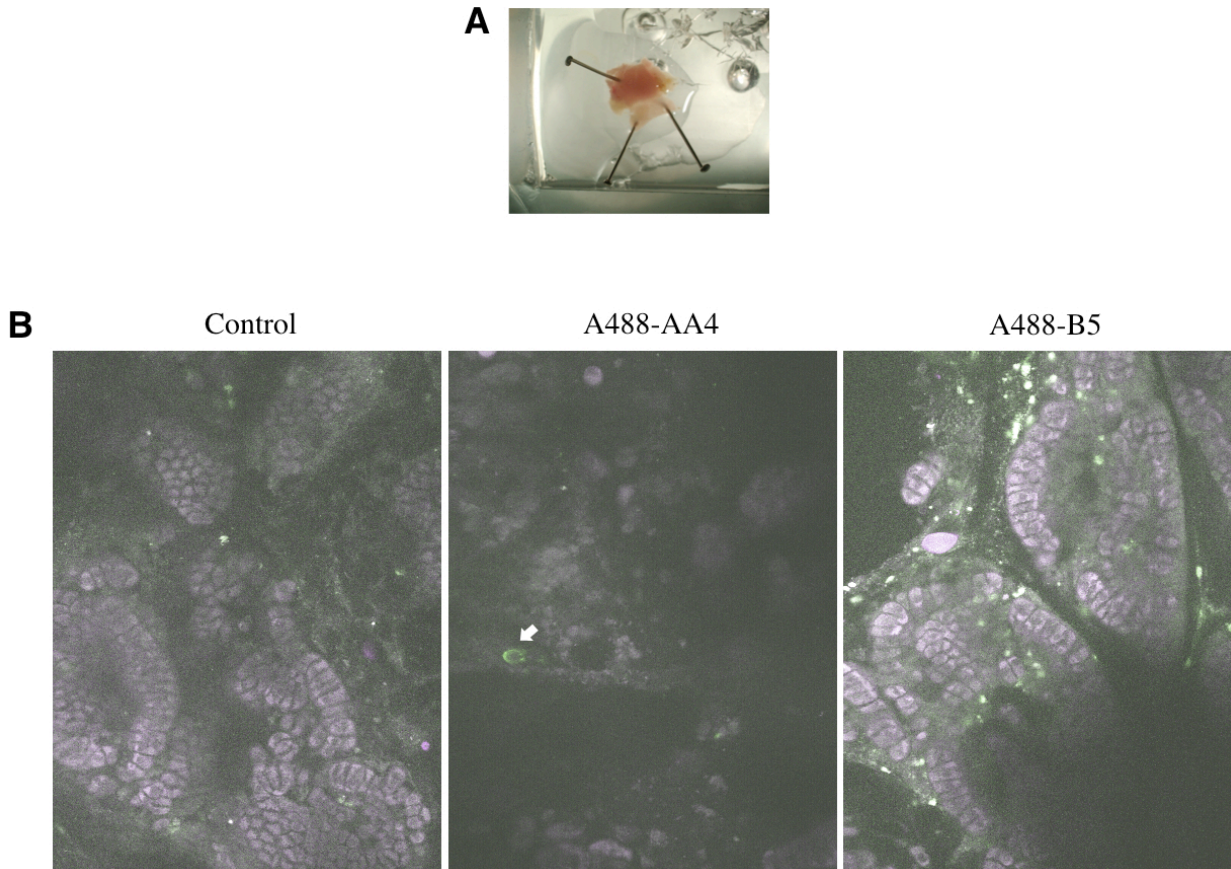


Figure 3.5. *In situ* multiphoton imaging of endogenous mast cells in *Trichinella*-infected rat small intestine. (A) Intact small intestine segment of a rat infected with *Trichinella spiralis* on a microscope stage. (B) Rats were infected with *T. spiralis* for 14 days, then small intestine sections were labeled with either Alexa488-AA4 monoclonal antibody, Alexa488-B5 anti-IgE monoclonal antibody, or incubated in PBS (Control) at 4°C for more than 1 hour. Images were taken using multiphoton confocal microscopy from the luminal side, and purple autofluorescent epithelial cells are seen in villi cross sections. 20x magnification.

To optimize visualizing conditions, we transferred previously labeled RBL-2H3 mast cells by tail vein injection, eliminating the issue of insufficient labeling of endogenous mast cells, and asked if we can see proper redistribution of RBL-2H3 mast cells to the mucosal tissue. As shown in Figure 3.6, we found labeled RBL mast cells that migrated to the intraepithelial region of duodenal segments (Fig. 3.5B, C, arrows), whereas we found only autofluorescent cells in sham-injected tissue segments (Fig. 3.6A). Figure 3.6C shows a blown-up image of the boxed region in Figure 3.6B. Taken together, these data provide evidence that RBL-2H3 mucosal mast cells can migrate into appropriate tissue sites where endogenous mucosal mast cells can also be found, and they appear to interact with mucosal intestinal tissue in the intraepithelial region in response to *T. spiralis* infection.

Discussion

A single layer of epithelial cells maintained by tight junctions (TJs) between cell covers the intestinal mucosa. Pathogenic viruses, bacteria, and parasites all take advantage of the chances for breaching the epithelial barrier by entering through junctions (23, 24). Intestinal infection by certain parasites, including *Trichinella spiralis*, induces mastocytosis throughout the effector phase of the inflammatory response. Friend et al., provided evidence that differentiated, tissue-residing mucosal mast cells that are found in submucosa or lamina propria of the intestine redistribute to the intraepithelial regions of the villi by examining histologic sections of jejunal tissue of

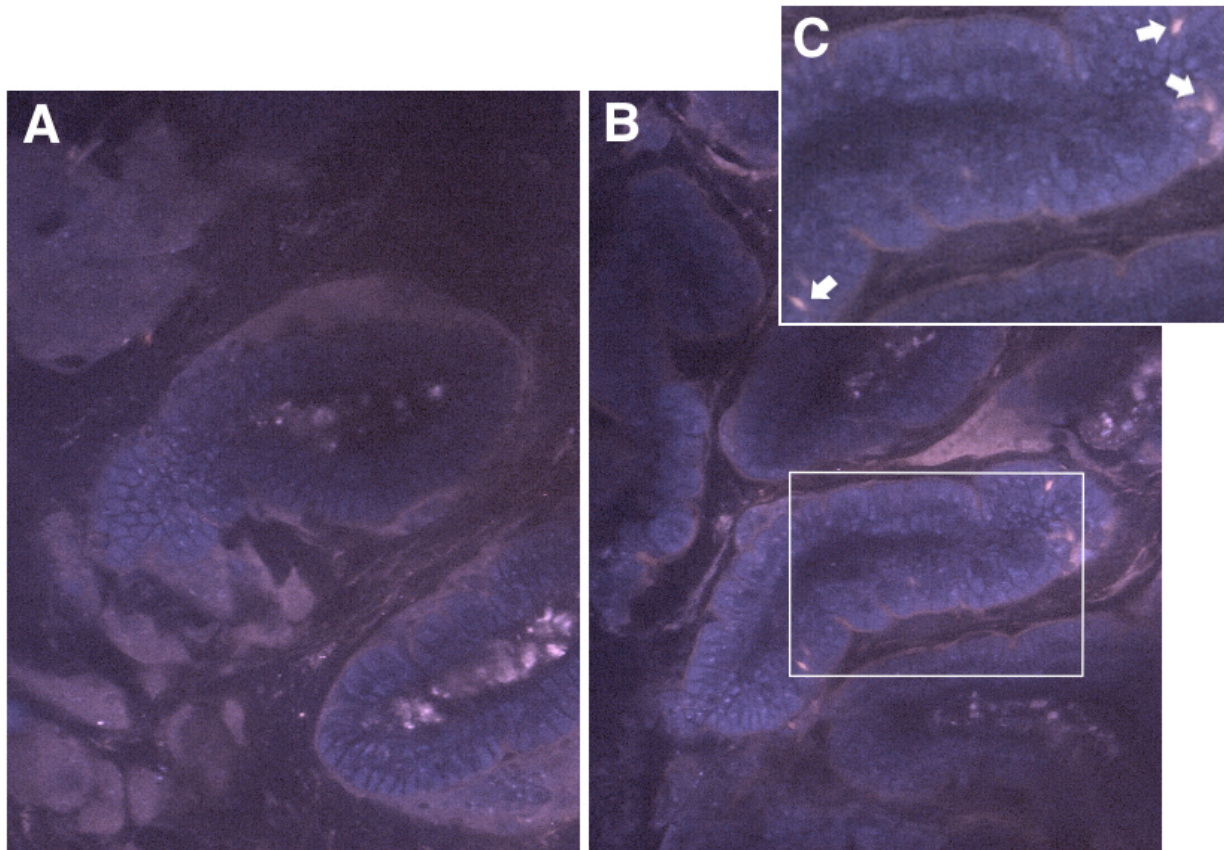


Figure 3.6. *In situ* multiphoton imaging of adoptively transferred RBL-2H3 mast cells in *Trichinella*-infected rat small intestine. Rats were infected with *T. spiralis* 14 days prior to i.v. tail vein injection of far-red DDAO-SE-labeled RBL cells (B), or media (A). 1 day after the injection, small intestine sections of live tissue were imaged. Pink autofluorescent cells in central lamina propria are seen in both samples, but pink DDAO-SE-labeled RBL cells between purple autofluorescent epithelial cells (C, arrows, zoomed-in section of boxed region in B) are seen only in (B) and (C). Images were taken using multiphoton confocal microscopy from the luminal side, and purple autofluorescent epithelial cells are seen in villi cross sections. 20x magnification.

T. spiralis infected mice (6), but very little is known about this process. In the current study, we demonstrated dynamic interactions between intestinal epithelia and mast cells *in vitro* and *in situ* by utilizing real-time imaging, a transwell co-culture system, and multiphoton microscopy.

We observed distinctive interactions between RBL-2H3 mast cells and polarized monolayers of the rat intestinal epithelial cell line SLC-44 (Fig. 3.2 and Supplementary Movie 3.1), in which the RBL mast cells displayed apical to basolateral transepithelial migration. It is known that MDCK epithelial cells grown on glass surfaces are polarized (25). Our data indicates that SLC-44 cells are polarized on glass surfaces as shown by their expression of the tight junction specific protein ZO-1 at cell-cell contacts (Fig. 3.1). Mucosal mast cells are preferentially located in the basolateral side of the intestinal epithelia *in vivo* (2). The Apical to basolateral crossing of mast cells that we observe (Fig. 3.2) could be a response to a homing signal from epithelial cells, or it could suggest the capability of mast cells to transmigrate in the direction of the luminal side of the intestine, then cross back to the lamina propria.

Transepithelial migration of other leukocytes has been observed previously (26-28). To assess whether mast cells can interact and undergo transepithelial migration when they are introduced from the basolateral side to mimic their *in vivo* niche, we utilized a transwell co-culture system (Fig. 3.3). When fluorescently labeled mast cells were added on the basolateral side of the polarized epithelial monolayers, we were able to visualize mast cells among the epithelial cells, suggesting transepithelial migration of mast cells (Fig. 3.4). Recently, a novel role for dendritic cells (DCs) in taking up bacteria

across the intestinal barrier was proposed (11, 29, 30). Specialized, myeloid-derived mucosal DCs were identified in the lamina propria of the intestine, with CX₃CR1 (fractalkine receptor)-dependent transepithelial dendrites poking through the intestinal lumen (30). These extensions have an unusual globular (30), or balloon (11) shape, and have been dynamically imaged *in vivo* (11). CX₃CR1 is a receptor for CX₃CL1 (fractalkine) that is expressed on the surfaces of intestinal epithelial cells and endothelial cells in the intestine (31, 32). It will be interesting to investigate whether the dynamic interactions we have observed between mast cells and intestinal epithelial monolayers are mediated by CX₃CR1 – CX₃CL1 interactions, and to characterize the surface components of the transepithelial protrusions of mast cells to gain more insights into their roles.

To further investigate the interactions between mucosal mast cells and intestinal epithelial cells, we imaged endogenous (Fig. 3.5) and adoptively transferred (Fig. 3.6) mast cells in the rat small intestine after *T. spiralis* infection *ex vivo*, using *in situ* multiphoton confocal microscopy. Even though we observed endogenous mast cells clearly surface-labeled with a fluorescently tagged antibody that binds to rat mast cell specific ganglioside, or cells labeled with Alexa488-rat anti-IgE antibody (Fig. 3.5), visualizing endogenous mast cells proved to be technically challenging. We did not see robust populations of fluorescently labeled mast cells by incubating the small intestine tissue sections with either fluorescently tagged anti-AA4 or anti-B5 monoclonal antibody. We suspected insufficient penetration of the antibody solution to the tissue, and subsequently decided to attempt injecting pre-labeled mast cells intravenously. As

shown in Figure 6, we observed transferred DDAO-SE labeled RBL-2H3 mast cells in the intraepithelial region of the intestinal villi. DDAO-SE labeled rat BMMCs were also injected to the rat in a parallel experiment (data not shown), but we observed more robust recruitment of RBL mast cells to the small intestine after *T. spiralis* infection. Dissimilar to RBL-2H3 cells, rat BMMCs do not express $\alpha_E\beta_7$ integrin subunit (D. Holowka, unpublished results), which is an integrin selectively expressed on mature intestinal mast cells that is likely to mediate their attachment to E-cadherin on epithelial cells of the gut (5). This could, at least in part, explain why we see less BMMCs recruited to the small intestine in response to *T. spiralis* infection when compared to RBL-2H3 recruitment. Together, these data suggest that mucosal mast cells actively interact with intestinal epithelial cells, possibly via the $\alpha_E\beta_7$ integrin that is present on these mast cells.

In summary, we provide evidence for RBL-2H3 mast cells and rat BMMCs interacting with SLC-44 rat intestinal epithelial monolayers when the mast cells are introduced from either the apical or basolateral side of the polarized epithelial monolayers using either real-time imaging or a transwell co-culture system. In these experiments, we observed dynamic crossing of mast cells from the apical to the basolateral side of the polarized epithelial monolayers. In addition, when mast cells are introduced from the basolateral side of the epithelial monolayers grown on a supported porous membrane filter, we found mast cells among the epithelial cells with transepithelial extensions, suggesting these mast cells have crossed the porous membrane and are interacting with the epithelial cells. We further investigated this

interaction *in situ*, and found endogenous mast cells as well as transferred mast cells redistributed to the intraepithelial regions of the intestinal villi in response to *T. spiralis* infection. Collectively, these data supports a dynamic, intimate interaction between mucosal mast cells and the epithelial layer that lines the intestinal interface.

REFERENCES

1. Abraham SN, St John AL. 2010. Mast cell-orchestrated immunity to pathogens. *Nat Rev Immunol* 10: 440-52
2. Miller HR, Pemberton AD. 2002. Tissue-specific expression of mast cell granule serine proteinases and their role in inflammation in the lung and gut. *Immunology* 105: 375-90
3. Groschwitz KR, Ahrens R, Osterfeld H, Gurish MF, Han X, Abrink M, Finkelman FD, Pejler G, Hogan SP. 2009. Mast cells regulate homeostatic intestinal epithelial migration and barrier function by a chymase/Mcpt4-dependent mechanism. *Proc Natl Acad Sci U S A* 106: 22381-6
4. McDermott JR, Bartram RE, Knight PA, Miller HR, Garrod DR, Grecis RK. 2003. Mast cells disrupt epithelial barrier function during enteric nematode infection. *Proc Natl Acad Sci U S A* 100: 7761-6
5. Hallgren J, Gurish MF. 2007. Pathways of murine mast cell development and trafficking: tracking the roots and routes of the mast cell. *Immunol Rev* 217: 8-18
6. Friend DS, Ghildyal N, Austen KF, Gurish MF, Matsumoto R, Stevens RL. 1996. Mast cells that reside at different locations in the jejunum of mice infected with *Trichinella spiralis* exhibit sequential changes in their granule ultrastructure and chymase phenotype. *J Cell Biol* 135: 279-90
7. Brightling CE, Bradding P, Symon FA, Holgate ST, Wardlaw AJ, Pavord ID. 2002. Mast-cell infiltration of airway smooth muscle in asthma. *N Engl J Med* 346: 1699-705
8. Anderson JM. 2001. Molecular structure of tight junctions and their role in epithelial transport. *News Physiol Sci* 16: 126-30
9. Tsukita S, Furuse M, Itoh M. 1999. Structural and signalling molecules come together at tight junctions. *Curr Opin Cell Biol* 11: 628-33

10. Porter JC. 2008. Epithelial Rho GTPases and the transepithelial migration of lymphocytes. *Methods Enzymol* 439: 205-17
11. Chieppa M, Rescigno M, Huang AY, Germain RN. 2006. Dynamic imaging of dendritic cell extension into the small bowel lumen in response to epithelial cell TLR engagement. *J Exp Med* 203: 2841-52
12. Seldin DC, Adelman S, Austen KF, Stevens RL, Hein A, Caulfield JP, Woodbury RG. 1985. Homology of the rat basophilic leukemia cell and the rat mucosal mast cell. *Proc Natl Acad Sci U S A* 82: 3871-5
13. MacDonald AJ, Pick J, Bissonnette EY, Befus AD. 1998. Rat mucosal mast cells: the cultured bone marrow-derived mast cell is biochemically and functionally analogous to its counterpart in vivo. *Immunology* 93: 533-9
14. Posner RG, Lee B, Conrad DH, Holowka D, Baird B, Goldstein B. 1992. Aggregation of IgE-receptor complexes on rat basophilic leukemia cells does not change the intrinsic affinity but can alter the kinetics of the ligand-IgE interaction. *Biochemistry* 31: 5350-6
15. Gosse JA, Wagenknecht-Wiesner A, Holowka D, Baird B. 2005. Transmembrane sequences are determinants of immunoreceptor signaling. *J Immunol* 175: 2123-31
16. Guo NH, Her GR, Reinhold VN, Brennan MJ, Siraganian RP, Ginsburg V. 1989. Monoclonal antibody AA4, which inhibits binding of IgE to high affinity receptors on rat basophilic leukemia cells, binds to novel alpha-galactosyl derivatives of ganglioside GD1b. *J Biol Chem* 264: 13267-72
17. Baniyash M, Alkalay I, Eshhar Z. 1987. Monoclonal antibodies specific to the alpha-subunit of the mast cell's Fc epsilon R block IgE binding and trigger histamine release. *J Immunol* 138: 2999-3004
18. Chastre E, Empereur S, Di Gioia Y, el Mahdani N, Mareel M, Vleminckx K, Van Roy F, Bex V, Emami S, Spandidos DA, et al. 1993. Neoplastic progression of human and rat intestinal cell lines after transfer of the ras and polyoma middle T oncogenes. *Gastroenterology* 105: 1776-89

19. Blum LK, Thrasher SM, Gagliardo LF, Fabre V, Appleton JA. 2009. Expulsion of secondary *Trichinella spiralis* infection in rats occurs independently of mucosal mast cell release of mast cell protease II. *J Immunol* 183: 5816-22
20. Zipfel WR, Williams RM, Christie R, Nikitin AY, Hyman BT, Webb WW. 2003. Live tissue intrinsic emission microscopy using multiphoton-excited native fluorescence and second harmonic generation. *Proc Natl Acad Sci U S A* 100: 7075-80
21. Estienne V, Brisbarre N, Blanchin S, Durand-Gorde JM, Carayon P, Ruf J. 2004. An in vitro model based on cell monolayers grown on the underside of large-pore filters in bicameral chambers for studying thyrocyte-lymphocyte interactions. *Am J Physiol Cell Physiol* 287: C1763-8
22. Basciano LK, Berenstein EH, Kmak L, Siraganian RP. 1986. Monoclonal antibodies that inhibit IgE binding. *J Biol Chem* 261: 11823-31
23. Bergelson JM. 2009. Intercellular junctional proteins as receptors and barriers to virus infection and spread. *Cell Host Microbe* 5: 517-21
24. O'Hara JR, Buret AG. 2008. Mechanisms of intestinal tight junctional disruption during infection. *Front Biosci* 13: 7008-21
25. Kreitzer G, Schmoranzler J, Low SH, Li X, Gan Y, Weimbs T, Simon SM, Rodriguez-Boulan E. 2003. Three-dimensional analysis of post-Golgi carrier exocytosis in epithelial cells. *Nat Cell Biol* 5: 126-36
26. Cramer EB, Milks LC, Ojakian GK. 1980. Transepithelial migration of human neutrophils: an in vitro model system. *Proc Natl Acad Sci U S A* 77: 4069-73
27. Taguchi M, Sampath D, Koga T, Castro M, Look DC, Nakajima S, Holtzman MJ. 1998. Patterns for RANTES secretion and intercellular adhesion molecule 1 expression mediate transepithelial T cell traffic based on analyses in vitro and in vivo. *J Exp Med* 187: 1927-40
28. Liu L, Zuurbier AE, Mul FP, Verhoeven AJ, Lutter R, Knol EF, Roos D. 1998. Triple role of platelet-activating factor in eosinophil migration across monolayers

- of lung epithelial cells: eosinophil chemoattractant and priming agent and epithelial cell activator. *J Immunol* 161: 3064-70
29. Rescigno M, Urbano M, Valzasina B, Francolini M, Rotta G, Bonasio R, Granucci F, Kraehenbuhl JP, Ricciardi-Castagnoli P. 2001. Dendritic cells express tight junction proteins and penetrate gut epithelial monolayers to sample bacteria. *Nat Immunol* 2: 361-7
 30. Niess JH, Brand S, Gu X, Landsman L, Jung S, McCormick BA, Vyas JM, Boes M, Ploegh HL, Fox JG, Littman DR, Reinecker HC. 2005. CX3CR1-mediated dendritic cell access to the intestinal lumen and bacterial clearance. *Science* 307: 254-8
 31. Muehlhoefer A, Saubermann LJ, Gu X, Luedtke-Heckenkamp K, Xavier R, Blumberg RS, Podolsky DK, MacDermott RP, Reinecker HC. 2000. Fractalkine is an epithelial and endothelial cell-derived chemoattractant for intraepithelial lymphocytes in the small intestinal mucosa. *J Immunol* 164: 3368-76
 32. Lucas AD, Chadwick N, Warren BF, Jewell DP, Gordon S, Powrie F, Greaves DR. 2001. The transmembrane form of the CX3CL1 chemokine fractalkine is expressed predominantly by epithelial cells in vivo. *Am J Pathol* 158: 855-66

CHAPTER 4

SUMMARY AND FUTURE DIRECTIONS

Cell migration is a foundational function in biology, and has been of avid interest of the scientific field for many years. For immune cells, motility is one of the key mechanisms to efficiently mount immune responses, including infiltration to inflammatory sites and relaying immunological information. Although homing of mast cell progenitors is relatively well characterized (1), many questions still remain unanswered in regard to migration of differentiated mast cells. This dissertation describes molecular mechanisms of basal and directed migration of mast cells. Below are summarized major findings and proposed future directions.

RBL-2H3 mast cells and rat bone marrow-derived mast cells (BMMCs) show spontaneous migration on glass surfaces, including often when the cell bodies move back and forth between the tracks defined by their protrusions. These two kinds of mast cells show similar motility characteristics: they adhere to glass surfaces, have extended protrusions on glass surfaces when plated at a low density, have roughly similar motility coefficients under the same condition, and their motility depends on actin polymerization. Similar to other leukocytes, the motility of RBL mast cells depends on Rho family GTPases and PI3K, which are both considered to be central regulators of cell motility in various cells types (2, 3). However, RBL cell motility was unaffected by PKC

inhibition, suggesting selectivity in the intracellular signaling pathways regulating mast cell motility.

During the course of this thesis work, we developed an imaging method to visualize mast cell chemotaxis in real-time video microscopy. Although mast cell chemotaxis toward antigen has been previously shown using a more traditional modified Boyden chamber assay, molecular mechanisms underlying this process are not yet well understood, and this method commonly suffers from the limitation that only a low percentage of cells actually migrate across the permeable membrane. We demonstrate that RBL mast cells and rat BMMCs show directed migration toward antigen in a dose dependent manner, with RBL mast cells showing a maximal response to 10 ng/ml antigen using real-time imaging. We provide evidence that Syk tyrosine kinase and Ca^{2+} mobilization are involved in regulating both spontaneous migration and chemotaxis of mast cells toward antigen.

Syk- mutant RBL cells exhibit impaired basal motility and chemotaxis toward antigen. Syk- cells show a modest reduction of about 30% in basal motility when compared to normal RBL cells, and they show a more severe reduction in chemotaxis toward antigen. To further gain insights to the role of Syk kinase in mast cell motility, chemotaxis of Syk- cells toward another chemoattractant besides antigen should be investigated to assess whether Syk requirement is specific to chemotaxis toward antigen or is more universal.

Inhibiting Ca^{2+} mobilization by either withdrawing extracellular Ca^{2+} from the environment or inhibiting Ca^{2+} influx reduces both basal motility and chemotaxis of mast cells toward antigen. Furthermore, knocking down Ca^{2+} entry channel protein Orai1 using shRNA inhibits both of these processes, further providing evidence that Ca^{2+} influx via Orai1 is important in regulating mast cell migration. Similarly to Syk-cells, Orai1 knock down in RBL mast cells causes a modest reduction in their motility coefficient but results in rather severely impaired chemotaxis toward antigen. We observed that chemotaxis of RBL mast cells toward S1P is independent of extracellular Ca^{2+} , suggesting that Ca^{2+} influx through Orai1 seems to play a more selective role in chemotaxis toward antigen. One approach to dissect the involvement of Ca^{2+} mobilization in mast cell chemotaxis is to investigate chemotaxis of either STIM1 or TRPC1 knocked down mast cells. Even though we did not observe severe inhibition in basal motility of either STIM1 or TRPC1 knocked down RBL mast cells, we cannot rule out the possibility of STIM1 or TRPC1 involvement in cell motility due to the limitations of knock down in our cells. Another approach is to investigate chemokinesis of either Syk-cells or RBL mast cells under Ca^{2+} mobilization inhibitory conditions, when they have chemoattractant in both directions, so the chemoattractant is present but gradient is absent. These approaches will help to further dissect the roles for Syk kinase and Ca^{2+} mobilization in regulating different steps of chemotaxis, including cell motility such as velocity, and sensing and turning of cells towards a chemotactic gradient.

We previously described the participation of TRPC channels in specifying initiation site of Ca^{2+} response (4). In particular, knockdown of TRPC1 and TRPC3 in this study shifted the site of Ca^{2+} wave initiation in response to antigen stimulation from cell protrusions to the cell body. This thesis work provides evidence for previously uncharacterized, spontaneous Ca^{2+} transients using genetically encoded Ca^{2+} sensor GCaMP3 and fast confocal imaging. We demonstrate that these Ca^{2+} transients are often found in cell protrusions, and are dependent on Ca^{2+} influx. In addition, when the same inhibitors of Ca^{2+} influx are used, Ca^{2+} transients have a similar pattern of inhibition as basal motility of mast cells, suggesting a potential correlation between cell motility and Ca^{2+} transients. It will be interesting to investigate the effects of Orai1, TRPC1, and STIM1 knockdown on these Ca^{2+} transients. Wei et al. reported that Ca^{2+} flickers promote turning of migrating fibroblasts, and that asymmetric Ca^{2+} flickers develop when migrating fibroblasts were exposed to a chemoattractant gradient (5). We made some attempts to correlate Ca^{2+} transients and cell motility by observing the movements of cell bodies while imaging Ca^{2+} transients, and noticed some tendency of cell bodies trying to move toward the direction of Ca^{2+} transients localized in cell protrusions. However, it was hard to observe prominent movements of cell bodies in a relatively shorter amount of observation time for Ca^{2+} transients (20 min). One solution might be to employ asymmetry-triggering signals such as a chemoattractant gradient to spatially coordinate the Ca^{2+} transients by observing Ca^{2+} transients of chemotaxing cells.

Redistribution of differentiated, tissue-residing mucosal mast cells in response to *T. spiralis* infection has been described several decades ago, yet this area of mast cell biology is understudied. In this dissertation, we further investigate mast cell migration in relation to their potential functions *in vivo*. We observe transepithelial migration of mast cells through polarized intestinal epithelial monolayers using real-time imaging and transwell co-culture system. Furthermore, we observe endogenous and adoptively transferred mast cells in the intraepithelial region of intestinal villi in response to *T. spiralis* infection *in situ* using multiphoton microscopy. One approach to further characterize this process *in vitro* is to investigate the chemotaxis of mast cells toward *Trichinella* antigen when cells are sensitized with anti-*Trichinella* IgE. In addition, given that we observed chemotaxis of mast cells toward DNP-BSA when cells are sensitized to anti-DNP IgE, monitoring transepithelial migration of mast cells when either DNP-BSA or *Trichinella* antigen is present in the lower part of the transwell transmigration assay system to generate a gradient of DNP-BSA or *Trichinella* antigen would permit us to test whether these mast cells can respond to an antigen gradient in this more physiologically relevant situation.

Single cell migration can be categorized into two types: amoeboid and mesenchymal. Amoeboid migration mimics features of the single cell behavior of the amoeba *Dictyostelium discodium*. In higher eukaryotes, hematopoietic stem cells, leukocytes, and certain tumor cells are known to use amoeboid migration, which is a fast 'crawling' type of movement that is driven by short-lived and relatively weak

interactions with the substrate (6, 7). In 3D environment, mesenchymal cells such as fibroblasts, myoblasts, single endothelial cells or sarcoma cells have a spindle-shaped, fibroblast-like morphology (8, 9). The elongated morphology is dependent on integrin-mediated adhesion dynamics and the presence of high traction forces (9, 10). In this dissertation, we observed mast cell morphology that is reminiscent of cell types with mesenchymal migration but with some heterogeneity, in which a subpopulation of cells show more amoeboid-like, faster migration. Literature suggests plasticity in the transition between amoeboid and mesenchymal migration, especially with changes in cell state and environmental conditions (11, 12).

In recent years, differences and similarities between cell migration in two-dimensional (2D) and three-dimensional (3D) environments have received growing interest. It was reported that cells have 3D interactions *in vivo* that are absent in 2D cell culture, which can affect cell migration (13). Using micropatterning technique to generate 1D fibrillar patterns to mimic 3D environment, Doyle et al. demonstrated that, in contrast to 2D, fibroblast migration is more rapid, dependent on myosin II contractility and microtubules, but independent of extracellular matrix (ECM) ligand density in 1D fibrillar patterns and in 3D (14). In 3D, dendritic cells migrate using myosin II dependent contraction when passing through narrow gaps, where a squeezing contraction of the trailing edge propels the rigid nucleus in an integrin independent manner (15). With respect to plasticity in mesenchymal and amoeboid migration, and differences in 2D versus 3D cell migration, further insight regarding mast cell migration might come from characterizing molecular mechanisms of mast cell basal motility and

chemotaxis in 3D. Modifying the real-time imaging methods described in this dissertation to accommodate 3D migration may help elucidate mechanisms and physiological functions of mast cell migration.

REFERENCES

1. Hallgren J, Gurish MF. 2007. Pathways of murine mast cell development and trafficking: tracking the roots and routes of the mast cell. *Immunol Rev* 217: 8-18
2. Etienne-Manneville S. 2004. Cdc42--the centre of polarity. *J Cell Sci* 117: 1291-300
3. Kolsch V, Charest PG, Firtel RA. 2008. The regulation of cell motility and chemotaxis by phospholipid signaling. *J Cell Sci* 121: 551-9
4. Cohen R, Torres A, Ma HT, Holowka D, Baird B. 2009. Ca²⁺ waves initiate antigen-stimulated Ca²⁺ responses in mast cells. *J Immunol* 183: 6478-88
5. Wei C, Wang X, Chen M, Ouyang K, Song LS, Cheng H. 2009. Calcium flickers steer cell migration. *Nature* 457: 901-5
6. Friedl P, Borgmann S, Brocker EB. 2001. Amoeboid leukocyte crawling through extracellular matrix: lessons from the Dictyostelium paradigm of cell movement. *J Leukoc Biol* 70: 491-509
7. Wang W, Wyckoff JB, Frohlich VC, Olynykov Y, Huttelmaier S, Zavadil J, Cermak L, Bottinger EP, Singer RH, White JG, Segall JE, Condeelis JS. 2002. Single cell behavior in metastatic primary mammary tumors correlated with gene expression patterns revealed by molecular profiling. *Cancer Res* 62: 6278-88
8. Grinnell F. 1994. Fibroblasts, myofibroblasts, and wound contraction. *J Cell Biol* 124: 401-4
9. Tamariz E, Grinnell F. 2002. Modulation of fibroblast morphology and adhesion during collagen matrix remodeling. *Mol Biol Cell* 13: 3915-29
10. Ballestrem C, Hinz B, Imhof BA, Wehrle-Haller B. 2001. Marching at the front and dragging behind: differential alphaVbeta3-integrin turnover regulates focal adhesion behavior. *J Cell Biol* 155: 1319-32

11. Mishima T, Naotsuka M, Horita Y, Sato M, Ohashi K, Mizuno K. 2010. LIM-kinase is critical for the mesenchymal-to-amoeboid cell morphological transition in 3D matrices. *Biochem Biophys Res Commun* 392: 577-81
12. Wolf K, Mazo I, Leung H, Engelke K, von Andrian UH, Deryugina EI, Strongin AY, Brocker EB, Friedl P. 2003. Compensation mechanism in tumor cell migration: mesenchymal-amoeboid transition after blocking of pericellular proteolysis. *J Cell Biol* 160: 267-77
13. Even-Ram S, Yamada KM. 2005. Cell migration in 3D matrix. *Curr Opin Cell Biol* 17: 524-32
14. Doyle AD, Wang FW, Matsumoto K, Yamada KM. 2009. One-dimensional topography underlies three-dimensional fibrillar cell migration. *J Cell Biol* 184: 481-90
15. Lammermann T, Bader BL, Monkley SJ, Worbs T, Wedlich-Soldner R, Hirsch K, Keller M, Forster R, Critchley DR, Fassler R, Sixt M. 2008. Rapid leukocyte migration by integrin-independent flowing and squeezing. *Nature* 453: 51-5

APPENDIX A

CHARACTERIZING MOTILITY OF RBL MAST CELLS ON DIFFERENT SUBSTRATES

Cell adhesion to the extracellular matrix (ECM) is essential for fundamental cellular processes such as survival, migration, and differentiation. Cell migration is regulated, in part, by the mechanical environment surrounding the cells. Cells in tissues are connected to their surrounding ECM by transmembrane integrin adhesion proteins. ECM ligand binds to the extracellular domain of integrins (1, 2), while the intracellular domain connects the plasma membrane to the actin cytoskeleton through various signaling complexes (3, 4). Changes in substrate stiffness are critical mechanical regulators of cell behavior for many cell types. Matrix stiffness can promote smooth muscle cell migration (5), stem cell differentiation (6), neuronal growth (7). Endothelial cells use traction forces to mechanically communicate through their substrate, and cells migrate towards each other to form cell-cell connections on sufficiently compliant substrates (8, 9). To understand the role of the mechanical properties and ligand density of matrix in regulating mast cell motility, we characterized mast cell spontaneous migration on different substrates using matrices of tailored stiffness and matrix presentation¹.

¹ These substrates were prepared in Dr. Cynthia Reinhart-King's lab at Cornell University.

Materials and Methods

Polyacrylamide gel fabrication

Polyacrylamide substrates were fabricated as previously described (10). Briefly, substrate stiffness was adjusted between 1 kPa and 10 kPa by changing the ratio of acrylamide to bis-acrylamide, then polyacrylamide gels were covalently bound to glutaraldehyde-activated glass coverslips. RGD peptide or Type I collagen (BD Biosciences) was covalently bound to the polyacrylamide gel using a bi-functional linker (10).

Motility assay

The polyacrylamide gel substrates bound to glass coverslips were put inside 35 mm culture dish, and RBL mast cells were plated at a low density onto the polyacrylamide gels. Next day, coverslips were imaged for 1.5 h in media while collecting images every 2 min. Cell motility was analyzed as described in Chapter 2.

Results and Discussion

As shown in Figure A.1, RBL mast cells plated on 1 kPa substrate without covalently linked ligand exhibit similar morphology to the cells plated on glass surfaces as shown in Chapter 2, often with the extended protrusions. However, cells plated on stiffer substrates of 2.5 kPa and 5 kPa without ligand rarely exhibit extended

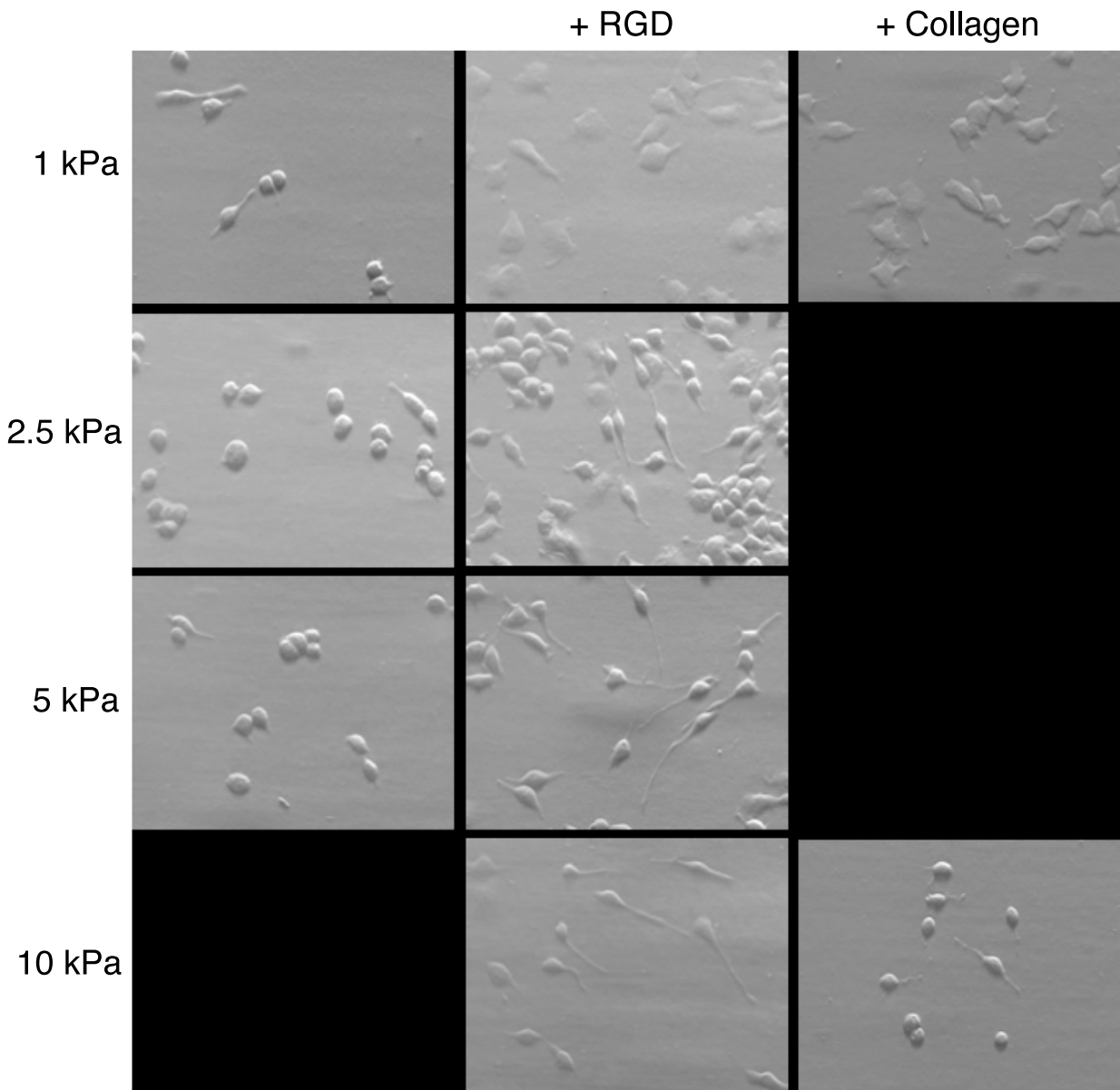


Figure A.1. Morphology of RBL mast cells on different substrates. Representative images showing morphology of RBL-2H3 mast cells on different substrates. Cells were plated on polyacrylamide gel substrate without any covalently linked ligand in different stiffness indicated by kPa on left. +RGD: polyacrylamide gel substrates covalently bound to RGD peptide. +Collagen: polyacrylamide gel substrates covalently bound to type I collagen.

protrusions and are generally rounded in their shape. In a stark contrast to this morphology, cells plated on substrates stiffer than 2.5 kPa that have been covalently linked with RGD peptide, which is a binding recognition sequence for integrins, exhibit longer and more prominent protrusions. RBL mast cells show more flattened and spread-out morphologies on compliant 1 kPa substrate that has been covalently linked with either RGD peptide or type I collagen (Fig. A.1), and these cells moved as if they were partly sinking to the gel substrates (data not shown). These data suggest that substrate stiffness and ligand composition affects mast cell morphology.

We also monitored spontaneous migration of RBL-2H3 mast cells on different substrates. Compared to the cells on substrates without ligand, cells show enhanced motility when they were on substrates with covalently linked ligand, as well as when they were on stiffer substrates (Fig. A.2). With substrate stiffness of 1 kPa and 10 kPa, cells on type I collagen linked substrates show about 4-fold higher average motility coefficients when compared to the cells on RGD peptide linked substrates, suggesting that under these conditions, collagen promotes spontaneous migration of mast cells more substantially. Taking into consideration that fibronectin-RGD motif has been previously shown to preferentially bind $\alpha 5\beta 1$ and $\alpha V\beta 3$ integrins (8, 9), and collagen to $\alpha 2\beta 1$ integrin (10), these results suggest a possibility of $\alpha 2\beta 1$ integrin involvement in regulating RBL mast cell migration.

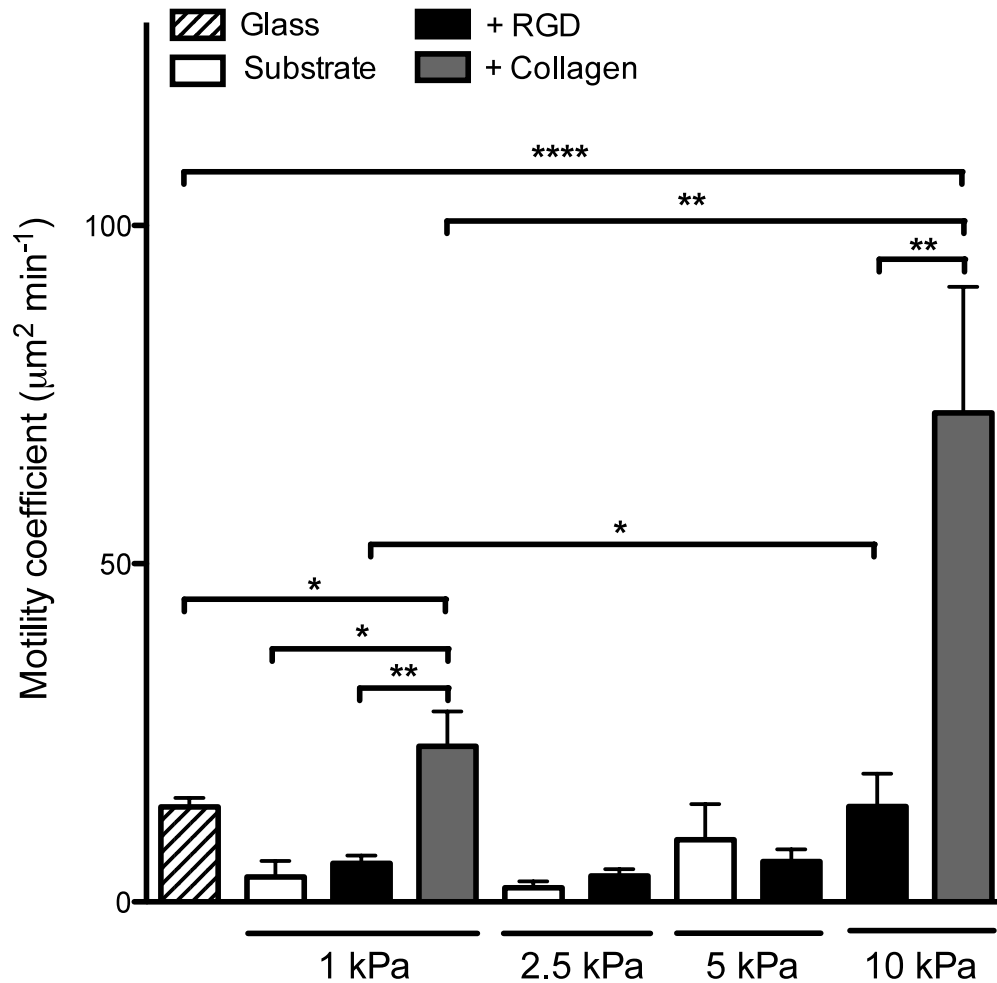


Figure A.2. Motility of RBL mast cells on different substrates. Spontaneous migration of RBL-2H3 cells plated on various polyacrylamide substrates was monitored for 1.5 h in media. Average motility coefficients are shown \pm SEM ($n = 8 - 35$ cells per each condition). Glass (striped bar): glass surface without polyacrylamide gel substrates. Substrate (white bars): polyacrylamide gel substrates without any covalently linked ligand. +RGD (black bars): polyacrylamide gel substrates covalently bound to RGD peptide. +Collagen (grey bars): polyacrylamide gel substrates covalently bound to type I collagen. Stiffness of the substrates is indicated below by kPa. * $P < 0.05$, ** $P < 0.01$ between indicated conditions.

In summary, these data suggest that mast cell morphology and motility are influenced by the mechanical characteristics such as stiffness of the substrates they are on, as well as by ECM composition.

REFERENCES

1. Humphries MJ. 2000. Integrin structure. *Biochem Soc Trans* 28: 311-39
2. Humphries JD, Byron A, Humphries MJ. 2006. Integrin ligands at a glance. *J Cell Sci* 119: 3901-3
3. Zaidel-Bar R, Itzkovitz S, Ma'ayan A, Iyengar R, Geiger B. 2007. Functional atlas of the integrin adhesome. *Nat Cell Biol* 9: 858-67
4. Byron A, Morgan MR, Humphries MJ. 2010. Adhesion signalling complexes. *Curr Biol* 20: R1063-7
5. Peyton SR, Putnam AJ. 2005. Extracellular matrix rigidity governs smooth muscle cell motility in a biphasic fashion. *J Cell Physiol* 204: 198-209
6. Engler AJ, Sen S, Sweeney HL, Discher DE. 2006. Matrix elasticity directs stem cell lineage specification. *Cell* 126: 677-89
7. Georges PC, Miller WJ, Meaney DF, Sawyer ES, Janmey PA. 2006. Matrices with compliance comparable to that of brain tissue select neuronal over glial growth in mixed cortical cultures. *Biophys J* 90: 3012-8
8. Wu C, Bauer JS, Juliano RL, McDonald JA. 1993. The alpha 5 beta 1 integrin fibronectin receptor, but not the alpha 5 cytoplasmic domain, functions in an early and essential step in fibronectin matrix assembly. *J Biol Chem* 268: 21883-8
9. Wu C, Hughes PE, Ginsberg MH, McDonald JA. 1996. Identification of a new biological function for the integrin alpha v beta 3: initiation of fibronectin matrix assembly. *Cell Adhes Commun* 4: 149-58
10. Hynes RO. 1992. Integrins: versatility, modulation, and signaling in cell adhesion. *Cell* 69: 11-25

APPENDIX B

CHARACTERIZING ROLES FOR FYN, SPHINGOSINE KINASES 1 AND 2, AND TEC FAMILY KINASES IN MOTILITY OF MOUSE BONE MARROW-DERIVED MAST CELLS

In mast cells, cross-linking of the high affinity receptor for IgE, FcεRI, activates sphingosine kinases (SphKs) leading to the production and secretion of lipid mediator sphingosine-1-phosphate (S1P) (1). It has been reported that Fyn kinase is required for the coupling of FcεRI to sphingosine kinase 1 (SphK1) and sphingosine kinase 2 (SphK2) and the ensuing S1P production (2), and both Fyn kinase defective and SphK inhibited mast cells are defective in chemotaxis (1, 2). To investigate the role of Fyn kinase and SphK1 and SphK2 in mast cell spontaneous migration, we took advantage of genetic manipulation strategies that are well developed for mice. We characterized the motility of mouse bone marrow-derived mast cells (BMMCs) from Fyn, SphK1, and SphK2 knockout mice¹.

Tec tyrosine kinases are non-receptor tyrosine kinases which comprise five family members: Bruton's tyrosine kinase (Btk), IL-2-inducible T-cell kinase (Itk), endothelial tyrosine kinase (Etk), resting lymphocyte kinase (Rlk), and Tec (3). Tec kinases act downstream of various receptors including FcεRI, and mast cells express four of these members except Etk (3). Btk has been documented to play a crucial role in

¹ These BMMCs were derived and differentiated in Dr. Juan Rivera's lab at NIH.

mast cell activation (4) and chemotaxis through activation of small Rho GTPase Rac and actin rearrangement after FcεRI aggregation (5). More recently, BMMCs from Btk and Itk double knockout mice were reported to have impaired Ca²⁺ responses and degranulation in response to FcεRI cross-linking (6). To characterize the role of Btk and Itk in mast cell basal motility, we investigated the motility properties of BMMCs derived from Itk and Btk knockout mice, and from Itk/Btk double knockout (DKO) mice².

Materials and Methods

BMMCs were maintained in RPMI containing 25 mM HEPES supplemented with MEM non-essential amino acid solution, penicillin-streptomycin, glutamine, sodium pyruvate solution, 2-mercaptoethanol, and 10% FBS. Cells were plated at a low density overnight on a fibronectin coated MatTek dishes, then time-lapse images were collected for 1-3 hours in every 2 min. To coat the MatTek dishes, bovine fibronectin solution (Sigma-Aldrich, St. Louis, MO) was added onto the glass part of MatTek dishes, incubated for at least 2 hours at room temperature, then washed with PBS. Cell motility was assessed by manually tracking cell movements using Manual Track Plugin for ImageJ, which then calculates velocity of a given cell based on its migration track.

² These BMMCs were derived and differentiated in Dr. Avery August's lab at Cornell University.

Results and Discussion

As shown in Figure B.1, Fyn null BMMCs show significantly decreased average velocity when compared to its wild type control BMMCs. Furthermore, BMMCs from SphK1 and SphK2 knockout mice show substantially decreased velocity as well, suggesting that Fyn kinase and SphKs contribute to spontaneous migration of mast cells. As introduced earlier, the Fyn kinase-SphKs signaling axis has been shown to regulate mast cell chemotaxis, and S1P is a known chemotactic ligand for mast cells. Together, these data implicate the Fyn kinase-SphKs axis in regulating mast cell motility even without chemotactic signals.

As shown in Figure B.2, Itk null and Btk null BMMCs did not show significant differences in their average velocity when compared to the average velocity of BMMCs from wild type control mice, demonstrating that either Itk or Btk alone is dispensable for mast cell spontaneous migration. In contrast, BMMCs from Itk/Btk DKO mice show a substantially increased average velocity in comparison with BMMCs from wild type control mice, suggesting redundant and/or exchangeable role for Itk and Btk in negatively regulating mast cell spontaneous migration.

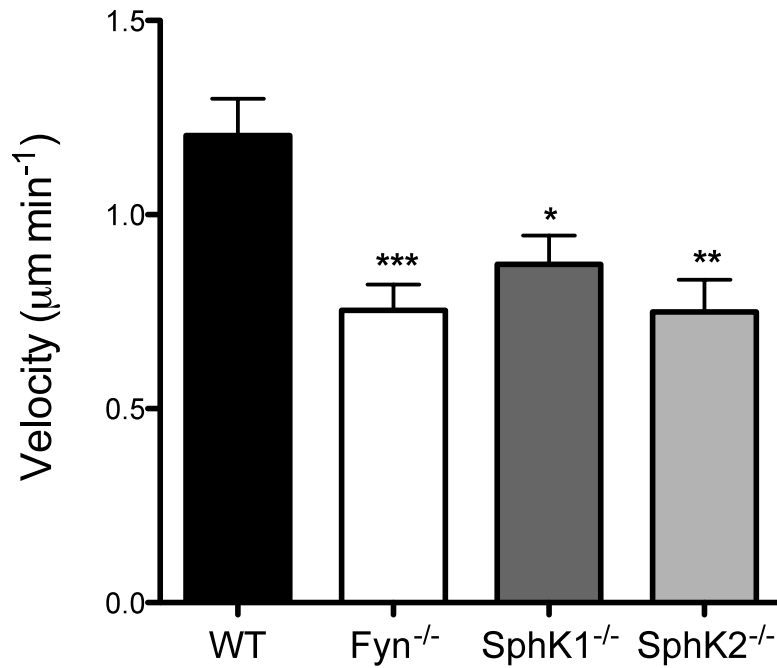


Figure B.1. Characterizing the role of Fyn and sphingosine kinases 1 and 2 in mouse BMMC motility. Motility of mouse BMMCs from Fyn knockout, SphK1 knockout, and SphK2 knockout mice were monitored for 1.5 h in media, and the average velocities are shown \pm SEM ($n = 27 - 68$ per each condition). WT, BMMCs from wild type control. * $P < 0.05$, ** $P < 0.01$, *** $P < 0.001$ compared to WT.

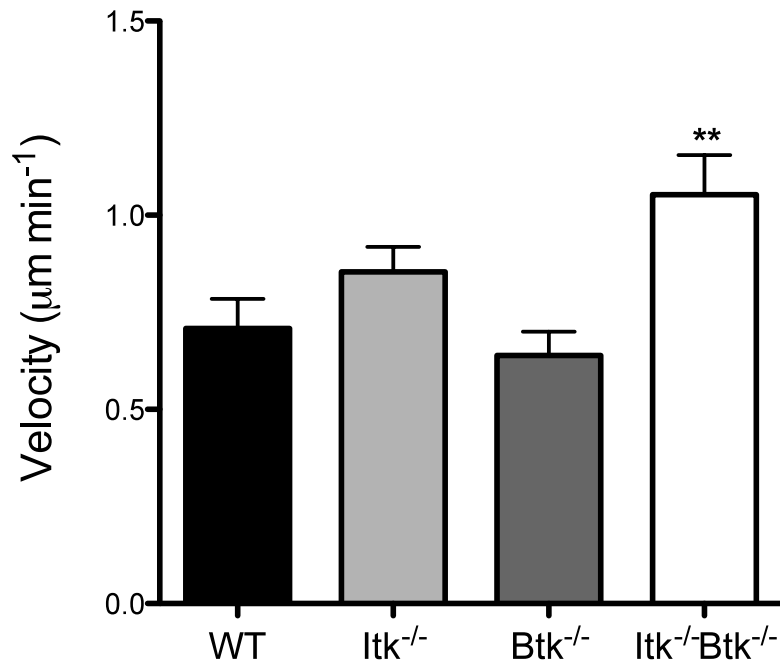


Figure B.2. Characterizing the role of Tec family kinases Itk and Btk in mouse BMMC motility. Motility of mouse BMMCs from Btk knockout, Itk knockout, and Itk/Btk double knockout mice were monitored for 1 h in media, and the average velocities are shown \pm SEM (n = 52 - 73 per each condition). WT, BMMCs from wild type control. ** $P < 0.01$ compared to WT.

REFERENCES

1. Jolly PS, Bektas M, Olivera A, Gonzalez-Espinosa C, Proia RL, Rivera J, Milstien S, Spiegel S. 2004. Transactivation of sphingosine-1-phosphate receptors by FcepsilonRI triggering is required for normal mast cell degranulation and chemotaxis. *J Exp Med* 199: 959-70
2. Olivera A, Urtz N, Mizugishi K, Yamashita Y, Gilfillan AM, Furumoto Y, Gu H, Proia RL, Baumruker T, Rivera J. 2006. IgE-dependent activation of sphingosine kinases 1 and 2 and secretion of sphingosine 1-phosphate requires Fyn kinase and contributes to mast cell responses. *J Biol Chem* 281: 2515-25
3. Gilfillan AM, Rivera J. 2009. The tyrosine kinase network regulating mast cell activation. *Immunol Rev* 228: 149-69
4. Iwaki S, Tkaczyk C, Satterthwaite AB, Halcomb K, Beaven MA, Metcalfe DD, Gilfillan AM. 2005. Btk plays a crucial role in the amplification of Fc epsilonRI-mediated mast cell activation by kit. *J Biol Chem* 280: 40261-70
5. Kuehn HS, Radinger M, Brown JM, Ali K, Vanhaesebroeck B, Beaven MA, Metcalfe DD, Gilfillan AM. 2010. Btk-dependent Rac activation and actin rearrangement following FcepsilonRI aggregation promotes enhanced chemotactic responses of mast cells. *J Cell Sci* 123: 2576-85
6. Iyer AS, Morales JL, Huang W, Ojo F, Ning G, Wills E, Baines JD, August A. 2011. Absence of Tec family kinases interleukin-2 inducible T cell kinase (Itk) and Bruton's tyrosine kinase (Btk) severely impairs Fc epsilonRI-dependent mast cell responses. *J Biol Chem* 286: 9503-13

APPENDIX C

SUMMARY OF CALCIUM MEASUREMENTS OF RAT BONE MARROW- DERIVED MAST CELLS

Ca²⁺ mobilization responses of rat bone marrow derived mast cells (BMMCs) have not been previously characterized. To assess Ca²⁺ responses after stimulation, including contributions of store operated Ca²⁺ entry (SOCE) and IP₃R to Ca²⁺ influx in rat BMMCs, we examined the effects of antigen and thapsigargin stimulation, and Ca²⁺ release-activated Ca²⁺ (CRAC) channel inhibitor GdCl₃, Ca²⁺ influx inhibitor 2-APB, and PLC γ inhibitor U-73122 on this process (1).

Materials and Methods

Intracellular Ca²⁺ levels were measured using an SLM 8100C steady state fluorimeter (SLM instruments, Urbana, IL). Rat bone marrow-derived mast cells (BMMCs) in suspension were loaded with the Ca²⁺ indicator, indo-1 (Invitrogen), and sensitized with anti-DNP IgE in BSS containing 0.5 mM sulfinpyrazone (Sigma). Cells were stimulated with 0.4 μ g/ml DNP-BSA, or 0.25 μ M thapsigargin (Sigma), and their Ca²⁺ response was monitored for about 600 sec. The cells were then treated with 1 μ M GdCl₃ and monitored for additional 150 sec, followed by an addition of either 10 μ M 2-APB, or 1 μ M U-73122 and monitored for additional 200 sec. Subsequently, cells were

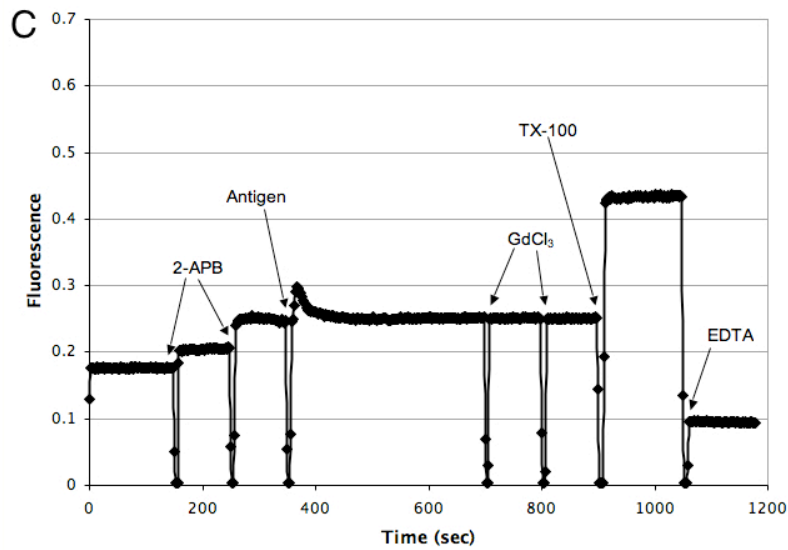
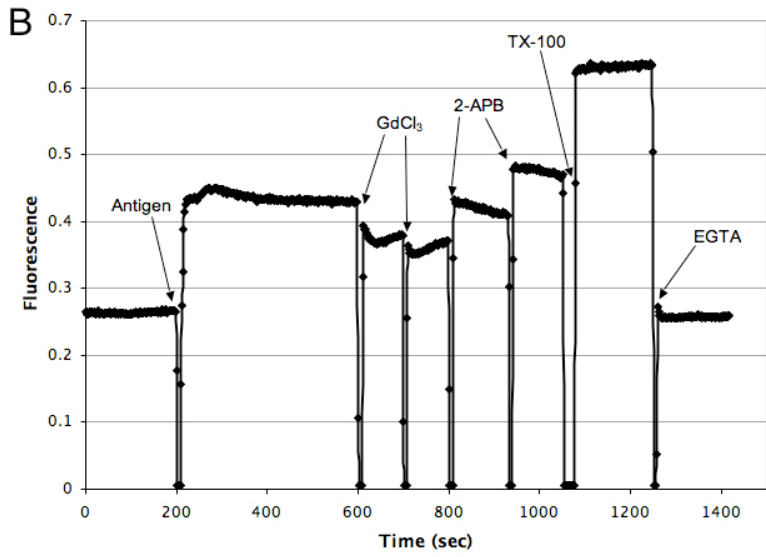
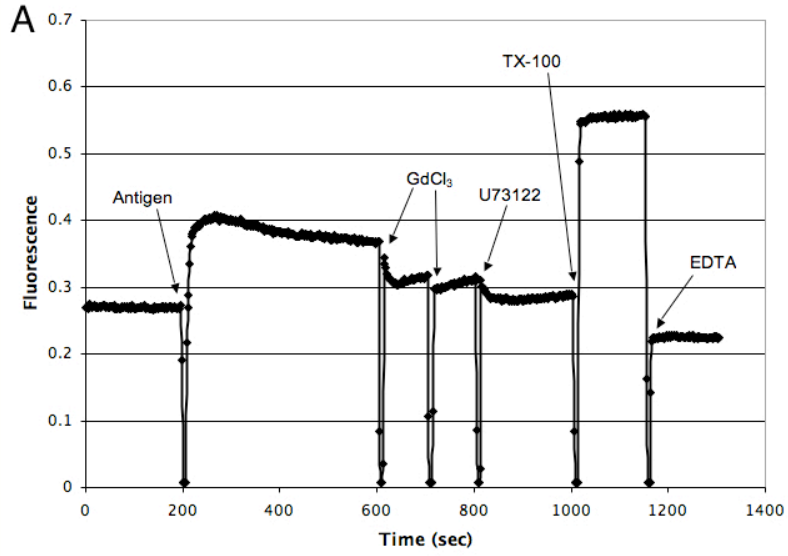
lysed by the addition of 0.1% TritonX-100 to obtain the maximal value of indo-1 fluorescence for each sample. The fluorescence was quenched by the addition of EDTA or EGTA to obtain the background indo-1 fluorescence levels. Representative Ca^{2+} responses were plotted as the change in fluorescence intensity of indo-1 versus time.

Results and Discussion

As shown in Figure C.1, representative plots demonstrate robust Ca^{2+} response to stimulation by 0.4 $\mu\text{g}/\text{ml}$ antigen (DNP-BSA). The influx phase represented by the plateau of the trace response is effectively inhibited by addition of 1 μM GdCl_3 , and a second addition of 1 μM GdCl_3 caused only a small additional increment of inhibition (Fig. C.1A, B). Subsequent addition of 1 μM U-73122 completely inhibited antigen stimulated Ca^{2+} influx (Fig. C.1A). In contrast, addition of 10 μM 2-APB aliquots caused incremental increases in indo-1 fluorescence following antigen and GdCl_3 , suggesting some non-specific effects (Fig. C.1B). When 10 μM 2-APB was added before antigen stimulation, similar fluorescence increases were noted, but the subsequent response to antigen was almost completely inhibited.

As shown in Figure C.2, thapsigargin mediated Ca^{2+} response was almost completely sensitive to addition of 1 μM GdCl_3 , suggesting that majority of the SOCE is caused by Orai1-dependent CRAC channels in rat BMMCs, similar to results with RBL-2H3 cells (2). Subsequent addition of 1 μM U-73122 without additional inhibition

Figure C.1. Antigen-stimulated Ca^{2+} response of rat BMMCs. Representative plots show Ca^{2+} responses to antigen stimulation (0.4 $\mu\text{g}/\text{ml}$ DNP-BSA), and effects of subsequent additions of 1 μM GdCl_3 , followed by either (A) U-73122 addition, or (B) two additions of 2-APB. (C) Two additions of 2-APB were added previous to antigen stimulation. All plots are representative of two independent experiments.



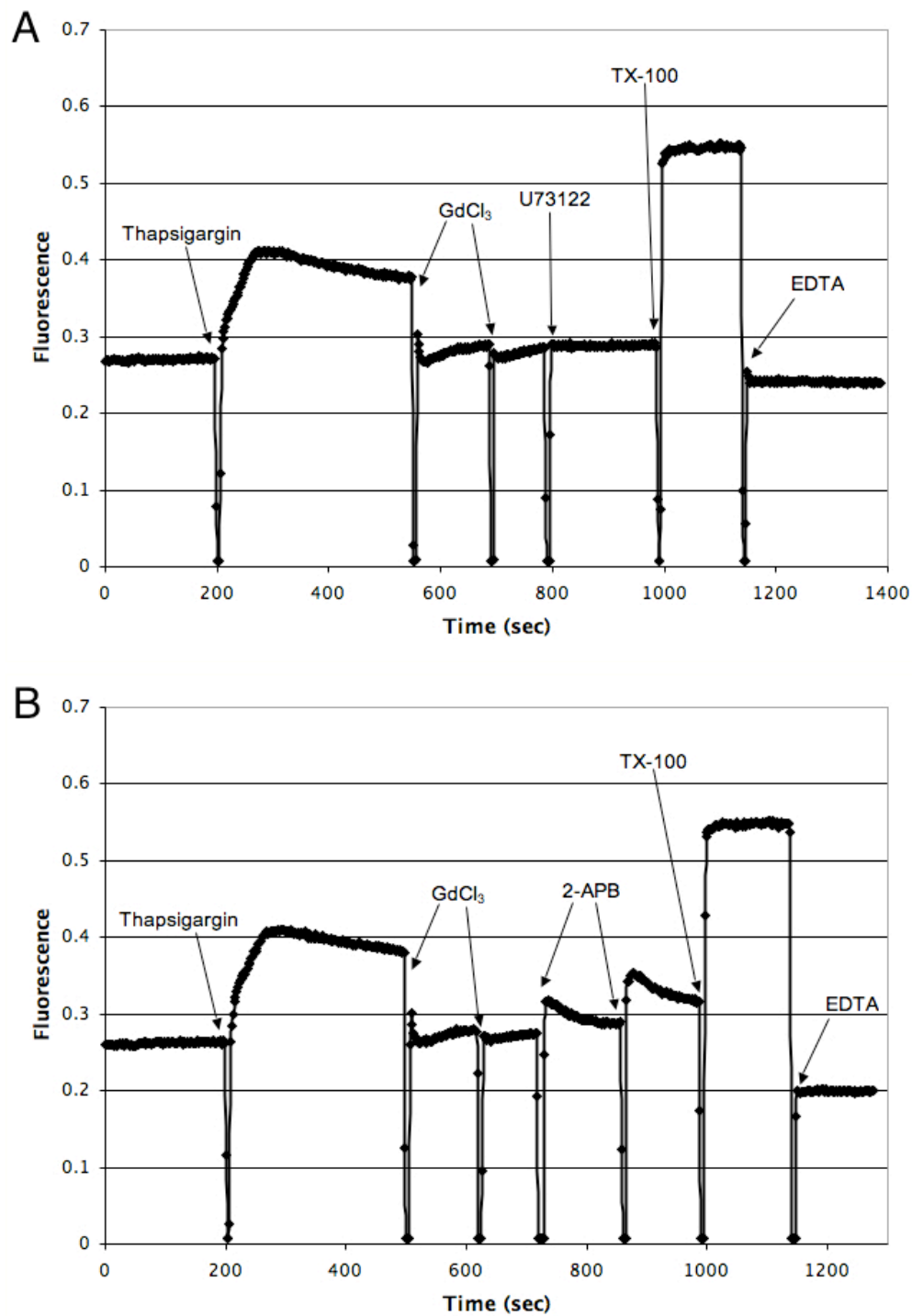


Figure C.2. Thapsigargin-stimulated Ca^{2+} response of rat BMMCs. Representative plots show Ca^{2+} responses to thapsigargin stimulation ($0.25 \mu\text{M}$), and effect of subsequent addition of GdCl_3 , followed by either (A) U-73122 addition, or (B) two additions of 2-APB. All plots are representative of two independent experiments.

further confirmed this conclusion (Fig. C.2A). Similarly to antigen-stimulated Ca^{2+} response (Fig. C.1B), two subsequent additions of 10 μM 2-APB after thapsigargin stimulation caused increase in indo-1 fluorescence (Fig. C.2B).

We also monitored Ca^{2+} response of rat BMMCs to antigen and thapsigargin stimulation in the absence of extracellular Ca^{2+} (Fig. C.3). In both cases, stimulation caused relatively small Ca^{2+} responses without sustained plateau phases as expected, and subsequent additions of 1 μM GdCl_3 and 1 μM U-73122 did not result in further inhibition of this Ca^{2+} response.

Collectively, these data demonstrate that the majority of Ca^{2+} influx in rat BMMCs is mediated by CRAC channels, and Ca^{2+} mobilization of these cells are sensitive to the known inhibitors of Ca^{2+} influx in RBL-2H3 cells such as GdCl_3 , 2-APB, and U-73122 that are also shown to inhibit the motility of both RBL mast cells and rat BMMCs in Chapter 2.

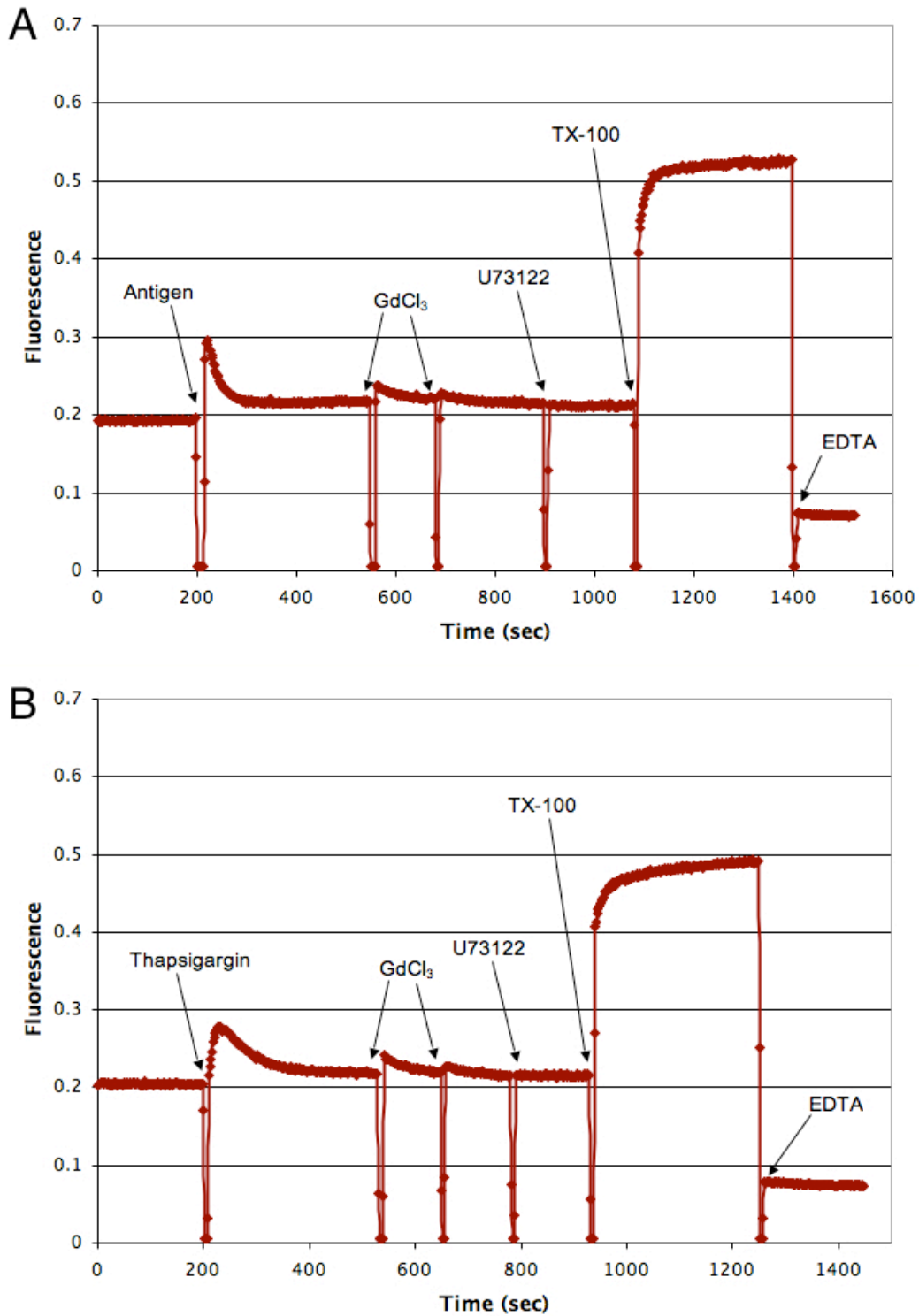


Figure C.3. Stimulated Ca^{2+} response of rat BMMCs in the absence of extracellular Ca^{2+} . Representative plots show Ca^{2+} responses to (A) antigen ($0.4 \mu\text{g}/\text{ml}$ DNP-BSA) or (B) thapsigargin ($0.25 \mu\text{M}$), and effect of subsequent addition of GdCl_3 , followed by two additions of U-73122. All plots are representative of two independent experiments.

REFERENCES

1. Cohen R, Torres A, Ma HT, Holowka D, Baird B. 2009. Ca²⁺ waves initiate antigen-stimulated Ca²⁺ responses in mast cells. *J Immunol* 183: 6478-88
2. Calloway N, Owens T, Corwith K, Rodgers W, Holowka D, Baird B. 2011. Stimulated association of STIM1 and Orai1 is regulated by the balance of PtdIns(4,5)P between distinct membrane pools. *J Cell Sci* 124: 2602-10

APPENDIX D

ADDITIONAL RESULTS FROM MAST CELL MOTILITY AND CHEMOTAXIS STUDY

One of the important aspects of cell motility is the capacity of cells to respond to chemotactic cues with directionally oriented movement. The basal motility of cells, as well as the capacity of cells to sense and direct themselves in response to a chemical gradient can both affect cell chemotaxis behavior. We have shown in Chapter 2 that both Syk protein tyrosine kinase and Ca^{2+} influx via Orai1 contribute to mast cell basal motility as well as to chemotaxis toward antigen. To better understand the relationship between basal motility and directed motion of cells under these conditions, we compared motility coefficient of spontaneously migrating RBL-2H3 cells and the chemotactic index of directionally migrating RBL-2H3 cells toward antigen. As shown in Figure D.1, Syk- cells show substantially decreased chemotaxis that cannot be fully accounted for by their decreased basal motility, suggesting that Syk also modulates directed motion of mast cells up a gradient of antigen. In contrast, the level of decrease in basal motility of cells in the absence of extracellular Ca^{2+} is comparable to that of chemotaxis of cells in excess EGTA (Fig. D.1). For cells with Orai1 knocked-down, the decrease in chemotaxis toward antigen is greater than that in basal motility, but only moderately so. Taken together, these data imply that Ca^{2+} influx via Orai1 regulates chemotaxis of mast cells toward higher concentrations of antigen primarily by affecting their basal motility.

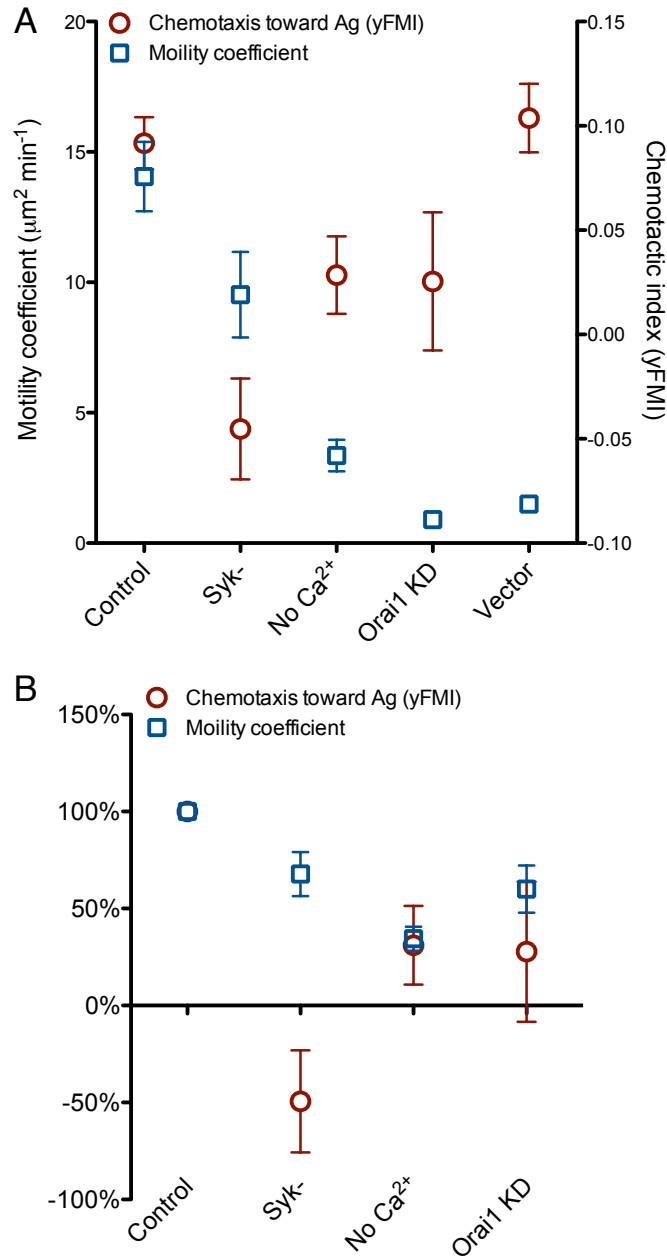


Figure D.1. Comparison of the motility coefficient and the chemotactic index of RBL-2H3 cells under various conditions. Motility coefficients of mast cells under spontaneous migration conditions (blue open rectangle) and chemotactic indices (yFMI) of mast cells in Ibidi chemotaxis μ -slide chambers with 10 ng/ml DNP-BSA as a chemoattractant (red open circle) are shown \pm SEM (n= 11 – 137). (A) Motility coefficients are represented on the left y axis, and chemotactic indices are represented on the right y axis. Control: RBL mast cells in complete medium. (B) Motility coefficients and chemotactic indices of RBL-2H3 cells shown in (A) are represented as percentages of controls, where respective controls for each condition are normalized to 100%.

APPENDIX E

MATLAB CODE FOR AUTOMATED TRACKING AND ANALYSIS¹

track_cells.m

```
function [AllxData AllyData] = track_cells(INFILE, OUTFILE, scale, fsize, rmax, threshval)
```

```
close all
```

```
if nargin<5, rmax = 15; end
```

```
if nargin<4, fsize = 40; end
```

```
if nargin<3, scale = .5; end
```

```
if nargin==1,
```

```
    endind = strfind(INFILE, '.avi');
```

```
    OUTFILE = [INFILE(1:endind-1) '.m'];
```

```
end
```

```
if nargin == 0,
```

```
    [INFILE INFILEPATH] = uigetfile('*.*avi', 'Select Movie File to Track');
```

```
    endind = strfind(INFILE, '.avi');
```

```
    defaultOUTFILE = [INFILE(1:endind-1) '.mat'];
```

```
    INFILE = [INFILEPATH INFILE];
```

```
    [OUTFILE OUTFILEPATH] = uiputfile('*.*mat', 'Select Output File', defaultOUTFILE);
```

```
    OUTFILE = [OUTFILEPATH OUTFILE];
```

¹ Developed by Dr. Sarah Veatch.

```

    [scale fsize rmax threshval] = tracking_parameters_dialog;
end

I = double(imresize(frame2im(aviread(INFILE, 1)), scale));

I = I/mean(mean(I))-1;

imagesc(I);

colormap gray

axis equal tight off

counter = 1;

[x y] = ginput(1);

while ~isempty(x)

    text(x, y, num2str(counter), 'horizontalalignment', 'center', 'color', 'r', 'fontsize', 14)

    xold(counter) = round(x);

    yold(counter) = round(y);

    counter = counter+1;

    [x y] = ginput(1);

end

screenshot_OUTFILE = [OUTFILE(1:length(OUTFILE)-4) '_firstframe.tif'];

M = getframe;

I2 = frame2im(M);

imwrite(I2, screenshot_OUTFILE, 'tif');

```

```

xstart = xold;

ystart = yold;
yold = ystart;

xold = xstart;

filt = zeros(fsize+1);

for i=1:length(xold)

    centerx = xold(i);
    centery = yold(i);

    rect = [round(centerx-fsize/2) round(centery-fsize/2) fsize fsize];

    if rect(1) <=0,
    elseif rect(2) <= 0,
    elseif rect(1)+rect(3)>size(I, 2),
    elseif rect(2)+rect(4)>size(I, 1),
    else
        filt = filt + double(imcrop(I, rect));
    end

    %imagesc(filt);

    %axis equal tight off

    %pause
end

```

```

Finfo = aviinfo(INFILE);

Nframes = Finfo.NumFrames;

AllxData = zeros(Nframes, length(xold));

AllyData = zeros(Nframes, length(yold));
for framenum = 1:Nframes,

    % read in image, filter, and find cell bodies

    I = double(imresize(frame2im(aviread(INFILE, framenum)), scale));

    I = I/mean(mean(I))-1;

    J = imfilter(double(I), filt);

    J = (J-min(min(J)))/(max(max(J))-min(min(J)));

    J = imhmin(J, threshval*graythresh(J));

    BW = imregionalmax(J, 8);

    [y2 x2] = find(BW);

    %imagesc(J);

    %axis equal tight off

    %hold on

    %plot(x2, y2, 'ro')

    %hold off

    %pause(1)

    % match up new cells with cells from last frame

```

```

xnew = zeros(size(xold));

ynew = zeros(size(yold));

for i=1:length(xold),

    %xold = x(i);

    %yold = y1(i);

    if xold(i)~=0,
        rsquaredvals =(x2-xold(i)).^2 + (y2-yold(i)).^2;

        if sum(rsquaredvals<=rmax^2)==1,

            %keepinds(i) = find(rvals<=rmax^2);

            xnew(i) = (x2(find(rsquaredvals<=rmax^2)));

            ynew(i) = (y2(find(rsquaredvals<=rmax^2)));

        elseif sum(rsquaredvals<=rmax^2)>1,

            ind = find(rsquaredvals==min(rsquaredvals));

            xnew(i) = x2(ind(1));

            ynew(i) = y2(ind(1));

        end

    end

end

end

% update filter;

filt = zeros(fsize+1);

for i=1:length(xnew)

    if xnew(i)~=0,

```

```

    centerx = xnew(i);

    centery = ynew(i);

    rect = [round(centerx-fsize/2) round(centery-fsize/2) fsize fsize];

    if rect(1) <=0,

    elseif rect(2) <= 0,

    elseif rect(1)+rect(3)>size(I, 2),

    elseif rect(2)+rect(4)>size(I, 1),

    else
        filt = filt + double(imcrop(I, rect));
    end

end

end

AllxData(framenumber, :) = xnew;

AllyData(framenumber, :) = ynew;

xold = xnew;

yold = ynew;

% plot tracks

imagesc(I);

hold on

plot(AllxData(1:framenumbe, :), AllyData(1:framenumbe, :), '-x')

plot(AllxData([1 framenumbe], :), AllyData([1 framenumbe], :), 'x')

```

```

hold off

axis equal tight off

title(['frame number ' num2str(framenumber)]);

pause(.01)

end

for i=1:length(xnew),

    text(xnew(i),ynew(i), num2str(i), 'horizontalalignment', 'center', 'color', 'k', 'fontsize',
14)

end

screenshot_OUTFILE = [OUTFILE(1:length(OUTFILE)-4) '_lastframe.tif'];

M = getframe;

I2 = frame2im(M);

imwrite(I2, screenshot_OUTFILE, 'tif');

AllxData = AllxData/scale^2;

AllyData = AllyData/scale^2;

save(OUTFILE, 'AllxData', 'AllyData', 'scale', 'fsize', 'rmax', 'xstart', 'ystart')

i = 1;

newcellxdata = {[['x cell ' num2str(i)]]; num2cell(AllxData(:, i))];

newcellydata = {[['y cell ' num2str(i)]]; num2cell(AllyData(:, i))];

XLS_tracking_data = [newcellxdata, newcellydata];

```

```

for i = 2:size(AllxData, 2);

    newcellxdata = [[[ 'x cell ' num2str(i)]]; num2cell(AllxData(:, i))];

    newcellydata = [[[ 'y cell ' num2str(i)]]; num2cell(AllyData(:, i))];

    XLS_tracking_data = [XLS_tracking_data, newcellxdata, newcellydata];

end

XLS_OUTFILE = [OUTFILE(1:length(OUTFILE)-4) '.xls'];

xlswrite(XLS_OUTFILE, XLS_tracking_data, 'Tracking data', 'A1')

%MSDdata = process_tracked_data(OUTFILE);

```

tracking_parameters_dialog.m

```

function varargout = tracking_parameters_dialog(varargin)
% TRACKING_PARAMETERS_DIALOG M-file for tracking_parameters_dialog.fig
%           TRACKING_PARAMETERS_DIALOG, by itself, creates a new
TRACKING_PARAMETERS_DIALOG or raises the existing
%   singleton*.
%
%           H = TRACKING_PARAMETERS_DIALOG returns the handle to a new
TRACKING_PARAMETERS_DIALOG or the handle to
%   the existing singleton*.
%
%
TRACKING_PARAMETERS_DIALOG('CALLBACK',hObject,eventData,handles,...)
calls the local
%   function named CALLBACK in TRACKING_PARAMETERS_DIALOG.M with the
given input arguments.
%
%           TRACKING_PARAMETERS_DIALOG('Property','Value',...) creates a new
TRACKING_PARAMETERS_DIALOG or raises the
%   existing singleton*. Starting from the left, property value pairs are
%   applied to the GUI before tracking_parameters_dialog_OpeningFcn gets called.
An

```

```

% unrecognized property name or invalid value makes property application
% stop. All inputs are passed to tracking_parameters_dialog_OpeningFcn via
varargin.
%
% *See GUI Options on GUIDE's Tools menu. Choose "GUI allows only one
% instance to run (singleton)".
%
% See also: GUIDE, GUIDATA, GUIHANDLES

% Edit the above text to modify the response to help tracking_parameters_dialog

% Last Modified by GUIDE v2.5 01-Jun-2009 11:54:22

% Begin initialization code - DO NOT EDIT
gui_Singleton = 1;
gui_State = struct('gui_Name',    mfilename, ...
    'gui_Singleton', gui_Singleton, ...
    'gui_OpeningFcn', @tracking_parameters_dialog_OpeningFcn, ...
    'gui_OutputFcn', @tracking_parameters_dialog_OutputFcn, ...
    'gui_LayoutFcn', [], ...
    'gui_Callback', []);
if nargin && ischar(varargin{1})
    gui_State.gui_Callback = str2func(varargin{1});
end

if nargout
    [varargout{1:nargout}] = gui_mainfcn(gui_State, varargin{:});
else
    gui_mainfcn(gui_State, varargin{:});
end
% End initialization code - DO NOT EDIT

% --- Executes just before tracking_parameters_dialog is made visible.
function tracking_parameters_dialog_OpeningFcn(hObject, eventdata, handles,
varargin)
% This function has no output args, see OutputFcn.
% hObject handle to figure
% eventdata reserved - to be defined in a future version of MATLAB
% handles structure with handles and user data (see GUIDATA)
% varargin command line arguments to tracking_parameters_dialog (see VARARGIN)

% Choose default command line output for tracking_parameters_dialog
handles.output1 = [];

```

```

handles.output2 = [];
handles.output3 = [];
handles.output4 = [];
% hObject;

% Update handles structure
guidata(hObject, handles);

% Make the GUI modal
set(handles.figure1, 'WindowStyle', 'modal')

% UIWAIT makes tracking_parameters_dialog wait for user response (see UIRESUME)
uiwait(handles.figure1);

% --- Outputs from this function are returned to the command line.
function varargout = tracking_parameters_dialog_OutputFcn(hObject, eventdata,
handles)
% varargout cell array for returning output args (see VARARGOUT);
% hObject handle to figure
% eventdata reserved - to be defined in a future version of MATLAB
% handles structure with handles and user data (see GUIDATA)

% Get default command line output from handles structure

varargout{4} = handles.output4;
varargout{3} = handles.output3;
varargout{2} = handles.output2;
varargout{1} = handles.output1;

% The figure can be deleted now
delete(handles.figure1);

%close(handles.figure1);
%varargout{1} = handles.output;

% --- Executes on button press in close_window_pushbutton.
function close_window_pushbutton_Callback(hObject, eventdata, handles)
% hObject handle to close_window_pushbutton (see GCBO)
% eventdata reserved - to be defined in a future version of MATLAB
% handles structure with handles and user data (see GUIDATA)

```

```

%tracking_parameters_dialog_OutputFcn(hObject, eventdata, handles);

handles.output4 = str2double(get(handles.threshval_edit, 'String'));
handles.output3 = str2double(get(handles.step_size_edit, 'String'));
disp(get(handles.step_size_edit, 'String'));
handles.output2 = str2double(get(handles.filter_size_edit, 'String'));
handles.output1 = str2double(get(handles.scale_edit, 'String'));
guidata(hObject, handles);
uiresume(handles.figure1);

function scale_edit_Callback(hObject, eventdata, handles)
% hObject   handle to scale_edit (see GCBO)
% eventdata reserved - to be defined in a future version of MATLAB
% handles   structure with handles and user data (see GUIDATA)

% Hints: get(hObject,'String') returns contents of scale_edit as text
%        str2double(get(hObject,'String')) returns contents of scale_edit as a double

% --- Executes during object creation, after setting all properties.
function scale_edit_CreateFcn(hObject, eventdata, handles)
% hObject   handle to scale_edit (see GCBO)
% eventdata reserved - to be defined in a future version of MATLAB
% handles   empty - handles not created until after all CreateFcns called

% Hint: edit controls usually have a white background on Windows.
%       See ISPC and COMPUTER.
if ispc && isequal(get(hObject,'BackgroundColor'),
get(0,'defaultUicontrolBackgroundColor'))
    set(hObject,'BackgroundColor','white');
end

function filter_size_edit_Callback(hObject, eventdata, handles)
% hObject   handle to filter_size_edit (see GCBO)
% eventdata reserved - to be defined in a future version of MATLAB
% handles   structure with handles and user data (see GUIDATA)

% Hints: get(hObject,'String') returns contents of filter_size_edit as text
%        str2double(get(hObject,'String')) returns contents of filter_size_edit as a double

% --- Executes during object creation, after setting all properties.
function filter_size_edit_CreateFcn(hObject, eventdata, handles)

```

```

% hObject handle to filter_size_edit (see GCBO)
% eventdata reserved - to be defined in a future version of MATLAB
% handles empty - handles not created until after all CreateFcns called

% Hint: edit controls usually have a white background on Windows.
% See ISPC and COMPUTER.
if ispc && isequal(get(hObject,'BackgroundColor'),
get(0,'defaultUicontrolBackgroundColor'))
    set(hObject,'BackgroundColor','white');
end

```

```

function step_size_edit_Callback(hObject, eventdata, handles)
% hObject handle to step_size_edit (see GCBO)
% eventdata reserved - to be defined in a future version of MATLAB
% handles structure with handles and user data (see GUIDATA)

% Hints: get(hObject,'String') returns contents of step_size_edit as text
% str2double(get(hObject,'String')) returns contents of step_size_edit as a double

```

```

% --- Executes during object creation, after setting all properties.
function step_size_edit_CreateFcn(hObject, eventdata, handles)
% hObject handle to step_size_edit (see GCBO)
% eventdata reserved - to be defined in a future version of MATLAB
% handles empty - handles not created until after all CreateFcns called

% Hint: edit controls usually have a white background on Windows.
% See ISPC and COMPUTER.
if ispc && isequal(get(hObject,'BackgroundColor'),
get(0,'defaultUicontrolBackgroundColor'))
    set(hObject,'BackgroundColor','white');
end

```

```

function threshval_edit_Callback(hObject, eventdata, handles)
% hObject handle to threshval_edit (see GCBO)
% eventdata reserved - to be defined in a future version of MATLAB
% handles structure with handles and user data (see GUIDATA)

% Hints: get(hObject,'String') returns contents of threshval_edit as text
% str2double(get(hObject,'String')) returns contents of threshval_edit as a double

```

```

% --- Executes during object creation, after setting all properties.
function threshval_edit_CreateFcn(hObject, eventdata, handles)
% hObject    handle to threshval_edit (see GCBO)
% eventdata  reserved - to be defined in a future version of MATLAB
% handles    empty - handles not created until after all CreateFcns called

% Hint: edit controls usually have a white background on Windows.
%       See ISPC and COMPUTER.
if      ispc      &&      isequal(get(hObject,'BackgroundColor'),
get(0,'defaultUicontrolBackgroundColor'))
    set(hObject,'BackgroundColor','white');
end

```

process_tracked_data.m

```

function MSDdata = process_tracked_data(INFILE, OUTFILE, frames, FINFOSTR)

if nargin ==0,

    [INFILE INFILEPATH] = uigetfile('*.mat', 'Select Data File to Process');

    [frames, fitinds, FINFOSTR] = process_parameters_dialog;

    endind = strfind(INFILE, '.mat');

    defaultOUTFILE = [INFILE(1:endind-1) '_' FINFOSTR '_processed.mat'];

    INFILE = [INFILEPATH INFILE];

    [OUTFILE OUTFILEPATH] = uiputfile('*.mat', 'Select Output File', defaultOUTFILE);

    OUTFILE = [OUTFILEPATH OUTFILE];

end

load(INFILE)

```

```

MSDdata = calculate_MSD(AllxData, AllyData, frames, fitinds, 1);

MSDdata.info = FINFOSTR;

MSDdata.frames = frames;

MSDdata.fitinds = fitinds;

save(OUTFILE, 'MSDdata');

MSD = MSDdata.MSD;

shortD = MSDdata.shortD;

confinedD = MSDdata.confinedD;

confinedAlpha = MSDdata.confinedAlpha;

MSD_XLS_data = {};

FIT_XLS_data = {'fit parameters'; 'short time D'; 'confined D'; 'alpha'};

for i=1:size(MSD, 1),

    MSD_XLS_data = [MSD_XLS_data [{'MSD cell ' num2str(i)}; num2cell(MSD(i, :))]];

    FIT_XLS_data = [FIT_XLS_data [{'cell ' num2str(i)}; num2cell([shortD(i);
confinedD(i); confinedAlpha(i))]];

end

AVG_FIT_data = {'Average fit parameters'; 'short time D'; 'confined D'; 'alpha'};

AVG_FIT_data = [AVG_FIT_data [{}; num2cell([MSDdata.shortAvgD;
MSDdata.confinedAvgD;MSDdata.confinedAvgAlpha])]];

XLS_OUTFILE = [INFILE(1:length(INFILE)-4) '.xls'];

```

```
xlswrite(XLS_OUTFILE, MSD_XLS_data, ['MSD data ' FINFOSTR], 'A1')
```

```
xlswrite(XLS_OUTFILE, FIT_XLS_data, ['Fit data ' FINFOSTR], 'A1')
```

```
xlswrite(XLS_OUTFILE, AVG_FIT_data, ['Fit data ' FINFOSTR], 'A7')
```

process_parameters_dialog.m

```
function varargout = process_parameters_dialog(varargin)
%PROCESS_PARAMETERS_DIALOG M-file for process_parameters_dialog.fig
%          PROCESS_PARAMETERS_DIALOG, by itself, creates a new
PROCESS_PARAMETERS_DIALOG or raises the existing
%  singleton*.
%
%          H = PROCESS_PARAMETERS_DIALOG returns the handle to a new
PROCESS_PARAMETERS_DIALOG or the handle to
%  the existing singleton*.
%
%          PROCESS_PARAMETERS_DIALOG('Property','Value',...) creates a new
PROCESS_PARAMETERS_DIALOG using the
%  given property value pairs. Unrecognized properties are passed via
%  varargin to process_parameters_dialog_OpeningFcn. This calling syntax produces
a
%  warning when there is an existing singleton*.
%
%          PROCESS_PARAMETERS_DIALOG('CALLBACK') and
PROCESS_PARAMETERS_DIALOG('CALLBACK',hObject,...) call the
%  local function named CALLBACK in PROCESS_PARAMETERS_DIALOG.M with
the given input
%  arguments.
%
%  *See GUI Options on GUIDE's Tools menu. Choose "GUI allows only one
%  instance to run (singleton)".
%
% See also: GUIDE, GUIDATA, GUIHANDLES

% Edit the above text to modify the response to help process_parameters_dialog

% Last Modified by GUIDE v2.5 29-May-2009 12:09:14

% Begin initialization code - DO NOT EDIT
gui_Singleton = 1;
```

```

gui_State = struct('gui_Name',    mfilename, ...
                 'gui_Singleton', gui_Singleton, ...
                 'gui_OpeningFcn', @process_parameters_dialog_OpeningFcn, ...
                 'gui_OutputFcn', @process_parameters_dialog_OutputFcn, ...
                 'gui_LayoutFcn', [], ...
                 'gui_Callback', []);
if nargin && ischar(varargin{1})
    gui_State.gui_Callback = str2func(varargin{1});
end

if nargout
    [varargout{1:nargout}] = gui_mainfcn(gui_State, varargin{:});
else
    gui_mainfcn(gui_State, varargin{:});
end
% End initialization code - DO NOT EDIT

% --- Executes just before process_parameters_dialog is made visible.
function process_parameters_dialog_OpeningFcn(hObject, eventdata, handles,
varargin)
% This function has no output args, see OutputFcn.
% hObject    handle to figure
% eventdata  reserved - to be defined in a future version of MATLAB
% handles    structure with handles and user data (see GUIDATA)
% varargin   unrecognized PropertyName/PropertyValue pairs from the
%           command line (see VARARGIN)

% Choose default command line output for process_parameters_dialog
handles.output = hObject;
handles.output1 = [];
handles.output2 = [];
handles.output3 = [];

% Update handles structure
guidata(hObject, handles);

% Make the GUI modal
set(handles.figure1, 'WindowStyle', 'modal')

% UIWAIT makes process_parameters_dialog wait for user response (see UIRESUME)
uiwait(handles.figure1);

```

```

% --- Outputs from this function are returned to the command line.
function varargout = process_parameters_dialog_OutputFcn(hObject, eventdata,
handles)
% varargout cell array for returning output args (see VARARGOUT);
% hObject handle to figure
% eventdata reserved - to be defined in a future version of MATLAB
% handles structure with handles and user data (see GUIDATA)

% Get default command line output from handles structure
varargout{3} = handles.output3;
varargout{2} = handles.output2;
varargout{1} = handles.output1;
% The figure can be deleted now
delete(handles.figure1);

% --- Executes on button press in close_window_pushbutton.
function close_window_pushbutton_Callback(hObject, eventdata, handles)
% hObject handle to close_window_pushbutton (see GCBO)
% eventdata reserved - to be defined in a future version of MATLAB
% handles structure with handles and user data (see GUIDATA)

frames = str2double(get(handles.minframenum_edit, 'String'));
str2double(get(handles.maxframenum_edit, 'String'));
fitpts = str2double(get(handles.fitptsmin_edit, 'String'));
str2double(get(handles.fitptsmax_edit, 'String'));
FILEINFOSTR = get(handles.discription_edit, 'String');

handles.output1 = frames;
handles.output2 = fitpts;
handles.output3 = FILEINFOSTR;
guidata(hObject, handles);
uiresume(handles.figure1);

function minframenum_edit_Callback(hObject, eventdata, handles)
% hObject handle to minframenum_edit (see GCBO)
% eventdata reserved - to be defined in a future version of MATLAB
% handles structure with handles and user data (see GUIDATA)

% Hints: get(hObject,'String') returns contents of minframenum_edit as text

```

```
%      str2double(get(hObject,'String')) returns contents of minframenum_edit as a
double
```

```
% --- Executes during object creation, after setting all properties.
function minframenum_edit_CreateFcn(hObject, eventdata, handles)
% hObject   handle to minframenum_edit (see GCBO)
% eventdata reserved - to be defined in a future version of MATLAB
% handles   empty - handles not created until after all CreateFcns called
```

```
% Hint: edit controls usually have a white background on Windows.
%   See ISPC and COMPUTER.
if      ispc      &&      isequal(get(hObject,'BackgroundColor'),
get(0,'defaultUicontrolBackgroundColor'))
    set(hObject,'BackgroundColor','white');
end
```

```
function filter_size_edit_Callback(hObject, eventdata, handles)
% hObject   handle to filter_size_edit (see GCBO)
% eventdata reserved - to be defined in a future version of MATLAB
% handles   structure with handles and user data (see GUIDATA)
```

```
% Hints: get(hObject,'String') returns contents of filter_size_edit as text
%      str2double(get(hObject,'String')) returns contents of filter_size_edit as a double
```

```
% --- Executes during object creation, after setting all properties.
function filter_size_edit_CreateFcn(hObject, eventdata, handles)
% hObject   handle to filter_size_edit (see GCBO)
% eventdata reserved - to be defined in a future version of MATLAB
% handles   empty - handles not created until after all CreateFcns called
```

```
% Hint: edit controls usually have a white background on Windows.
%   See ISPC and COMPUTER.
if      ispc      &&      isequal(get(hObject,'BackgroundColor'),
get(0,'defaultUicontrolBackgroundColor'))
    set(hObject,'BackgroundColor','white');
end
```

```
function discription_edit_Callback(hObject, eventdata, handles)
% hObject   handle to discription_edit (see GCBO)
% eventdata reserved - to be defined in a future version of MATLAB
```

```

% handles    structure with handles and user data (see GUIDATA)

% Hints: get(hObject,'String') returns contents of discription_edit as text
%    str2double(get(hObject,'String')) returns contents of discription_edit as a double

% --- Executes during object creation, after setting all properties.
function discription_edit_CreateFcn(hObject, eventdata, handles)
% hObject    handle to discription_edit (see GCBO)
% eventdata  reserved - to be defined in a future version of MATLAB
% handles    empty - handles not created until after all CreateFcns called

% Hint: edit controls usually have a white background on Windows.
%    See ISPC and COMPUTER.
if    ispc    &&    isequal(get(hObject,'BackgroundColor'),
get(0,'defaultUicontrolBackgroundColor'))
    set(hObject,'BackgroundColor','white');
end

function maxframenum_edit_Callback(hObject, eventdata, handles)
% hObject    handle to maxframenum_edit (see GCBO)
% eventdata  reserved - to be defined in a future version of MATLAB
% handles    structure with handles and user data (see GUIDATA)

% Hints: get(hObject,'String') returns contents of maxframenum_edit as text
%    str2double(get(hObject,'String')) returns contents of maxframenum_edit as a
double

% --- Executes during object creation, after setting all properties.
function maxframenum_edit_CreateFcn(hObject, eventdata, handles)
% hObject    handle to maxframenum_edit (see GCBO)
% eventdata  reserved - to be defined in a future version of MATLAB
% handles    empty - handles not created until after all CreateFcns called

% Hint: edit controls usually have a white background on Windows.
%    See ISPC and COMPUTER.
if    ispc    &&    isequal(get(hObject,'BackgroundColor'),
get(0,'defaultUicontrolBackgroundColor'))
    set(hObject,'BackgroundColor','white');
end

```

```

function fitptsmin_edit_Callback(hObject, eventdata, handles)
% hObject    handle to fitptsmin_edit (see GCBO)
% eventdata  reserved - to be defined in a future version of MATLAB
% handles    structure with handles and user data (see GUIDATA)

% Hints: get(hObject,'String') returns contents of fitptsmin_edit as text
%    str2double(get(hObject,'String')) returns contents of fitptsmin_edit as a double

% --- Executes during object creation, after setting all properties.
function fitptsmin_edit_CreateFcn(hObject, eventdata, handles)
% hObject    handle to fitptsmin_edit (see GCBO)
% eventdata  reserved - to be defined in a future version of MATLAB
% handles    empty - handles not created until after all CreateFcns called

% Hint: edit controls usually have a white background on Windows.
%    See ISPC and COMPUTER.
if ispc && isequal(get(hObject,'BackgroundColor'),
get(0,'defaultUicontrolBackgroundColor'))
    set(hObject,'BackgroundColor','white');
end

function fitptsmax_edit_Callback(hObject, eventdata, handles)
% hObject    handle to fitptsmax_edit (see GCBO)
% eventdata  reserved - to be defined in a future version of MATLAB
% handles    structure with handles and user data (see GUIDATA)

% Hints: get(hObject,'String') returns contents of fitptsmax_edit as text
%    str2double(get(hObject,'String')) returns contents of fitptsmax_edit as a double

% --- Executes during object creation, after setting all properties.
function fitptsmax_edit_CreateFcn(hObject, eventdata, handles)
% hObject    handle to fitptsmax_edit (see GCBO)
% eventdata  reserved - to be defined in a future version of MATLAB
% handles    empty - handles not created until after all CreateFcns called

% Hint: edit controls usually have a white background on Windows.
%    See ISPC and COMPUTER.
if ispc && isequal(get(hObject,'BackgroundColor'),
get(0,'defaultUicontrolBackgroundColor'))
    set(hObject,'BackgroundColor','white');
end

```

confined_diffusion_func.m

```
function y = confined_diffusion_func(P, x)
```

```
A = P(1);
```

```
B = P(2);
```

```
if length(P)<3,
```

```
    C = 0;
```

```
else
```

```
    C = P(3);
```

```
end
```

```
y = A*x.^B+C;
```

calculate_MSD.m

```
function MSDdata = calculate_MSD(AllxData, AllyData, frames, fitinds, flag)
```

```
% if nargin == 0,
```

```
% [FILE FILEPATH] = uigetfile('*.m', 'Select data file to process');
```

```
% FILE = [FILEPATH FILE];
```

```
% end
```

```
%
```

```
% load(FILE);
```

```
%frames = frames1;
```

```

%fitinds = 5:10;

xData = AllxData(frames, :);
yData = AllyData(frames, :);
cellnumbers = 1:size(AllxData, 2);

totpoints = zeros(size(xData, 1), 1);
sumMSD = zeros(size(xData, 1), 1);
totdMSD= zeros(size(xData, 1), 1);
MSD = zeros(length(cellnumbers), size(xData, 1));
dMSD = zeros(length(cellnumbers), size(xData, 1));

for cellnumber = cellnumbers ,

    x = xData(:, cellnumber)';
    y = yData(:, cellnumber)';
    r = [x; y];
    if sum(x==0),
        inds = find(y==0);
        max_framenum = inds(1)-1;
    else
        max_framenum = length(x);
    end

    clear rdiffsquared

    if max_framenum>1,

```

```

for i=1:max_framenum;
    for j=1:max_framenum-i,
        rdiffsquared(j) =sum((r(:, j+i)-r(:, j)).^2);
    end
    MSD(cellnumber, i) = mean(rdiffsquared);
    dMSD(cellnumber, i) = std(rdiffsquared)./sqrt(length(rdiffsquared));
    totpoints(i) = totpoints(i)+1;
    sumMSD(i) = sumMSD(i)+MSD(cellnumber, i);
    totdMSD(i) = sqrt(sum(totdMSD(i)^2 + dMSD(cellnumber, i)^2));
end

%totpoints = totpoints + ones(1, max_framenum);
%sumMSD = sumMSD + MSD(cellnumber, :);

P1 = polyfit(fitinds, MSD(cellnumber, fitinds), 1);
shortD(cellnumber) = P1(1);

t = 0:min(50, max_framenum)-1;
fitinds2 = 1:min(max_framenum, 50);
P2 = lsqcurvefit('confined_diffusion_func', [10 1], t(fitinds2), MSD(cellnumber,
fitinds2));
confinedD(cellnumber) = P2(1);
confinedAlpha(cellnumber) = P2(2);

```

```

    if flag,
        plot(t, MSD(cellnumber, fitinds2), '.')
        hold on
        plot(t, confined_diffusion_func(P2, t))
        hold off
        xlabel('time (frames)')
        ylabel('mean squared displacement')
        title(['cell number ' num2str(cellnumber)])
        pause(.01)
    end
end

%plot(1:i, MSD(cellnumber, 1:i), '*', inds, polyval(P, inds))

%pause

end

avgMSD = sumMSD./totpoints;
totdMSD = totdMSD./totpoints;

P = polyfit(fitinds', avgMSD(fitinds), 1);
shortAvgD = P(1);
[n xout] = hist(shortD, 25);

[nDc xDc] = hist(confinedD, 25);

```

```

[nAc xAc] = hist(confinedAlpha, 25);

t = 0:length(x)-1;

fitinds2 = 1:length(x);

P2 = lsqcurvefit('confined_diffusion_func', [10 1], t(fitinds2), avgMSD(fitinds2));

confinedAvgD = P2(1);

confinedAvgAlpha = P2(2);

if flag

    figure(1)

    errorbar(1:length(x), avgMSD, totdMSD, '-.')

    hold on

    plot(fitinds, polyval(P, fitinds), 'g-')

    plot(t(fitinds2), confined_diffusion_func(P2, t(fitinds2)), 'r-')

    hold off

    xlabel('time (frames)')

    ylabel('mean squared displacement')

    title('Average mean squared displacement curve')

    figure(2)

    bar(xout, n)

    hold on

    plot(shortAvgD*[1 1],[0 max(n)], 'r-')

    hold off

```

```

ylabel('number of cells')
xlabel('average short time diffusion constant')

figure(3)
subplot(1, 2, 1)
bar(xDc,nDc)
hold on
plot(confinedAvgD*[1 1],[0 max(nDc)], 'r-')
hold off
ylabel('number of cells')
xlabel('average confined diffusion constant')
subplot(1, 2, 2)
bar(xAc,nAc)
hold on
plot(confinedAvgAlpha*[1 1],[0 max(nAc)], 'r-')
hold off
ylabel('number of cells')
xlabel('average confinement exponent')

end

MSDdata.MSD = MSD;
MSDdata.dMSD = dMSD;
MSDdata.avgMSD = avgMSD;

```

MSDdata.totdMSD = totdMSD;

MSDdata.shortD = shortD;

MSDdata.shortAvgD = shortAvgD;

MSDdata.confinedD = confinedD;

MSDdata.confinedAlpha = confinedAlpha;

MSDdata.confinedAvgD = confinedAvgD;

MSDdata.confinedAvgAlpha = confinedAvgAlpha;